**The Lifting of Mineral Aerosols in an Arid Environment**


**by**


**Douglas G. Halleaux**


A dissertation submitted in partial fulfillment
of the requirements for the degree of
Doctor of Philosophy
(Atmospheric, Oceanic, and Space Sciences)
in The University of Michigan
2014


Doctoral Committee:

     Professor Nilton O. Rennó, Chair
     Professor John R. Barker
     Professor Martin M. Kaufman
     Research Scientist Frank J. Marsik

**DEDICATION**

To Savannah, for your tireless support and encouragement (and English tutoring),

to Timmy, for being my side-kick, from our one-bedroom apartment to the farm,

and

to Jeremy, for sending me off every morning with a smile.

# ACKNOWLEDGEMENTS

Like every campaign, great or small, futile or destined, there is no single individual to whom credit for completion of this dissertation is owed. Instead, the chorus, sometimes cacophonic and sometimes harmonic, provided the foundation, background, fuel, and (sometimes, though only when appropriate) friction guiding its path. I beg the reader's patience, as a non-traditional student like myself owes much to many. Among all of those below, however, I am particularly grateful to the dedicated, my wife Savannah and sons Timmy and Jeremy, and to my advisor of these past 4 ½ years, Nilton Rennó.

The passing phrase, "I think I'd like to give a Doctoral program a try," turned into a half-decade of research, toil, failure, and success because of the encouragement and oft-drawn-upon excitement of my wife, Savannah. Since then, we've seen two Army deployments together, occupied five different places we've called "home," raised two fantastic boys, and built stability among the chaos of it all, and none of it would have been possible without Savannah's love. At the many points where I wished to quit, and the two or three moments when I was dedicated to doing so, Savannah gave me what I needed to continue. Usually it was a hopeful glance at the not-too-distant future, but at the more difficult times, it was a harsh reminder of the consequences to the boys of leaving that encouraged me to continue. It is in deep gratitude of this, and acknowledging completion of this degree as not an individual, but a family accomplishment, that I dedicate this dissertation to her.

Of everyone to whom I owe thanks, only one has been with me in person from the beginning to the end. Timmy and I began this trek together, in a tiny, one-bedroom apartment, managing the stress of a full, graduate-level course load while coping with Mommy's deployment to Iraq. We carried on through the qualification exam and candidacy, reminding each other along the way (though always by subtle means) that there were more important things to worry about than a poor exam grade or not getting a favorite toy at daycare. Timmy's love of family before toys, of hugs before cartoons, drove me to, more than once, think, "what the hell am I doing?" before putting down my lab book at home and sharing an episode of Spongebob.

Of course, this chapter (both literally, the text, and figuratively, the past 5 years) would not be complete without Jeremy, my smile-out-the-door every morning before braving rush-hour traffic. Usually that smile comes from a happy 2-year-old, excited that another day will bring him something new to see. Sometimes, the smile is amusement at a random antic to wear pajamas all day. Either way, Jeremy's hugs and kisses have a way of saying, "Don't worry about that poor paper review, you'll figure it out and be just fine." It's this psychological safety net provided by my two boys that I must admit I've relied upon many times, and I hope I reciprocate.

Without a doubt, the most significant professional influence in this dissertation and professional support through the past 5 years has been from my advisor, Nilton Rennó. Nilton gave me a wide berth to plan, lead, and conduct the ACI project, giving me his trust that, at the time, was in a relatively unknown student. More than the educational freedom and funding to grow into an independent research, though, Nilton provided me what others could not- honest, unabashed (though always constructive) criticism. Within my desk drawer sit three finished, but unpublished papers from my early days within the Ph.D. program. To each, Nilton opined, "This will not be published." As I progressed through my research and wrote other papers that were (eventually) published, I would take a glance through that drawer, and month by month, my appreciation for Nilton's candid opinions of my writing grew. Without his advice and counsel, this dissertation would have taken much longer to finish, if it were ever to be completed. Thank you, Nilton.

I'm deeply grateful for the professional support I've been given from inside and outside academia. Thank you, ACI team, Steve Musko, Robb Gillespie, Curt Cooper, and my driving buddy, Ron Rizor. Thank you, too, to my predecessors, Manish Mehta and Jasper Kok, my Ann Arbor colleagues, Shaneen Braswell, Harvey Elliott, German Martinez, Rachael Kroodsma, and Eric Fisher, my Flint colleagues, Randy Repic and Laura Binder, and a special thanks to Bill Kuhn, who listened patiently to my gripes more than once. Thank you, Mark Torregrossa, Glenn Willey, and Todd Borek for teaching me everything I know about being a weatherman. And, of course, I owe deep thanks to my doctoral committee, Frank Marsik, John Barker, Marty Kaufman, and Nilton Rennó, for reading, commenting, and signing (since these acknowledgements are published) my dissertation!

I would also like to acknowledge the support I received through the past five years from the support staff in the Atmospheric, Oceanic, and Space Sciences department. Thank you, Margaret Reid, Marti Moon, Sandra Pytlinski, Bryan White, and Katie Abdou! I also owe thanks to the University of Michigan's administrative staff for their extraordinary efforts to speed along the paperwork allowing the ACI project to be deployed to the field. Thank you, Katie Abdou, Judith Kirkdorffer, and Timothy Slottow.

Any achievement in our family is a family achievement, and in that theme, I would also like to thank my parents, whom I relied upon frequently for emotional support and (quite often) daycare. I never asked unless I really needed it, but when I asked, you bent over backward to help me, Savannah, Timmy, and Jeremy. Thank you, too, to my parents-in-law, John and Laura, for supporting my family through the past 5 years, whether with babysitting, the lake house, or just an ear to hear Savannah and me complain. I'm also very grateful for the support my sister, Beth and her family gave to mine. Coincidence brought you to live near us, but your kindness took care of us when we really needed a hand. Thank you, too, to my brother, Tom, and sister, Kelly, to Bill, Adam, and Laura, also my grandma, Arla, whose letters were a reminder that the world doesn't revolve around Ann Arbor, my grandpa, Ernie, my uncles, Mike, Dave, Duane, Danny, Mike, and Dave and my aunts, Geri, Barb, Kathy, Annette, Pam, my godfather, Brian, my godmother, Carol, my legion of cousins, nieces, and nephews, and Mrs. Joan Metzger, for taking my side in every complaint I had.

I would also like to acknowledge the patience and support I received from my military family. My doctoral studies were interrupted by a 12-month deployment to the middle-east, and through the support of my commanders and soldiers, I was able to make the transition back to research smoothly afterward. Thank you, Lt. Col. Dawn Dancer, Majors Rob Frazer and John Hall, Captains Matt Sawyer, Arnold Williams, Myron Bishop, Lieutenant Takura Nyamfukudza, Master Sergeant Tony Saladine, Sergants First Class Derren Mazza and Colin Mullins, the soldiers of the 126th Press Camp Headquarters, and my soldiers of 2nd Platoon, B-Battery, 1/182nd Field Artillery.

Finally, I would like to thank my friends and colleagues who have been my academic companions through all my years at Michigan. Thank you, Mike Boguth, Noelle Grulke, Bridget DeRosa, Nicole Shevsky, and Michael Jankowski!

**PREFACE**

The central theme of this dissertation is the successful implementation of the Aerosols-Climate Interaction project at Owens Lake, California. Chapter 1 provides the background and motivation for the field project, while Chapter 2 describes the development and tests of a new type of instrument for making measurements in convective vortices. Although Chapter 3 describes the instrumentation, data, and overall science themes behind the project in detail, it does not discuss the seemingly endless meetings and tedious bureaucratic dealings that occupied a large portion of the planning phase of the experiment.

The ACI project is the culmination of a series of field studies led by the overall Principal Investigator, Dr. Nilton Rennó. Previous field campaigns in Nevada and Niger used some of the ACI equipment for making opportunistic measurements of wind speeds, pressures, and electric fields in dust devils and dust storms. The 2-year field campaign at Owens Lake will also include the University of Michigan's electric field sensor, however at the time of this dissertation, they are not yet deployed.

Although each instrument deployed with the ACI project has been used previously, they had not been used together for extended periods of time, nor had they been set up for remote data transmittal. Steve Musko, the project's chief engineer, oversaw the development of the instrument assembly and data transmittal and storage system. The Space Physics Research Laboratory engineering team led by Steve also developed the instrument computer unit and power system.

The ACI project encountered a serious delay two months before deployment when the State of California, on whose lands the ACI project was to be deployed, and the University of Michigan (UM) found the project's lease agreement to be incompatible with each other's regulations. It was only through the kind efforts of the California Land Commission's Drew

Simpkin and the University of Michigan's Judith Kirkdorffer (who managed to drive through a 4-month approval process in 3 days) that engineer Ron Rizor and I were able to begin the 3-day journey to the California desert for deploying the instruments.

The nature of the lease agreement between UM and California prevented vehicles to be driven on the Owens Lake bed (details are described in Appendix C). Considering the nature of the ACI project studies, such driving would have been ill-advised, anyway. Unfortunately, much of the ACI equipment was heavy, and the project site is nearly 150 meters from the closest access road. What took 2 hours to load at the Space Research Building loading dock took 2 days to unload at the field site because the equipment had to be carried across high desert dunes in the dry conditions of early December. Specifically, carrying the 500-pound foundation sled upon which sits the solar panel assembly was nothing short of an adventure.

The fruit of this labor is what you read here. The three central chapters (Chapters 2, 3, and 4) have been submitted for publication. Chapter 2 has already been published as explained in Appendix B.

# TABLE OF CONTENTS

readings (green) as the dust devil passes the sensor are shown as a reference.

friction velocities are required to initiate saltation, but that dust is ejected more efficiently when saltation does occur.

# LIST OF TABLES

# LIST OF APPENDICES

# CHAPTER 1
# INTRODUCTION


Dust particles suspended in the atmosphere as aerosols are among the least understood atmospheric components with respect to the strength with which they drive natural processes [*Jacobson et al.,* 2000; *Tegen et al.,* 2004]. Of primary concern are the processes by which dust enters the atmosphere and their subsequent impact on the natural environment [e.g. *Zender et al.,* 2004; *Pilewskie,* 2007]. Understanding how dust particles enter suspension in the atmosphere is currently a major research problem because of the need for a solid foundation for estimates of aerosol concentrations and their effects on climate [*Shannon and Lunt,* 2011]. Once in suspension, dust particles affect radiative forcing directly by scattering and absorbing solar radiation [*Haywood and Boucher,* 2000] and indirectly by increasing the albedo and lifespan of clouds [*Twomey,* 1977; *Albrecht,* 1989; *Lohmann and Feichter*, 2005; *Li et al.,* 2011]. Indeed, beyond natural processes, studies of aerosols are pertinent to anthropogenic climate impacts because human activity may account for up to 50% of atmospheric dust concentrations through direct ejection mechanisms (e.g. motor vehicle operation) and indirect means (e.g. desertification) [*Tegen and Fung*, 1995]. Our understanding of the relationship between mineral aerosols and climate has been improving steadily, but radiative forcing by mineral dust aerosols is still one of the most uncertain processes in current climate models [*Sokolik et al.,* 2001; *IPCC,* 2007; *Laurent et al.,* 2009].

In Earth's climatological history, periods of peak stratospheric aerosol concentrations correlate well with depressed global temperatures [*Cole-Dai,* 2010], an effect mostly attributed to volcanic eruptions injecting particulate matter into the stratosphere (Fig. 1.1). On a regional scale, more common dust-lifting phenomena like mesoscale or synoptic scale winds and dust devils drive more frequent injections of dust into the boundary layer [*Neakrase et al.,* 2006; *Neakrase and Greeley,* 2010; *Kaplan et al.,* 2011; *Jiang et al.,* 2011]. These meteorology-driven perturbations in suspended dust concentrations can produce significant variations in the local and

global solar and terrestrial radiation fluxes and surface temperatures [*Tegen et al.,* 1996; *Prospero et al.,* 2002]. On any spatial scale, the capability of suspended aerosols to scatter, absorb, or emit radiation and thus alter atmospheric temperature and moisture profiles and meteorological patterns is highly complex, presenting challenges for effective modeling, even if the micro-processes of the individual particles' influence on radiative transfer is well understood [*e.g., Yang et al.,* 2007; *Alexander et al.,* 2013]. We believe that accurately estimating the concentrations of mineral aerosols by understanding their source processes is an important first step to developing accurate aerosol-radiation interaction models.

The concentration of mineral aerosols (or dust) is a function of the overall dust budget, balancing sources and sinks of suspended dust. The natural sources of terrestrial dust emission are those phenomena that can impart strong enough wind shear at a soil surface to initiate soil particle motion and include wide-scale phenomena like geostrophic wind flow to small, discrete events like dust devils and haboobs. Dust sinks, although not an investigative focus in this study, include gravitational setting and wet deposition, or "rain out" of particles, from the atmosphere [*Tegen and Schepanski,* 2009]. These sources and sinks define the atmospheric dust budget and are integral to understanding dust concentrations.

In this dissertation, I seek to contribute to the overall understanding of the processes that inject dust into the atmosphere and the role that dust has in impacting local climate through (i) testing and implementation of a novel instrument designed to accurately measure static and stagnation pressures within a dust devil, a unique and potentially significant source of atmospheric dust in arid environments, (ii) design and performance of a field campaign to measure the physical parameters characterizing saltation, dust ejection, and radiative flux changes at the surface, and (iii) introduction of a new theory for changes in a soil's ability to eject dust during saltation when soil moisture conditions change.

In the next section, I discuss the natural process of dust ejection from a soil surface. This is followed by a brief outline of this dissertation and its specific goals.
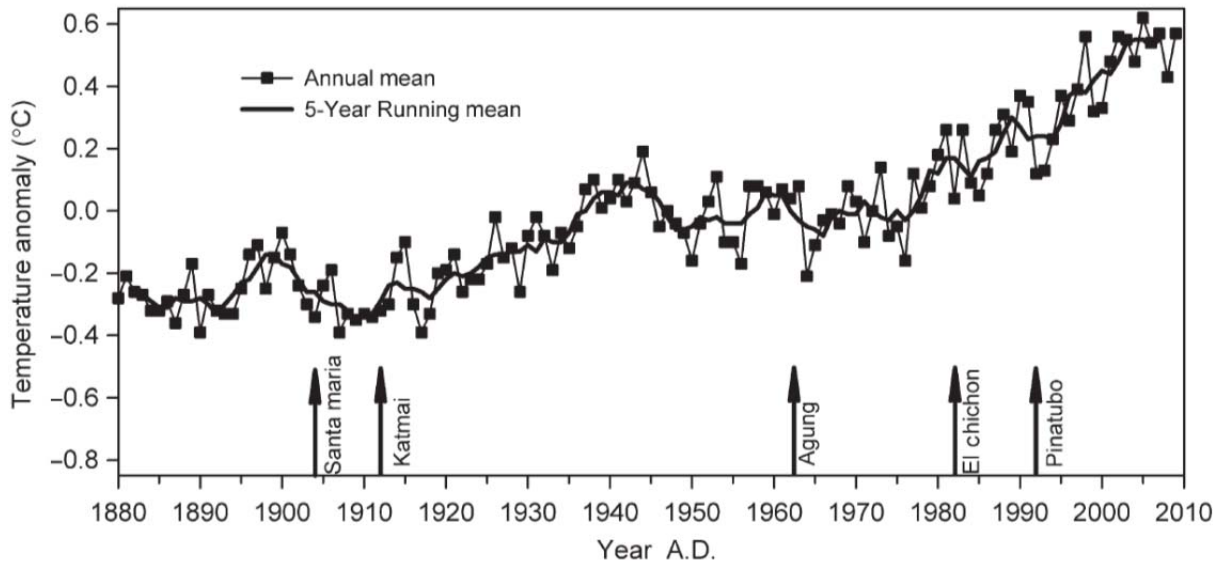
Figure 1.1: Global temperature anomaly from 1880. Global temperatures demonstrate a noticeable drop after significant volcanic eruption events produce an increase in stratospheric aerosol particles, an example of the possible effects aerosols play in global climate concerns. [*Cole-Dai*, 2010].

## 1.1 DUST LIFTING

Mineral particles enter into suspension in the atmosphere through aerodynamic lifting or when mechanically ejected by the impact of sand particles. Aerodynamic lifting occurs when drag and lifting forces on a particle remove it from the soil bed when these forces overcome the gravitational and interparticle forces acting on it. Figure 1.2 illustrates these forces on a soil particle.

The strengths of the various forces acting on a soil particle all depend upon the particle's size. Two forces drive their motion, the drag and the lift force. The drag force, $F_d$, is modeled by

$$F_d = K_d \rho_a D_p^2 u_*^2 \tag{1.1}$$

where $K_d$ is a dimensionless coefficient, $\rho_a$ is the air density, and $u_*$ is the friction velocity, a measurement of wind shear against the surface that scales with the square of the particle size ($D_p$) because larger particles present a larger surface area against which the wind can push [*Greeley and Iversen*, 1985]. The lift force, $F_l$, is typically small compared to the drag force for

saltation in air and is assumed negligible [*Saffman*, 1965; *McLaughlin*, 1991; *Kok et al.,* 2012]. Of those forces inhibiting motion, the gravitational force, $F_g$, modeled by

$$F_g = \frac{\pi}{6}(\rho_p - \rho_a)gD_p^3 \qquad (1.2)$$

where $\rho_p$ is the particle density, scales with the mass, and thus the cube of the particle size, and the interparticles forces, $F_i$, are a compilation of water adsorption forces, Van der Waals forces, and electrostatic forces that, as a whole, are found experimentally to scale with the particle size alone [*Hamaker*, 1937; *Johnson et al.,* 1971; *Herminghaus,* 2005]. In this manner, very large particles are dominated by gravitational force and tend to resist motion in nature. Likewise, very small particles, of which suspendable aerosols are a part, are dominated by interparticle forces and remain at rest for all but the most extreme natural wind shears.
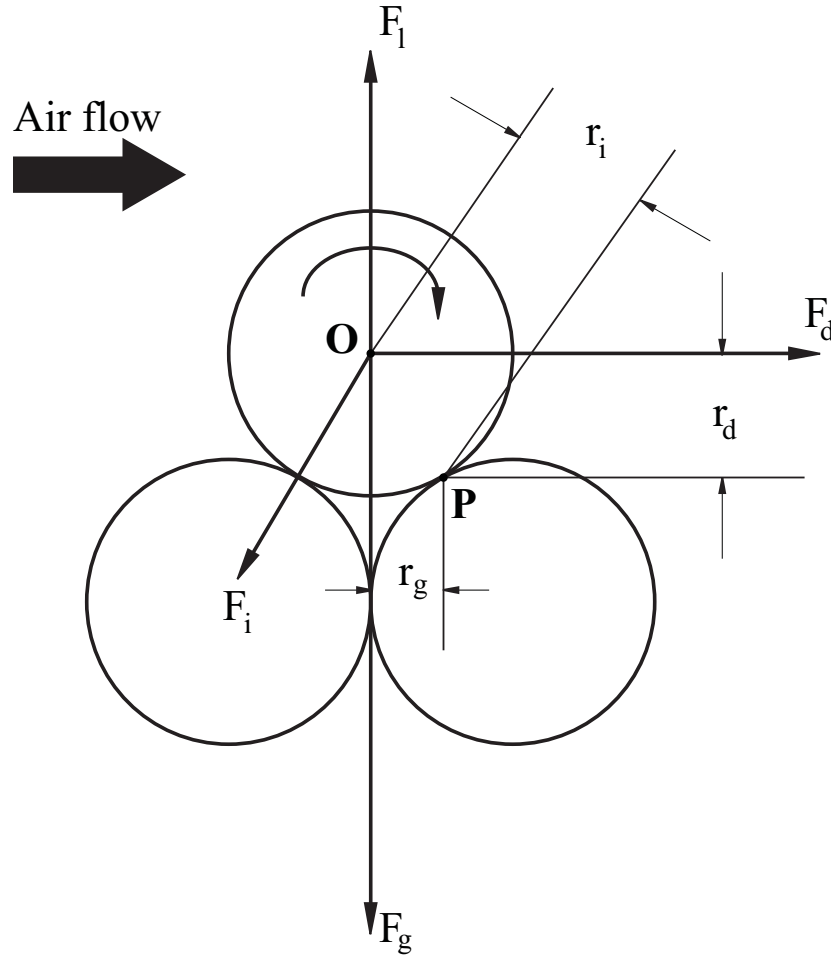
Figure 1.2: Aerodynamic force balance on a soil particle at rest. A particle (represented by circle O in the figure) moves when the drag force $F_d$ imparted by the wind shear is strong enough to overcome interparticle forces $F_i$ and the gravitational force $F_g$, allowing the particle to pivot over its neighbor at point $P$ [*Shao and Lu*, 2000].

These forces' disparete dependence on powers of particle sizes implies a middle range of particle sizes that are most likely to be aerodynamically lifted by a given wind shear. The Hjuldstrom diagram in Figure 1.3 demonstrates the minimum (or threshold) friction velocity necessary to push a particle of diameter $D$ into motion. Friction velocity ($u_*$) is a function of the strength of the wind shear against the surface and is related to wind speed by

$$u(z) = \frac{u_*}{\kappa} ln \frac{z}{z_0} \qquad (1.3)$$

where $u$ is the horizontal wind speed at height $z$, $\kappa$ is the von kármán constant ~0.4, and $z_o$ is the surface roughness length.

As aerosol particles are mostly smaller than 10 μm, and friction velocity even in strong windstorms is usually less than 0.5 m/s, direct entrainment of dust aerosols by the wind is rare [*Loosmore and Hunt*, 2000]. Instead, dust is ejected through mechanical forcing when larger particles aerodynamically lifted impact the surface at the termination of their trajectories into the air [*Alfaro et al.*, 2004]. Understanding the motion of these medium-sized particles is a critical first step toward understanding the overall aerosol budget.
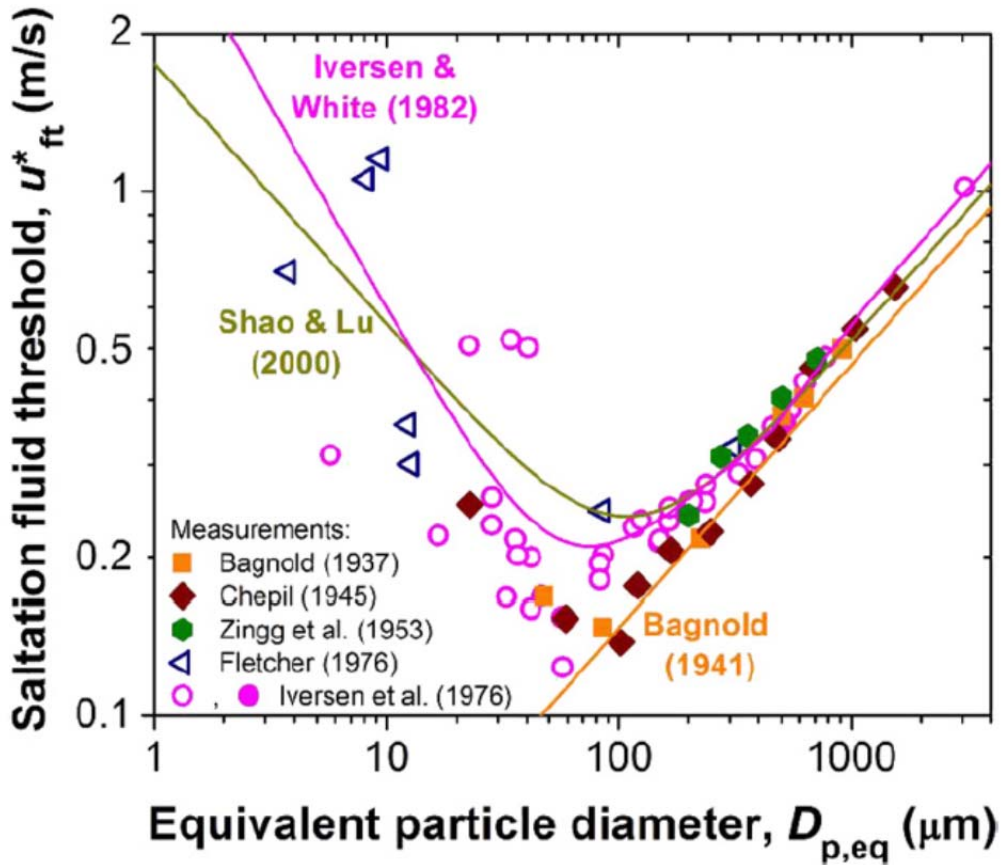


Figure 1.3: Modeled (solid lines) and measured (various symbols) threshold friction velocities for the direct lifting of soil particles from the surface. Particles with large enough diameters not to be dominated by interparticle forces but small enough not to be too heavy enter saltation at the minimum in threshold friction velocity [*Kok et al.*, 2012].

### 1.1.1 Saltation

Saltation is the primary vehicle by which mineral dust enters suspension and is physically manifested by the hopping motion of soil particles along the surface [*Bagnold*, 1941]. In saltation, particles are lifted aerodynamically in the presence of a sufficiently strong wind shear. Saltating particles then continue to move along a trajectory defined by their initial liftoff angle

and velocity, the particle's geometry, and the surrounding environmental conditions [*Kok and Rennó,* 2009]. When these particles return to the surface, they create a "splash," ejecting additional particles upward [*Shao and Li,* 1999; *Kok and Rennó,* 2009]. If the particles ejected during the splashes have a small enough diameter and large enough initial upward velocity, they may enter into suspension as dust.
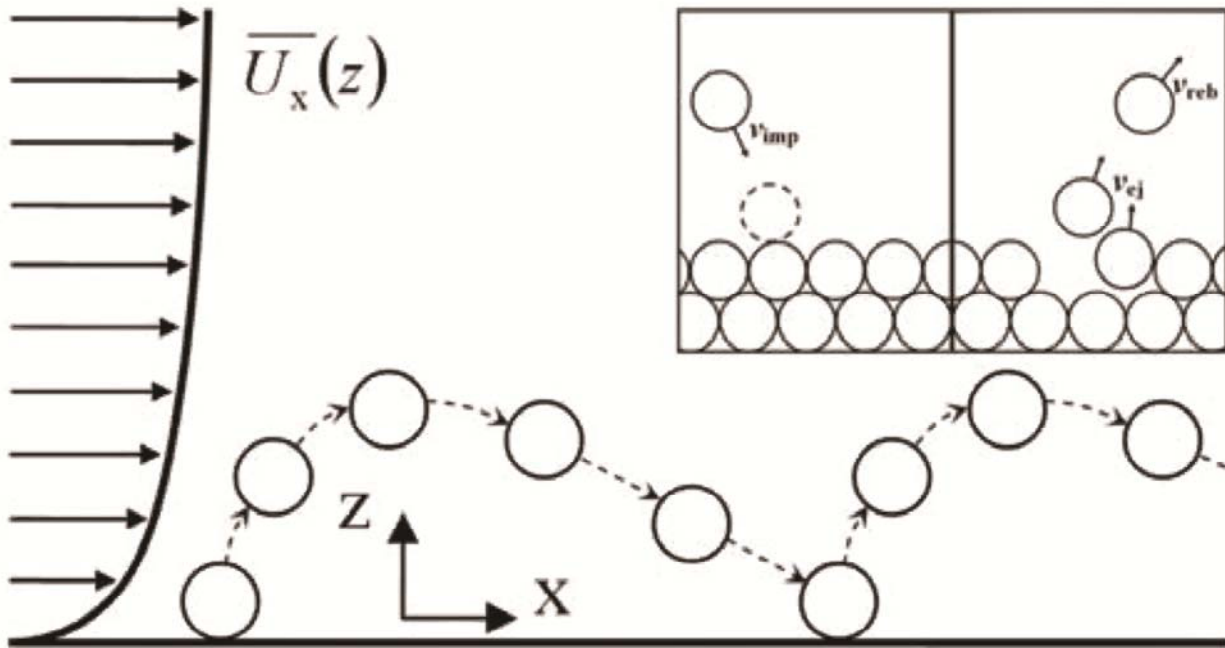


Figure 1.4: Saltation is characterized by the bouncing motion of moderate-sized particles along a soil surface, pushed into that motion by a wind gradient ($\overline{U}_x(z)$) providing a shearing force against the surface. When these particles re-impact the ground, they may eject other particles, some of which are small enough to be suspended as dust aerosols [*Kok and Renno,* 2009].

Saltation occurs when the vertical forces imparted on a particle, particularly the aerodynamic lift and the drag of the wind against the particle surface, exceed the vector sum of the downward gravitational pull on the particle [*Shao et al.,* 1993; *Kok and Rennó,* 2009] and the interparticle forces [*Kok et al.,* 2012] that keep it at rest.

Saltation depends on the particle's size, shape, and mass. Although there have been some attempts to define the particle size associated with saltation (> 106 μm in *Hagen et al.* [2010], for instance), the mechanics of saltation demand that the upper and lower particle size limits for grains in this motion to be dependent upon the imparting shear velocity [*Owen,* 1964].

### 1.1.2 Bombardment

Bombardment occurs when saltating particles impact the soil bed at the termination of their aerodynamic trajectories and transfer mechanical energy to other particles within the bed, ejecting them into the air [*Shao et al.,* 1993; *Grini et al.,* 2002]. If these particles ejected by bombardment are small enough, they may be lifted above the saltation layer, where they may be entrained by turbulent eddies in the boundary layer, becoming aerosols [e.g. *Park et al.,* 2007]. Here, we use a common definition of the saltation layer as the near-surface atmospheric layer containing 50% of the saltating particles at a given time [e.g. *Kok and Rennó,* 2009]. Aerosol-sized particles can also be released when saltating particles that are aggregates of smaller particles break [*Shao,* 2008; *Kok et al.,* 2012]. When particle aggregates impact the surface, they break apart, releasing the smaller particles into the air as aerosols [*Shao,* 2008]. Bombardment is the primary process through which aerosols are ejected from the surface. Saltation, which drives bombardment, and the cohesive interparticle forces that aggregate particles together are the critical processes linking wind shear to dust ejection.
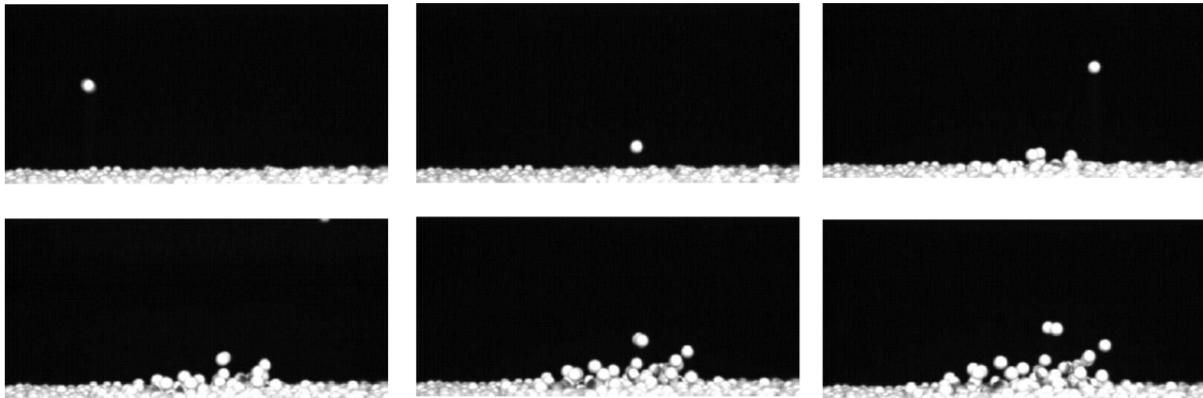


Figure 1.5: The bombardment process captured with a high-speed camera, from immediately before a bombarding particle's impact (upper-left) to "splash" and ejection of additional surface particles (lower-right). Reprinted figure with permission from *Beladjine et al.* [2007].

The interparticle forces binding soil particles together can be significantly strengthened by the presence of water [*Sherman et al.,* 1998; *Herminghaus,* 2005], and while these forces generally work to impede the onset of saltation, they can also enhance the creation of particle aggregates that can saltate more easily. The capacity of water to bind soil particles together depends strongly on soil type [*Fécan et al.,* 1999]. Water in sandy soils is more efficient at creating capillary bridges and strong cohesive bonds than in clayey soils, where a larger

proportion of the water is adsorbed as thin films onto the soil particles, resulting in less water being available for creating capillary forces, especially in high relative humidities (> 65%) [*Nickling and McKenna Neuman*, 2009]. This suggests that in sandy soils, capillary forces play a dominant role in binding soil particles together. In clay-rich soils, or on soils in low relative humidity (< 65%) environments, hygroscopic forces, or bonding forces between water layers adsorbed on the soil particles, dominate. In sandy soils in low relative humidity environments, neither capillary bridges nor hygroscopic forces play a significant role in contributing to interparticle forces [*Hillel*, 1980], but other chemical constituents in the soil may modify this moisture effect. For example, the presence of salt can increase the overall soil moisture content through deliquescence and enhance capillary forces [*Cantrell et al.,* 2002].

### 1.1.3  Saltation in nature

Saltation is the result of wind shearing against a surface containing loose particles, and such shear is typically a result of strong synoptic-scale meteorological pressure gradients or locally extreme weather events like dust devils and haboobs. Globally, aerosol emission is largest in arid regions characteristic of loose, dry soil with small surface roughness lengths where saltation would be expected to be ubiquitous [*Tegen et al.,* 2002; *Giles,* 2005]. Most researchers estimate that North African dust emissions represent a majority of all global emissions, while more temperate regions like North America and South America are typically relatively unimportant dust sources [*e.g., Huneeus et al.,* 2011; *Ginoux et al.,* 2001].

Saltation driven by synoptic-scale winds forced by ideally-aligned pressure gradients or a low-level jet is common in arid regions [*e.g., Yin et al.,* 2005], especially in channelized topography such as mountain valleys [*Washington et al.,* 2006]. Pressure gradients aligning with a mountain valley containing loose soil impart a shallow boundary layer and a steeper wind shear gradient against the surface. Such conditions can see friction velocity values exceeding 0.5 m/s and often drive persistent, long-lasting saltation events. Figure 1.6 shows a synoptic pattern over the Owens Valley in California that is a typical driver of strong saltation.
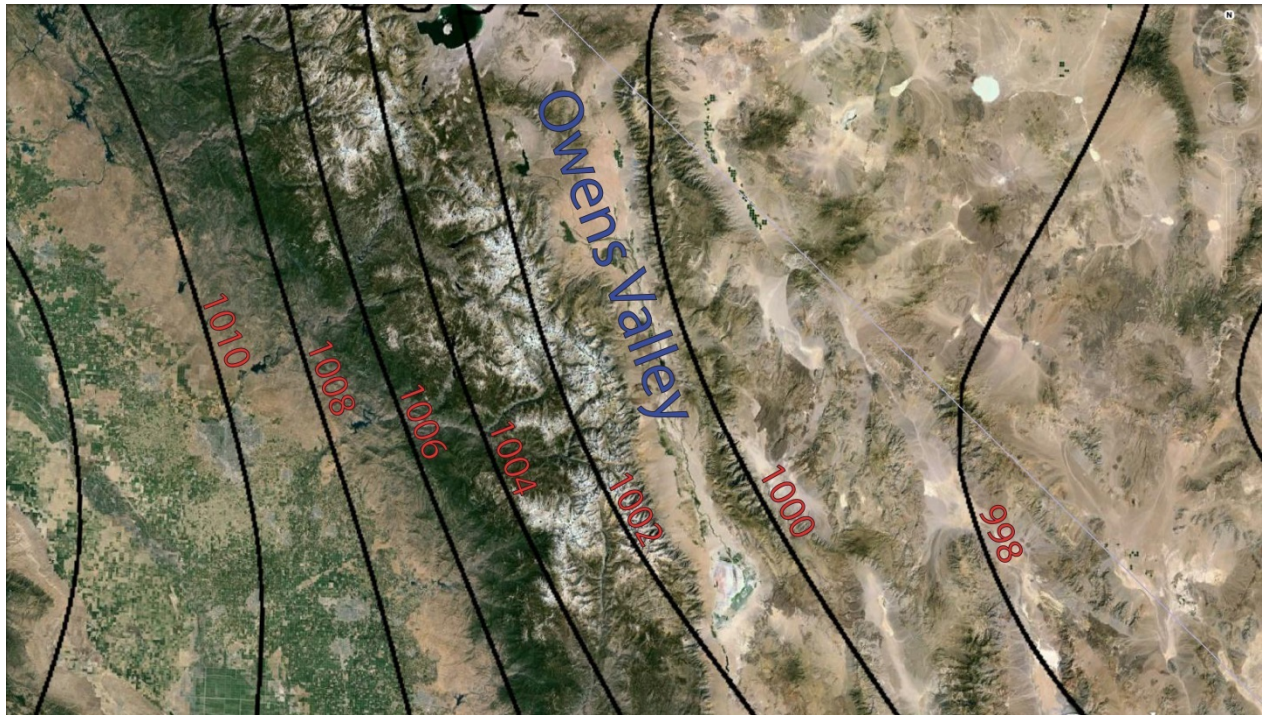
Figure 1.6: Pressure gradient (hPa) aligned with the channelized topography of Owens Valley on April 8, 2013. Alignment such as that shown here is a primary driver of the strong synoptic scale-driven wind shear against the dry, sandy soil of the valley that is characteristic of vigorous saltation events. Topographic map courtesy of Google Earth.

Dust devils are one of the most striking features of arid environments and as their name suggests, characteristically eject dust into the atmosphere [*Ringrose,* 2005]. As with synoptic-scale events, dust devils impart a strong wind shear that initiates saltation to remove dust-sized particles from the surface [*Balme et al.,* 2003]. Because they are convective vortices with a strong vertical wind component, dust devils also inject aerosols deep into the atmospheric boundary layer [*Balme and Greeley*, 2006]. Studies of dust devils are complicated by their intermittent nature, making it difficult to predict where they occur and thus to place instruments on them [e.g. *Sinclair*, 1964]. Further, among the most important measurements in a dust devil are static pressure and wind speed which are difficult to measure because of the dust devils' small scale and dynamic behavior.

Figure 1.7: Dust Devils at Owens Lake, California. Although the surface area of dust ejection within these convective phenomena is localized, their characteristic vertical winds lift particles high into the planetary boundary layer.

Thunderstorm gust fronts produce strong wind shear at the surface. When these gust fronts occur over an easily erodible surface and eject large quantities of dust, they are known as haboobs [*Roberts and Knippertz,* 2012]. A single haboob event can eject up to 1 Tg of dust into the atmosphere [*Bou Karam et al.,* 2010], demonstrating the importance of such discrete phenomena to the overall aerosol budget.

### 1.1.4 Owens Lake, California

The salty playa of Owens Lake in California is this dissertation's physical focus of study and the site of the Aerosols-Climate Interaction study. Until 1913, Owens Lake was the final destination of the Owens River and had held water continuously for more than 800 millennia. By the mid-1920s, water diversion of the Owens River into the Los Angeles Aqueduct reduced the lake to the sandy playa it is today [*Maisel,* 2005]. Its history as an evaporative pool accounts for the high salt content of the lake bed's soil [*Titus et al.,* 2002], dominated by sodium

11

carbonate [*Dahlgren et al.,* 1997] and containing smaller amounts of calcium and magnesium chloride salts [*Quick and Chadwick*, 2011]. The groundwater at Owens Lake is shallow with a high pH (~10) resulting from the alkaline nature of dissolved sodium carbonate solution and is anoxic, properties that also restrict vegetative growth in the lake bed [*Dahlgren et al.,* 1997].
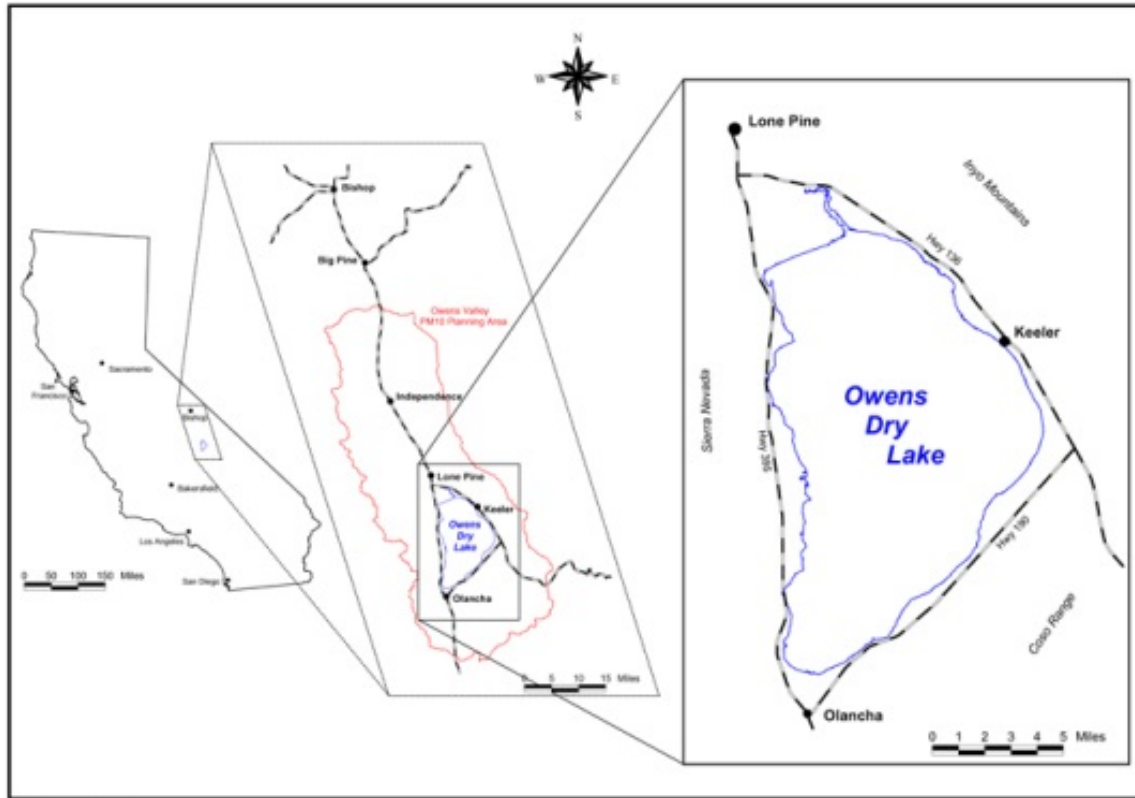


Figure 1.8: Owens Dry Lake is located in eastern California, at the southern end of the Owens Valley. Reproduced with permission from Great Basin Unified Air Pollution Control District.

Owens Lake is located at the south end of the Owens River, in the high desert of eastern California (Fig. 1.8). Its position within the longitudinally-oriented Owens River valley provides a source of strong wind shear when synoptic-scale wind gradients align with the valley and are channelized, and the dry, sandy, salty soil of its surface provides an abundance of saltatable material. The remote location of Owens Lake also reduces anthropogenic dust sources that may otherwise interfere with local measurements, making the dry lake an ideal location for investigating this study's research goals.

## 1.2 RESEARCH GOALS AND THESIS OUTLINE

The goal of this dissertation is to improve our understanding of the physical processes that initiate saltation and thus lift dust into suspension. It does so by addressing three questions:

1) *What drives the peak wind speeds of dust devils?*

   As a common dust-lifting weather phenomenon, dust devils are a natural focus of any research on dust aerosols. The capacity of these vortices to eject dust is a function of their overall strength (characterized by their vortex wind speeds or maximum vortex pressure drop) and duration. In Chapter 2, I support the study of these phenomena through the testing and implementation of a novel instrument for accurately measuring the static and stagnation pressures within a convective vortex, measurements that are important for the modeling and prediction of dust devils' strength.

2) *What role do environmental factors like humidity, wind speeds, and soil composition play in supporting saltation and dust lifting?*

   In Chapter 3, I describe a field project that was designed, deployed, and performed for the purpose of collecting and analyzing direct measurements of saltation's strength (via saltating particle flux and frequency), vertical dust flux, surface radiative flux, and the environmental properties within which saltation and dust lifting occur. Initial results from the field project show increases of dust flux with increases in soil relative humidity. This unexpected result may imply the existence of critical processes at the project site involving dust aggregation or soil crusting, two processes that affect the capability of an environment to eject dust.

3) *How do changes in soil moisture affect the vertical dust flux from saltation, and how is the saltating particles' efficiency at ejecting dust related?*

   The surprising result that vertical dust flux increases with soil moisture content led to the development of a theory to explain these changes. Chapter 4 introduces and discusses this new theory, which suggests that for most environmental conditions in which saltation is vigorous, increases in bombarding particles' dust-lifting efficiency with soil moisture enhances the vertical dust flux despite coincident increases in

threshold friction velocity.  The new theory sheds light on a previously alluded to, but not investigated, influence of moisture on dust lifting.

**CHAPTER 2**

**THE MICHIGAN PRANDTL SYSTEM: AN INSTRUMENT FOR ACCURATE**

**PRESSURE MEASUREMENTS IN CONVECTIVE VORTICES**

**2.1 INTRODUCTION**

This chapter describes a new instrument developed at the University of Michigan to measure the static pressure, the total (or stagnation) pressure, and the velocity in flows whose direction and intensity change rapidly.  Specifically, this system was designed to measure the static and stagnation pressures in dust devils.  Dust devils, as their name suggests, are a significant mover of mineral aerosols in arid environments.  As convective vortices, their strong wind shear on the soil surface produces vigorous saltation that ejects large amounts of dust into the air [*Sinclair,* 1973], while their vertical velocities lift these particles deep into the boundary layer.

The ever-changing wind vectors in convective vortices are a challenge for making accurate measurements on them.  Accurate measurements of the static pressure are particularly problematic because they require the sensor air intake to be aligned perpendicular to the wind direction.  This chapter describes calibrations and tests of the Michigan Prandtl System (MPS) and, in particular, the characterization of the errors in the static pressure measurements as a function of misalignments between the Prandtl tube and the wind vector.  This chapter shows that the MPS measures the pressure with a relative error of 3.5% for wind flows whose direction is within about 10° of the MPS tube direction.  It also shows that the MPS adjusts to changes in wind direction of 90° in about 1.5 s, the average rate of change expected in a typical dust devil of about 15 m of radius travelling at 10 m s$^{-1}$ [*Rennó et al.,* 1998]. Field tests indicate that misalignments between the MPS and the wind vector are usually smaller than ~30° during

measurements in dust devils, and that these misalignments always cause increases in the static pressure measured and decreases in the total pressure measured.

## 2.2 INSTRUMENT THEORY

This chapter describes the University of Michigan Prandtl System (MPS), developed to measure the wind vectors and the static and total pressures in flows with rapidly changing direction and intensity, and reports results of its characterization in a wind tunnel to:

1. Accurately measure static and total pressures within convective vortices.
2. Make high-frequency (10 Hz) measurements of these pressures.
3. Study the relationships between changes in static pressures and kinetic energy.

The MPS was developed to make *in situ* pressure measurements in dust devils and dust plumes. *Rennó* [2008] proposed a theory for convective vortices that predicts decreases in static pressure when the kinetic energy increases along streamlines of the inflow to the center of these vortices by

$$-(1-\gamma\eta)\frac{\Delta p}{\rho_s} + \gamma\eta\left[\left(c_p\Delta T + l_v\Delta q\right) + W_{irr}\right] + \Delta\phi + \frac{\Delta\upsilon^2}{2} = 0 \qquad (2.1)$$

where $\gamma \sim 1$ is the fraction of the mechanical dissipation of energy occurring at the heat input branch of the convective circulation, $\eta$ is the thermodynamic efficiency, $\left(c_p\Delta T + l_v\Delta q\right)$ is the change in enthalpy, $W_{irr}$ is the irreversible work of expansion, $\rho_s$ is the density of the air at the surface, $\Delta\phi$ is the change in potential energy, and $\left(\Delta\upsilon^2\right)/2$ is the change in specific kinetic energy. Eq. (2.1) is a generalization of the Bernoulli equation, which sheds light on the formation of the spiral bands that lift dust particles. In moisture-rich convective vortices such as tornadoes, the lifting condensation level lowers in these spiral bands while they intensify producing the "wall clouds" [*Moller,* 1978].

Here, dust devils are defined as low-pressure, warm-core vortices strong enough to initiate saltation and lift dust particles [*Rennó et al.,* 1998]. *Rennó et al.* [2010] show evidence

that in dust devils the changes in kinetic energy and static pressure are consistent with those predicted by the generalized Bernoulli equation, that is Eq. (2.1). The center of the typical dust devil analyzed by *Rennó et al.,* [2010] passed over stationary instruments in about 20 s. During the passage of the dust devil, the wind direction changed by as much as 22° between individual measurements 100 ms apart, and the wind direction typically changed by nearly 90° in about 3 s. The vortex that passed directly over the instruments caused a pressure drop of 1.1 hPa from the static pressure in the nearby environment to the lowest static pressure in the vortex walls. A more complete analysis of the data collected during our field campaigns will be described in a companion article.

Accurate pressure measurements are critical for testing theories such as that proposed by *Rennó* [2008], but are difficult to obtain because of the rapid changes in wind direction and intensity observed in dust devils and the modest changes in the static and total pressures (static and total pressure perturbations smaller than 0.5% of the atmospheric pressure in the strongest dust devils [*Rennó et al.*, 1998]). Previous measurements of static pressures and kinetic energy, though prevalent in the quasi-steady flows of wind tunnels, have been problematic in natural phenomena such as convective vortices, because current instruments do not make simultaneous measurements of pressure and wind velocity with sensors that have the air intake aligned with the flow. We show that the MPS described in this chapter is capable of making accurate measurements of static pressure, total pressure, and the wind vector in natural phenomena such as convective vortices.

## 2.3 MEASUREMENT APPROACH

Accurate measurements of static pressure and the wind vector are critical for testing theoretical ideas such as the generalized version of the Bernoulli equation proposed by *Rennó* [2008]. Even though existing instruments, such as sonic anemometers, are capable of performing accurate wind measurements even when the wind directions change rapidly, measurements of the static pressure are a challenge because they require the air intake of the pressure sensor to be aligned perpendicular to the wind. The MPS accomplishes this through a Prandtl probe capable of quickly aligning with the wind as its direction changes.

Prandtl probes measure the total pressure with a port directed into the flow and the static pressure with ports orthogonal to the flow. These measurements are generally used to calculate the flow speed in wind tunnels and airplanes and do so using the classical Bernoulli equation:

$$\Delta p = \tfrac{1}{2} \rho \upsilon^2 \qquad\qquad (2.2)$$

where $\Delta p$ is the difference between static and total pressures, $\rho$ is the fluid density, and $\upsilon$ is the flow speed [e.g., *Zucrow and Hoffman*, 1976]. In the MPS, the static and total pressures are measured with a Prandtl probe [*Prandtl*, 1952], and the static pressure is the primary measurement of interest. The total pressure is measured only to determine the alignment of the MPS with the flow through comparison with the measurements of the wind speed made with a Campbell "CSAT" 3D Sonic Anemometer [*Campbell Scientific Inc.*, 2012].

In addition to independent measurements of the 3D wind vectors and the static and total pressures, the MPS measures the wind direction with the vane, which points the instrument towards the flow. *Saca et al.* [2010] have successfully used the sensor to study dust devils.

## 2.4 SCIENCE REQUIREMENTS

The requirements for studies of kinetic energy and pressure perturbations in terrestrial dust devils are:

1. Pressure ranging from 850 to 1100 hPa. This range is required for making measurements in dust devils in areas with altitudes ranging from slightly below sea-level, such as Death Valley, to elevations exceeding 1000 m, such as California's High Desert where dust devils are ubiquitous.

2. Pressure measurement with resolution of $\pm 1$ Pa. Measurements should be accurate enough to describe typical dust devils' pressure perturbations of about 2.5 hPa [*Rennó et al.*, 1998].

3. Time with resolution of 0.1 s. This resolution is high enough for sampling typical dust devils with diameter of 15 m traveling at about 5 m s$^{-1}$ [*Rennó et al.*, 1998].

4. Wind speed ranging from 0 to 35 m s$^{-1}$. This range is necessary for making measurements in typical dust devils, which have peak tangential velocity of about 15 m s$^{-1}$ [*Rennó et al.*, 1998].

## 2.5 THE PROTOTYPE INSTRUMENT

The MPS consists of a Prandtl tube, a 3D sonic anemometer, and the supporting data processing electronics and mounting hardware shown in Fig. 2.1. A standard Prandtl tube, developed for measuring the static and the total pressures on aircraft [*Marks*, 1934], measures pressures in the MPS. As shown in Fig. 2.2, a single sensing port with radius of 0.85 mm at the forward tip of the sensor measures the total pressure, while eight ports with radii of 0.25 mm orthogonal to the longitudinal axis of the tube and 33 mm from the tip measure the static pressure. The static pressure ports are connected to a single pressure sensor. The Prandtl tube is attached to a trapezoidal double panel with a surface area of 710 cm$^2$, which acts as a vane to orient the tube towards the wind.
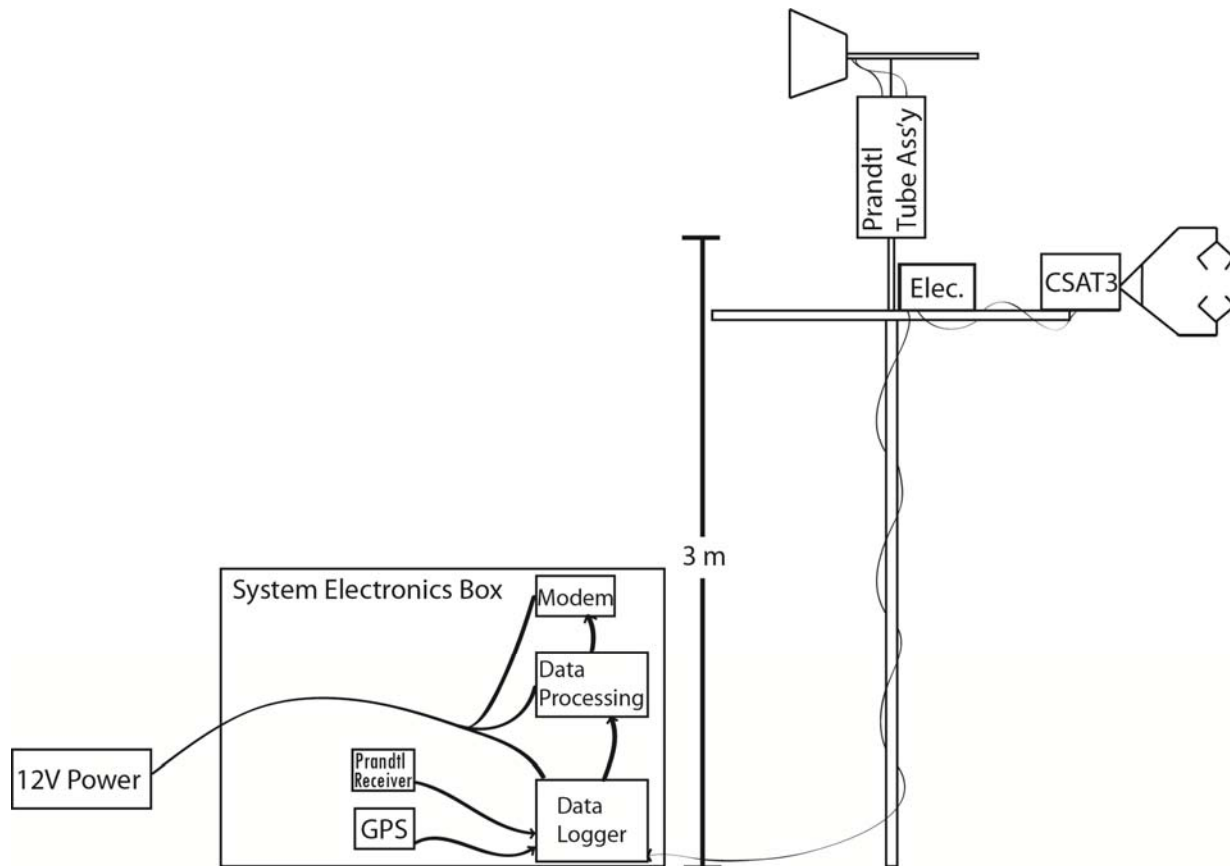
Figure 2.1: The Michigan Prandtl System (MPS). The MPS includes the Prandtl tube subsystem (top) and a 3D sonic anemometer (CSAT3, right). The Prandtl tube assembly freely rotates at the top of the mast and provides static and total pressure measurements in the wind flow, while the wind direction (used to verify proper alignment of the Prandtl tube to the wind flow direction) and speed are measured with the sonic anemometer. The data processing and storage electronics are located in a box (not drawn to scale) near the base of the mast.

Plastic tubing connects the static and total pressure ports to pressure transducers mounted in the electronics cylinder on the instrument post. The pressure transducers convert pressures into DC voltage for transmittal to a data logger with time response of about 500 ms. Disparate time responses between the static and total pressure transducers due to differing tube lengths are smaller than the time resolution of the transducers' measurements and negligible.
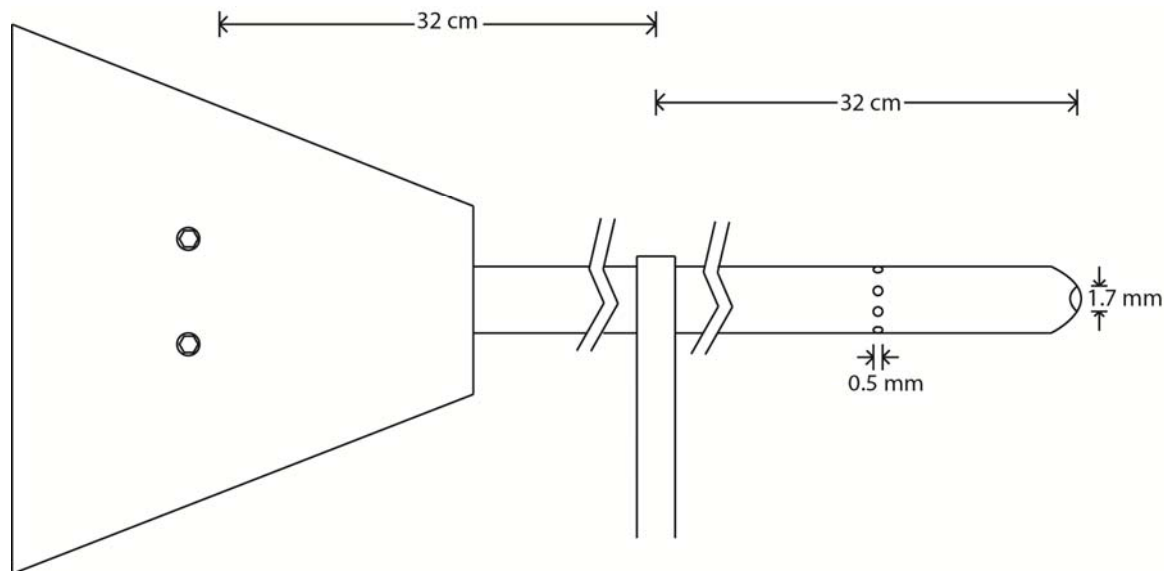
Figure 2.2: The pressure sensing portion of the MPS. Static pressure is measured via a port on the tip of this modified Prandtl tube, and total pressure is measured via eight orthogonal ports, all connected to a single pressure transducer. The vane on the aft portion of the tube aligns the tube with surrounding wind direction.

The entire pressure measuring system, including the Prandtl tube, vane, and cylinder, rotates freely as a single unit with changes in wind direction. A slip ring provides power to the rotating portion of the MPS.

The Prandtl tube system's response to change in wind direction depends on the moment of inertia of the entire rotating portion of the MPS. We first calculate moments of inertia for each separate component of the rotating portion of the MPS by integrating the product of the individual masses with their distance from the axis of rotation. We then calculate the total moment of inertia of the vane by adding the components' moments of inertia. The total moment of inertia is indicated in Table 2.1.

21

Table 2.1: Physical parameters of the MPS vane used

| Parameter | Value |
|---|---|
| Moment of Inertia ($J$) | $0.12$ kg m$^2$ |
| Vane panel surface area ($S$) | $0.071$ m$^2$ |
| Distance from rotational axis to center of wind force on vane ($r_v$) | $0.30$ m |
| Initial angle of wind vane to air flow ($\theta_0$) | $11°$ |
| Wind flow speed ($v$) | $5$ m/s |
| Air density (kg/m$^3$) | $1.25$ kg/m$^3$ |

The vane responds as a damped oscillator to changes in wind direction. That is

$$\theta(t) = \theta_0 \exp\left\{\frac{-D}{2J}t\right\}\cos(-2\pi\omega t) \tag{2.3}$$

where $\theta$ is the angle of the vane to the wind vector, $\theta_0$ is the initial angle of the vane, $J$ is the moment of inertia of the rotating portion of the MPS, $D$ is the aerodynamic damping of the vane, and $\omega$ is the damped oscillation frequency [*Wieringa*, 1967].

The damping ratio $\zeta$, defined as the ratio of the actual aerodynamic damping of the vane to its critical damping value $D_0$, is

$$\zeta = \frac{D}{D_0}. \tag{2.4}$$

It follows from *Wieringa* [1967] that it is given by

$$\zeta = 0.395\sqrt{\frac{a_v r_v^3 S}{J}} \tag{2.5}$$

where $r_v$ is the distance from the axis of rotation to the center-of-mass of the vane panel, $S$ is the area of the panel, and $a_v$ is the torque parameter of the vane, determined experimentally to be approximately 7 for a flat-plate fin with an angle-of-attack of 10°.

Neglecting the friction in the bearings, the MPS vane has a damping ratio of 0.13, implying that it is a subcritically damped oscillator. From this damping ratio, the natural oscillation period of the vane is found to be

$$t_0 = \frac{\pi r_v}{\upsilon \zeta}$$ (2.6)

where $\upsilon$ is the wind speed. The torque parameter $a_v$ can be used to calculate the torque on the vane as a function of wind speed

$$N = \tfrac{1}{2} \rho \upsilon^2 r_v S a_v$$ (2.7)

where $\rho$ is the air density. It follows from *Wieringa* [1967] that the damped oscillation period of the vane is

$$t_d = \frac{1}{\omega} = \frac{2\pi}{\sqrt{\dfrac{N}{J} - \left(\dfrac{D}{2J}\right)^2}} \quad .$$ (2.8)

Table 2.1 lists the values of the parameters used in Eq. (2.3) to calculate $\theta(t)$ for the MPS. The method proposed by *Wieringa* [1967] simplifies the second-order differential equation governing motion of the vane by approximating $\sin(\theta)$ to $\theta$. Thus, we apply this method only for small angles. Further, this expected response neglects the possible effects of suspended dust, which may increase the local air density and friction between the air flow and vane. Fig. 2.3 displays the expected angular response of the vane, indicating that the damped oscillation period is 1.4 s and the overshoot is 65.5%.
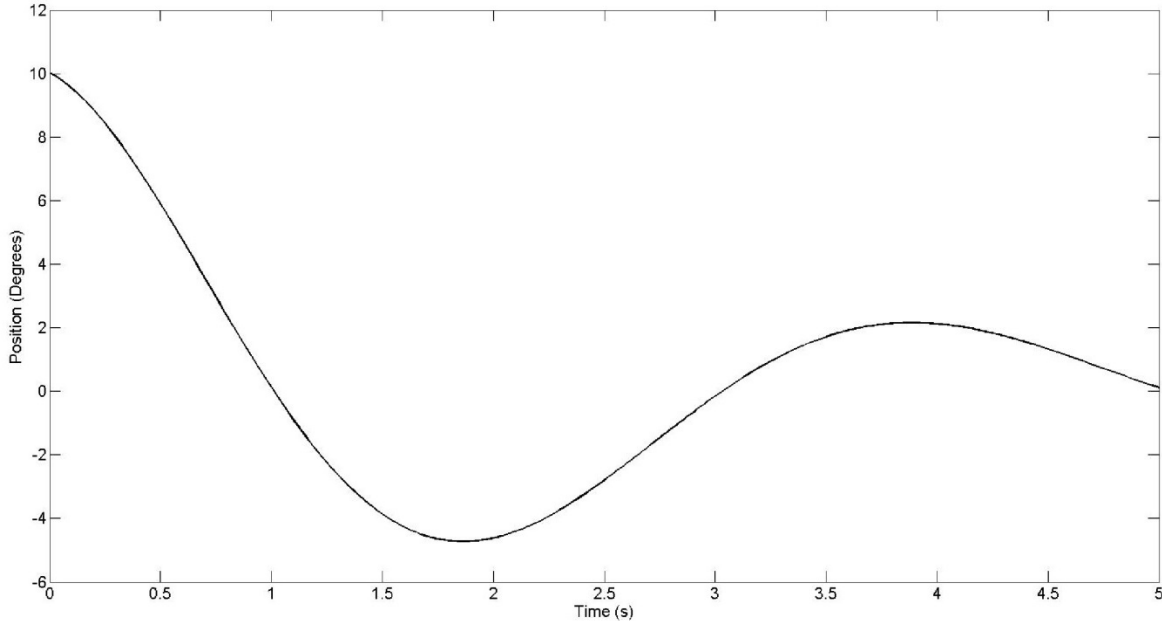
Figure 2.3: Predicted oscillation behavior of the MPS rotating frame. For an initial angle between the MPS vane and wind flow of $\theta = 11°$, the damped harmonic oscillation of the vane has a period of $t_d = 1.4$ s with an overshoot of 65.5%.

Measurements of the total pressure with the MPS when its tube is not aligned with the wind will always be smaller than those obtained with a tube in perfect alignment. This results from the decrease in the component of the flow into to the pressure port as the angle of misalignment increases. In a flow of velocity $v$ when the misalignment of the MPS vane with the flow is 90°, the decrease in the total pressure $p_{tot}$ is the dynamic pressure $p_d$ found by

$$p_d = p_{tot} - p_s = \tfrac{1}{2}\rho v^2 \tag{2.9}$$

where $p_s$ is the static pressure. The decrease in the total pressure is estimated to be 133 Pa for dry air at 25°C in a typical dust devil, whose peak wind speed is $v \approx 15$ m s$^{-1}$.

Measurements of the static pressure by the MPS when its tube is not aligned with the wind will always be larger than those obtained with a tube perfectly aligned with the flow. For a misalignment of 90°, the MPS tube acts as a cylinder with the longitudinal axis perpendicular to the flow. The Reynolds number of the flow around this cylinder is

24

$$\mathrm{Re} = \frac{vd}{\upsilon} \tag{2.10}$$

where the cylinder diameter is $d = 0.005$ m and, for dry air at 25°C, the kinematic viscosity is $v = 15.7 \times 10^{-6}$ m$^2$ s$^{-1}$. A flow speed of $\upsilon = 15$ m s$^{-1}$, the peak flow speed in an average dust devil, yields a Reynolds number of Re $= 4.8 \times 10^3$. Table 2.2 lists pressure coefficients along the surface of a cylinder in a flow with a Reynolds number of this order of magnitude [*Kravchenko and Moin*, 2000]. As the misalignment between the MPS vane and the flow increases, the total pressure decreases and the static pressure increases.

Table 2.2: Pressure coefficients along the surface of a cylinder whose longitudinal axis is perpendicular to a fluid flow at Re = 3900. $\theta$ is the angle made from the forward-most point of the cylinder, relative to the fluid flow [*Kravchenko and Moin, 2000*].

| $\theta$ [deg] | $\dfrac{p_{tot} - p_s}{\frac{1}{2}\rho\upsilon^2}$ |
|---|---|
| 0 | 1.0 |
| 45 | -0.5 |
| 90 | -1.0 |
| 135 | -0.9 |
| 180 | -0.9 |

A Campbell Scientific 3D sonic anemometer (CSAT) is integrated into the MPS, providing high-frequency measurements of the wind vector. The measurements with the 3DSA are used to detect and quantify misalignments between the Prandtl tube direction and the wind direction, in addition to the wind speed values used for calculation of the kinetic energy of the flow. The CSAT provides wind speed measurements with accuracy of 0.08 m s$^{-1}$ and wind direction measurements with accuracy of 0.2 degrees on a typical dust devil peak wind speed of 15 m s$^{-1}$ [*Campbell Scientific Inc.*, 2012].

## 2.6 INSTRUMENT CHARACTERIZATION

### 2.6.1 Tests

Three sets of measurements are made to characterize the MPS, which determine the accuracy of the static and total pressure measurements made with the MPS. To assess the MPS's accuracy when subjected to the abrupt changes in wind direction observed in convective vortices, we determine the accuracy of the MPS measurements when the sensor is not properly aligned with the wind flow.

The first set of measurements is conducted to calibrate the MPS in the range of conditions that the instrument will encounter during measurements on dust devils. To achieve this goal, the MPS is subjected to wind speeds ranging from 5 to 35 m s$^{-1}$. The flow speed is calculated using the MPS pressure measurements, which is compared to the wind tunnel flow speed measured with a Dwyer 641RM hot-wire anemometer, whose accuracy is 3%. The air density is used to estimate the flow velocity using Eq. (2.2), and is calculated using the air temperature measured inside the wind tunnel, and the atmospheric pressure measured by a mercury barometer at the wind tunnel facility. As explained below, this indicates that the flow speed calculated using the MPS pressure measurements is accurate over the full range of wind conditions expected in dust devils, beyond 15 m s$^{-1}$, the peak tangential velocity expected in typical dust devils [*Rennó et al.*, 1998].

The sensor is then tested for errors in pressure measurements resulting from misalignment between the wind flow and the Prandtl tube. Pressure measurements are made while the sensor is locked at angles ranging from 0° to 90°, both to the left and to the right of the wind direction with respect to the flow. The measurement error is calculated from the deviation of the pressure measurements made at the misaligned angles from those obtained when the sensor is aligned with the flow. These data are useful for estimating the measurement error when wind directions shift more rapidly than the sensor can respond.

Finally, a set of measurements is made to determine the response time of the MPS to changes in the wind direction. The MPS wind vane is placed at angles relative to the wind tunnel's flow ranging from 0° to 90°, locked in this position, and then released. The change in the direction of the vane as a function of time is recorded while it adjusts to the flow direction.

**2.6.2  Results**

The difference between static and total pressures measured by the MPS is found to have a mean error of 7.7% from the pressure differentials estimated by Eq. (2.2). This deviation between the expected pressure drop and the pressure drop measured by the MPS decreases as the flow speed increases, reducing to 4.8% at flow speeds above 5 m s$^{-1}$ (Fig. 2.4).  We hypothesize that this deviation is mostly the result of flow perturbations around the Prandtl tube and imperfect seals between the pressure ports on the tube and the pressure transducers.
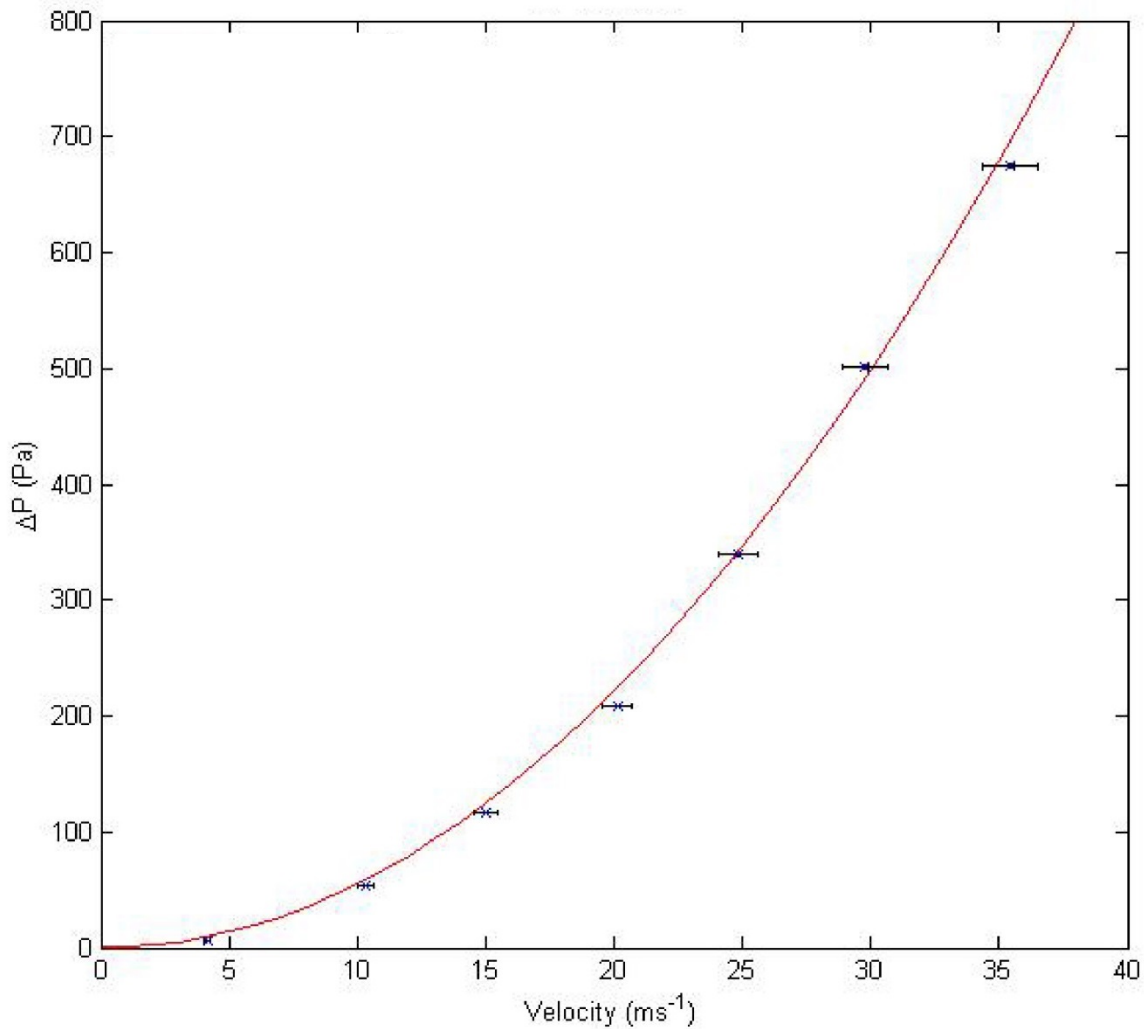
Figure 2.4: Calibration of the Michigan Sensor. The solid line indicates theoretical pressure differences ($\triangle$P) between static and total pressure from Eq. (2.2), while error bars represent wind speed measurement instrument accuracy in the wind tunnel. Data points (x) are pressure differences calculated from the static and total pressures measured by the MPS. The data deviates from the expected pressure differences by an average of 7.7% over the entire range of use. Mean relative error for tests at wind speeds faster than 5 m s$^{-1}$ is 4.9%.

Measurements of the static pressure always increase as misalignments between the Prandtl tube and the wind increase. Therefore, the correct static pressure is the minimum value that can be measured. The tests show that when the sensor is placed at angles with the flow direction that do not exceed 18°, the error in the differences between the static and total pressures from those measured at the zero-degree reference are smaller than +12% (Table 2.3). When placed at an angle of 12° to the flow, the error in the differences between static and total

28

pressures is about +3.5%. As expected, increases in the angles produce larger errors; at angles of 27° the error is +37%. At greater angles, the error increases significantly. More importantly, the error is always positive, indicating that misalignments of the Prandtl tube with the flow always produce decreases in the difference between the static and total pressures under the conditions tested here.

Table 2.3: Measurement error as a function of misalignments between the Prandtl tube and the wind vector. The MPS vane direction was locked at various angles to the left and right of the flow direction while the static and total pressures were measured. Deviation is from the difference between the static and total pressures when the Prandtl tube is aligned with the flow, $\Delta p(0°)$, and when misaligned by an angle $\alpha$ with respect to the flow, $\Delta p(\alpha)$. The wind tunnel flow speed was maintained at 5.0 m s$^{-1}$ during these measurements. The measurement error increases strongly for angles larger than 30°.

| Sensor Angle $\alpha$ (Direction) [deg] | $\lvert\Delta p(0°)-\Delta p(\alpha)\rvert$ [Pa] | Relative Error [%] |
|---|---|---|
| 12 (Right) | 0.28 | +3.5 |
| 18 (Left) | 1.09 | +12 |
| 27 (Right) | 2.97 | +37 |
| 30 (Left) | 2.89 | +32 |
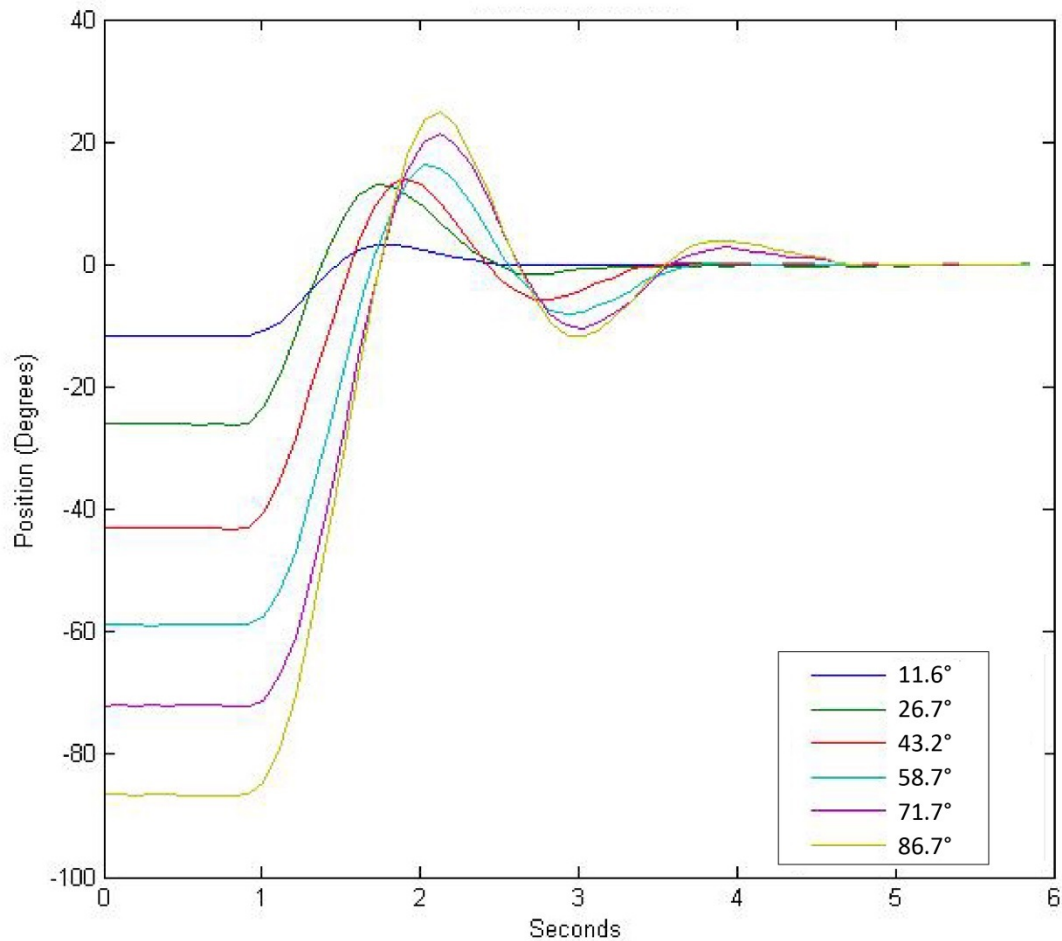
Figure 2.5: Timescale for the MPS to align with the wind flow when subjected to abrupt changes in wind direction. The Prandtl tube was locked at angles to the wind flow, then released at $t = 0$ s to test its response to rapidly changing wind directions. Even the most extreme wind test here—nearly 90°—displays the sensor's orientation returning to a small angle from the wind flow direction within 1.5 s of release of the sensor.

Fig. 2.5 shows the timescale for the MPS to adjust to changes in the flow direction as a function of flow speed. In the most extreme case studied here (the gold-colored line in Fig. 2.5), the MPS wind vane rotates 25° in 1 s. The wind vane operates like a damped oscillator; within 3 s of release, the Prandtl tube aligns with the flow direction even in flow speeds as slow as 5.0 m s$^{-1}$, a lower limit for the values expected in a dust devil. Our test at small angles with the flow shows a smaller overshoot than predicted in section 4. We hypothesize that this is caused mostly by friction within the bearings of the rotating base. Under the test conditions, the Prandtl tube changed direction with a maximum rate of 14° in a single measurement interval of 100 ms. Typical dust devils produce changes in wind direction at similar rates. For example, the case

30

analyzed by *Rennó et al.* [2010] shows average wind shifts of 1.4° in 100 ms with standard deviation of 5.7°. Statistically, 95% of values fall within two standard deviations of the mean value, therefore 95% of the 100 ms wind shifts in this strong dust devil are smaller than 11.4°. Our results indicate that the error caused by the misalignments expected during measurements in this dust devil, of which 95% are 11.4° or less, is not larger than 4%. Moreover, comparison of the flow direction measured with the sonic anemometer to that collected from the vane can be used to quantify misalignments between the Prandtl tube and the wind flow during field measurements, as shown with data from *Rennó et al.* [2010] in Fig. 2.6.
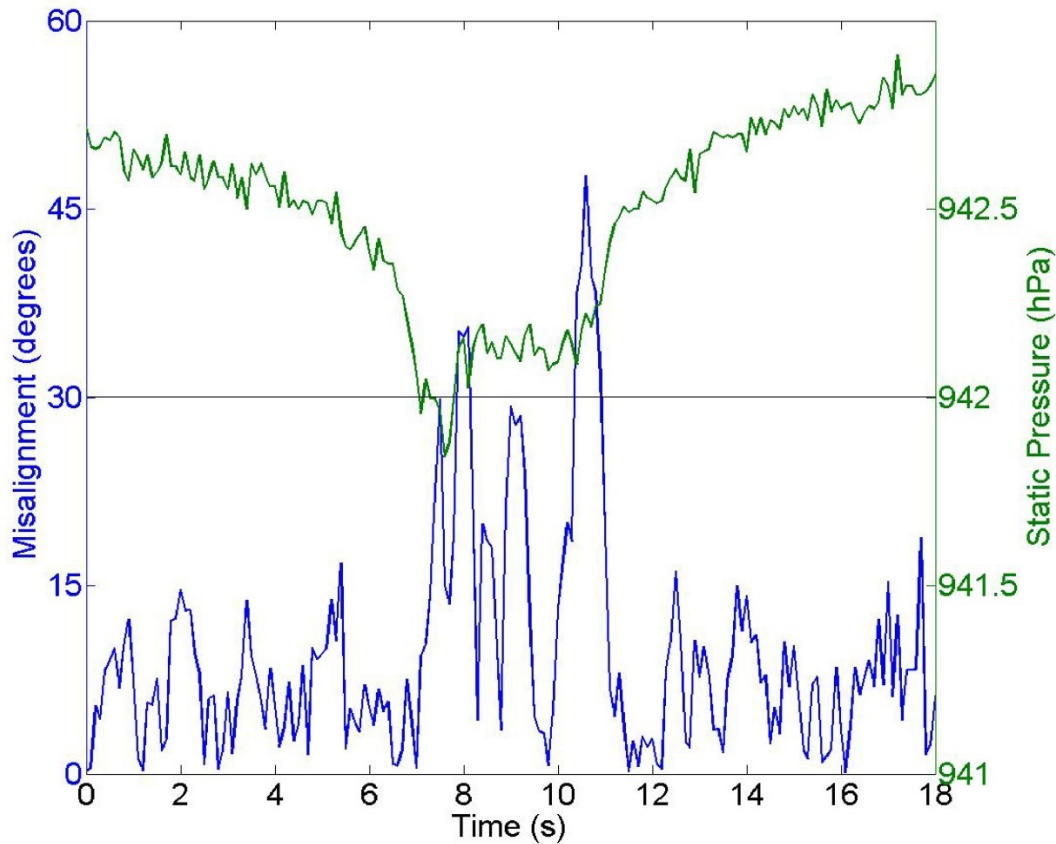


Figure 2.6: MPS alignment with wind direction during measurements in a dust devil. The differences in wind direction measured by the MPS vane and those measured by the 3D sonic anemometer show misalignment is rare, even during the passage of a dust devil over the sensors, as is shown here. The difference between directional measurements (blue) remains below 30° for all but the most extreme wind shifts in the dust devil. Static pressure readings (green) as the dust devil passes the sensor are shown as a reference.

## 2.7 CONCLUSION

The instrument described in this chapter makes high-frequency measurements of the 3D wind vector as well as static and total pressures in a wind of changing direction, such as those expected in dust devils. The difference between the static and total pressures measured by the MPS has an average error of less than 7.7% for flow speeds up to 35 m s$^{-1}$. The MPS is also able to maintain alignment between its pressure measuring system and the wind direction to within 30° for nearly all of the severe wind shifts expected in strong dust devils and within 12° for the majority of the dust devil wind measurements in general. This results in measurement errors caused by misalignment to be less than +4% in most cases. The fact that the error shown in Fig. 2.6 is always positive indicates that misalignments always produce an increase in the static pressure measurement. Therefore, the MPS is stand-alone system capable of making accurate measurements of static and total pressure as well as wind speed and direction in convective vortices.

# CHAPTER 3

# THE AEROSOLS-CLIMATE INTERACTION PROJECT

## 3.1 INTRODUCTION

The University of Michigan Aerosols-Climate Interaction (ACI) project was designed to study dust lifting by weather systems ranging in size from microscale to synoptic scale, in one of the largest sources of mineral dust aerosols in North America, the Owens Lake salty playa in California [*Groeneveld et al.,* 2010]. The ACI project has been conducting simultaneous measurements of the processes that force saltation and eject dust into the air, providing the data necessary for testing models of saltation and dust lifting. In addition, the ACI project has been measuring the changes in the flux of solar radiation at the surface and its correlation with dusty events. Change in the flux of solar radiation is an important quantity for understanding the impact of mineral dust aerosols on climate because the direct and indirect effects of aerosols are currently among the least understood of atmospheric constituents' effects on surface radiative forcing [*IPCC,* 2007]. This chapter describes initial results of the project, discusses the quality of the data, and proposes two hypotheses to explain the surprising result described below.

The unexpected result of our measurements at the Owens Lake salty playa is that the vertical fluxes of dust are higher when larger amounts of moisture are available to be absorbed by the soil. The fact that the dust flux is higher is surprising because previous theories for saltation predict increases in the threshold friction velocity with increases in soil moisture [e.g., *Fécan et al.,* 1999]. However, this unexpected dependence is consistent with qualitative observations in other salty playas reported in the literature [*Reynolds et al.,* 2007]. The detailed measurements of the ACI project provide motivation for two hypotheses capable of explaining the initial result.

We hypothesize that the observed increase in dust flux might be caused by the formation of dust particle aggregates that then become available for saltation, or alternatively by the formation of more readily erodible soil crusts, both by the absorption of moisture by salty

particles. These two hypotheses are consistent with previously published studies of dust lifting mechanics [*Castellanos,* 2005; *Reynolds et al.,* 2007].

### 3.1.1 The mechanics of dust lifting

Understanding the role of aerosols in climate necessitates understanding the sources of aerosols that mark the beginning of the dust cycle. The atmospheric portion of the dust cycle starts with the onset of saltation, the process by which soil particles are forced to move by the wind and skip along the surface, ejecting smaller, harder to lift, dust particles into the air [*Bagnold,* 1941]. The dust-size particles ejected into the air by saltation are then entrained by turbulent eddies and lifted into suspension [*Shao et al.,* 1993]. The amount of dust emitted by dust-ejecting weather events is a function of the capability of the events to force saltation and of the events' characteristic vertical wind velocities. Understanding how natural phenomena initiate saltation, eject dust into the air, and then lift this dust into the atmosphere is critical to the understanding and accurate modeling of the dust cycle.

The largest natural generators of suspended dust are the weather systems that initiate saltation and force dust lifting. The four dust lifting weather phenomena that the ACI project is designed to study are dust devils [*Rennó et al.*, 1998], non-rotating convective dust plumes [*Koch and Rennó,* 2005], thunderstorm gust fronts capable of producing saltation and lifting large quantities of dust particles (named haboobs) [*Chen and Fryrear,* 2002; *Williams*, 2008], and synoptic-scale, saltation-producing weather systems [*Kok et al.,* 2012]. The ACI project was designed to quantify the vertical dust flux and the intensity of saltation forced by these four types of weather phenomena while also measuring the friction velocity and the properties of the soil where saltation occurs.

### 3.2 THEORY AND HYPOTHESES

### 3.2.1 Aeolian saltation and dust lifting

A particle's size strongly influences its ability to enter saltation [*Shao and Lu,* 2000]. On Earth, the particles that enter saltation generally have diameters between 20 and 500 μm, but the size distribution is a function of the wind shear stress at the surface [*Owen*, 1964]. Soil particles of diameter $d$ in a wind profile that causes a friction velocity $u_*$ that exceeds the minimum value

necessary to cause them to saltate (the threshold shear velocity $u_{*_t}$) are lifted aerodynamically and then forced into a trajectory defined by their initial liftoff angle and velocity, the particle's geometry, and the surrounding environmental conditions. The smaller particles are not lifted directly by aerodynamic forces because they are subject to stronger interparticle forces relative to the particle size, while the larger particles are impeded from lifting by their large weight.

Bombardment is the primary natural process by which mineral dust-sized particles enter suspension in the atmosphere [*Gillette,* 1981; *Shao et al.,* 1993]. It is the process by which the momentum of saltating particles is transferred to surface particles where they impact, ejecting some of these surface particles from the soil bed. This process is also referred to as "splashing" [*Alfaro et al.,* 2004]. If the particles released by bombardment are small enough, they may enter into suspension as mineral aerosols.

3.2.1.1  Saltation modeling

Models of saltation have evolved to accommodate the complex environments in which saltation occurs. Earlier models of saltation usually assumed monodisperse soil particles [*Shao,* 2005], but recent models include heterogeneous particle size distributions [*Kok and Rennó,* 2009]. Saltation models usually assume steady state, where the wind profile above the surface remains constant over time except for changes due to momentum transfers between saltating particles and the air [*Kok and Rennó,* 2009]. Published models of saltation do not explicitly include wind profiles that are externally (i.e., wind changes that are not a result of the exchange of momentum with saltating particles) variable with time, a particular limitation that the ACI project must account for through statistical means when comparing results of field measurements with those of numerical simulations, as described in section 3.3.1.

The modeling of saltation begins with an estimation of the threshold shear velocity $u_{*_t}$, the minimum friction velocity strong enough to force soil particles to move. The value of $u_{*_t}$ depends on the physical characteristics of the soil bed, including particle size distribution, soil composition, and soil moisture content. The value of $u_{*_t}$ is estimated by *Shao and Lu* [2000] to be

$$u_{*t} = A_N \sqrt{\sigma_p g d + \frac{\gamma}{\rho d}} \qquad (3.1)$$

where $\sigma_p$ is the particle to air density ratio, $g$ is gravitational acceleration, $d$ is the particle diameter, $\rho$ is the air density, and $\gamma$ is a dimensional parameter representing the interparticle forces resisting initial particle motion.

Eq. (3.1) implies that $u_{*t}$ increases with increases in interparticle forces. Some types of interparticle forces are a function of soil chemical composition and particle size and therefore approximately constant in a given soil. Other types of interparticle forces vary on short timescales, primarily resulting from changes in soil moisture that cause attractive capillary forces between particles.

Increases in soil moisture content inhibit saltation by increasing the strength of capillary forces [*Marticorena and Bergametti,* 1995]. However, the capillary forces can also create dust aggregates, which can skew the soil particle distribution toward larger diameters when compared to that of dry soil [*Castellanos,* 2005]. In addition, in soils with large clay content, moisture can encourage surface crusts to form, severely inhibiting the onset of saltation [*Rajot et al.,* 2003]. *Fécan et al.* [1999] developed a parameterization of the increase in $u_{*t}$ with increases in soil moisture content by comparing the value of $u_{*t}$ of wet soil to that of dry soil:

$$\begin{aligned} \frac{u_{*tw}}{u_{*td}} &= 1 & w < w' \\ \frac{u_{*tw}}{u_{*td}} &= \left[1 + A(w - w')^{b'}\right]^{1/2} & w > w' \end{aligned} \qquad (3.2)$$

where $u_{*tw}$ and $u_{*td}$ are the threshold shear velocities of wet and of dry soil, respectively, $w$ is the volumetric soil moisture content, $A$ and $b'$ are empirically derived constants whose values are found to be 1.3 and 0.7, respectively, and $w'$ is a constant that depends on the soil type

$$w' = 0.0014(\%clay)^2 + 0.17(\%clay). \qquad (3.3)$$

This study uses the volumetric soil moisture content $w$ as a representative value for moisture content within the soil due to its frequent use in the literature on saltation. Although $w$ may indeed change without the addition of moisture due to changes in the soil particle density, changes in the soil particle density are assumed to be negligible. In environments with frequent soil packing, the mass soil moisture content may be more appropriate.

The relationship expressed in Eq. (3.3) implies that $u_{*_t}$ increases more strongly with moisture in sandy soil than in clayey soil. This is because in sandy soil, moisture almost exclusively results in capillary forces that strengthen interparticle forces, whereas in clayey soils water is adsorbed by clay and therefore larger amounts of water are required for capillary forces to be affected significantly.

The ACI project studies the dependence of saltation's strength on friction velocity and soil properties through direct measurements of saltating particle counts against a piezoelectric sensor, collection and analysis of saltating grains, and measurements of the soil properties and the wind profile that determine the threshold friction velocity and the actual friction velocity. Analysis of the data from these measurements and comparisons of the data with results of simulations with idealized saltation models are used to study the physical processes that drive saltation.

3.2.1.2   The COMSALT saltation model

The COMSALT model [*Kok and Rennó*, 2009] simulates saltation as a function of friction velocity and the soil particle size distribution, predicting the vertical and horizontal particle mass flux as a function of height within the saltation layer. COMSALT is a steady-state model applicable to soils of heterogeneous particle size distributions. It estimates the motion of saltating particles, the change to the near-surface $u_*$ caused by momentum transfer between the particles and the air, and the ejection of surface particles by "splashing." COMSALT accurately predicts several key properties of saltation, including the adjusted wind shear velocity and the vertical mass flux profiles of saltated material in steady state saltation [*Kok and Rennó*, 2009].

The ACI project utilizes COMSALT as a theoretical tool for determining the intensity of saltation and the size distribution of saltating particles. COMSALT's predictions are compared to the ACI project's unique data set. In the cases on which COMSALT does not predict the

measured saltation particle size distribution accurately, the surrounding environmental conditions are analyzed to investigate the physical reasons for the discrepancies. Inconsistencies between the results of the simulations and the ACI project data provide insights into how dust flux estimation and dust lifting models can be improved to more fully incorporate processes observed in places with atypical soil and weather conditions like the Owens "Dry" Lake.

### 3.2.1.3  Modeling dust lifting

In the presence of local turbulent eddies, dust particles ejected by splashing during saltation can be lifted well above the 'saltation layer', defined as the near surface atmospheric layer containing 50% of the saltating particles [e.g., *Kok and Rennó*, 2009]. The vertical dust flux is enhanced significantly when saltation is forced by weather phenomena with strong vertical wind components, such as dust devils, dusty plumes, and haboobs. The rate of dust ejection from saltation is a function of the kinetic energy of the saltating particles bombarding the surface, which depends on $u_*$, and the resistance of the dust to separation from the soil bed, which is quantified by $u_{*_t}$.

When saltation is forced by nearly horizontal wind flow, dust is ejected from the surface and lifted above the saltation layer with a flux that is strongly dependent on the friction velocity. This dust flux is expressed as

$$F_d = C_F \rho_a u_{*_t} \left( u_*^2 - u_{*_t}^2 \right)$$

(3.4)

where $F_d$ is the vertical dust flux, $\rho_a$ is the air density, and $C_F$ is a proportionality constant with units kg/J representing the fraction of energy of particles bombarding the surface available to overcome the interparticle forces holding the dust particles onto the surface [*Shao et al.,* 1993; *Kok et al.,* 2012]. Field measurements support the power law dependence of the vertical dust mass flux on friction velocity suggested by Eq. (3.4) [*Fratini et al.,* 2007]. Typical friction velocities range from 0.1 to 0.6 m/s, causing vertical dust fluxes ranging from $10^{-5}$ to 10 mg/m$^2$s that are dependent on the soil properties [*Fratini et al.,* 2007; *Sow et al.,* 2009]. The vertical dust flux increases significantly when saltation is forced by convective weather phenomena like dust devils, dusty plumes, and haboobs.

The vertical dust flux can be orders of magnitude larger in dust devils and dusty plumes than in saltation driven solely by horizontal winds. Dust fluxes as large as 2 g/m$^2$s have been measured in large dust devils [*Gillette and Sinclair,* 1990]. *Koch and Rennó* [2005] estimate dust fluxes of around 0.7 g/m$^2$s in typical dust devils and around 0.1 g/m$^2$s in non-rotating dusty plumes. The proximity of the area of strong saltation to the area of strong vertical velocity allows these dust devils and dusty plumes to lift dust deep into the convective boundary layer where it can increase ambient dust concentrations long after the passage of the dusty event. In arid regions, even in the absence of strong winds, the background dust concentrations are generally around 10 μg/m$^3$ [*Ito et al.,* 2010], while in areas of frequent dust devils and dusty plumes dust concentrations can be as large as ~100 μg/m$^3$ [*Metzger,* 1999].

Haboobs are significant sources of suspended dust [*Marsham et al.,* 2011; *Roberts and Knippertz,* 2012]. In addition to producing strong friction velocities over large areas, these convection-driven dusty gust fronts have strong vertical velocities capable of lifting dust deep into the convective layer. The total dust emission from a single haboob has been estimated to be of the order of 1×10$^9$ kg [e.g., *Bou Karam et al.,* 2010]. Near surface particle concentrations exceeding 1 g/m$^3$ have been measured in a haboob [*Chen and Fryrear*, 2002]. It is conceivable, though, that the dust emission by haboobs is tempered somewhat by wet deposition in the parent thunderstorm.

Measurements of dust flux as a function of the strength of saltation support the ACI project's goal of studying the mechanisms that lift dust from the surface. Vertical dust flux caused by convective activity is studied separately from the dust flux caused by nearly horizontal winds. This approach is motivated by the fact that the discrete nature of convective phenomena and their strong vertical velocities produce dust fluxes that are much larger than those produced by the turbulent eddies in the nearly horizontal winds. This approach also allows the analysis of individual convective events and their effect on the surface radiation budget.

### 3.2.2 Aerosol-radiation feedbacks

Mineral aerosols are important to earth science because of their large effects on climate. Aerosols affect climate directly by scattering and absorbing solar radiation [*Haywood and Boucher,* 2000] and indirectly by increasing the albedo and lifespan of clouds [*Twomey,* 1977; *Albrecht,* 1989; *Lohmann and Feichter*, 2005]. Studies of aerosols are pertinent to

anthropogenic climate impacts because human activity accounts for up to 50% of atmospheric dust concentrations [*Tegen and Fung*, 1995]. Our understanding of the relationship between mineral aerosols and climate has been improving steadily, but radiative forcing by mineral dust aerosols is still one of the most uncertain processes in current climate models [*IPCC,* 2007].

Mineral aerosols' scattering and absorbing of incoming solar radiation increases the local optical depth of the atmosphere. The contribution of aerosols to the total atmospheric optical depth is referred to as the Aerosol Optical Depth (AOD) and is the primary quantity used to characterize the impact of aerosols on radiative forcing [*Holben et al.,* 2001]. Globally, aerosols are estimated to reduce the solar radiation flux incident at the surface by -0.12 to -0.25 W/m$^2$ [*Tegen et al.,* 1996; *Hansen et al.,* 1998]. On a local scale, the reduction in radiative flux can be much larger than the global mean value. For instance, *Gu et al.* [2006] estimate a radiative flux perturbation of -51 W/m$^2$ for mineral aerosols of size 2.0 μm and producing an AOD of 0.2 in aerosol studies in southern China.

The short-term change in AOD can be estimated by comparing surface-based solar radiative flux measurements to top-of-atmosphere (TOA) flux using Beer's law,

$$\tau = -\cos(\theta)\ln\left[\frac{I}{I_{TOA}}\right] \tag{3.5}$$

where $\theta$ is the solar zenith angle, $I$ is the measured surface irradiance, and $I_{TOA}$ is the calculated TOA irradiance. Over a few hours, the perturbation in total optical depth is assumed to be due only to perturbations in suspended aerosols when meteorological conditions remain the same and cloud cover is negligible. This is a common assumption because other contributors to the atmosphere's optical thickness vary on timescales larger than a few hours [*Smirnov et al.,* 2002]. Although this method does not provide absolute AOD values, it does provide reliable values for the change in the AOD over short time-scales. This change in the AOD, together with the measured change in aerosol concentration, sheds light on the capability of local suspended dust to alter the surface radiation budget.

Measurements of changes in AOD with changes in local aerosol concentration contribute to the ACI project's study of effects of suspended dust on climate by unveiling how effective locally lifted dust particles are at scattering and absorbing solar radiation.

## 3.3 METHODS AND INSTRUMENTATION

### 3.3.1 ACI field site and instrument arrangement

The ACI project's field site is located near Keeler, California in the dry bed of Owens Lake, a salty playa which contains a surface layer of dry, loose, salty [*Titus et al.,* 2002] soil that is prone to saltation and erosion by the wind (Figure 3.1). Government-sponsored dust remediation efforts have been intermittent at Owens Lake [*Groeneveld et al.,* 2010], and much of the area is still a large source of mineral aerosols. The prevailing wind direction at the project field site is from about 330°, parallel to the direction of the Owens River valley, and a direction that provides a homogeneous, flat terrain fetch for more than 1500 m. In addition to its unique suitability for the science goals of the ACI study due to the high frequency of saltation events and a variety of dusty weather phenomena, Owens Lake is a location where instruments can be emplaced for extended periods of time without interruption and within range of wireless telecommunications services, providing a convenient mode for remote data collection.
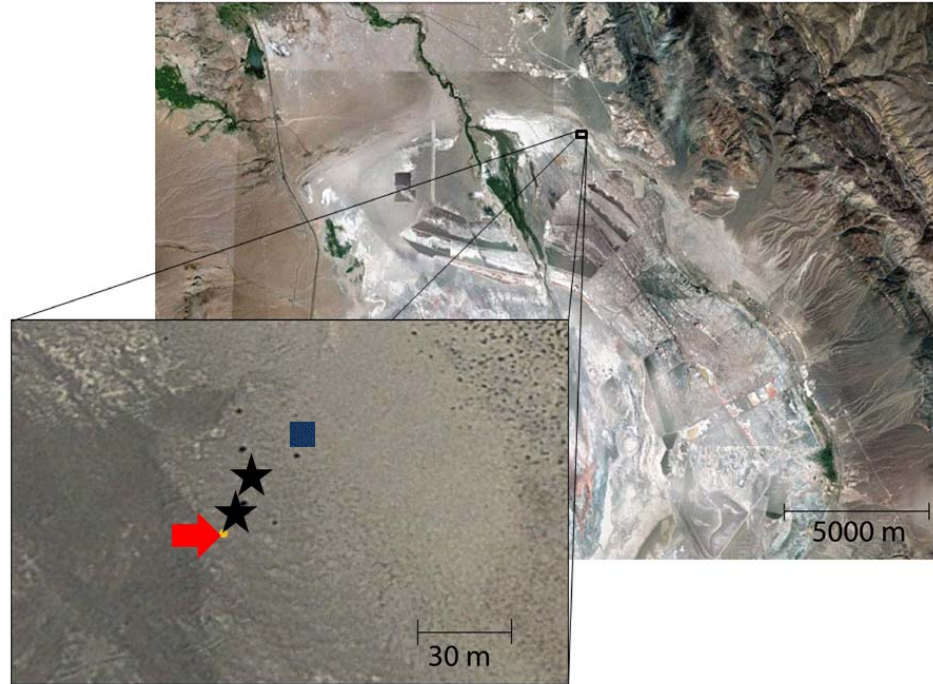
Figure 3.1: The ACI project site is located in the northeast portion of Owens Lake. The locations of the instrument towers (stars), solar power system (square) and dust collection traps (circle, with arrow indicating location) are indicated.

The ACI instruments, detailed in Appendix A, are arranged on two towers located 15 m apart as shown in Figure 3.2. Tower 1 is a 3 m steel Rohn tower and tower 2 is a 2 m Campbell Scientific tripod tower. Each tower is grounded via cable and copper rods and supports a unique suite of instrumentation as listed in Table 3.1.

Figure 3.2: View of the ACI project site at Owens Lake, facing east. The system includes, from left, the solar power system, tower 2, electronics box, tower 1, and the BSNE collection array.

Table 3.1: Instrumentation of the ACI Project. Instrumentation details are in *Appendix A*.

| Platform | Instrument | Manufacturer | Model Number | Height |
|---|---|---|---|---|
| Tower 1 | 4x 3-cup anemometer | Campbell-Scientific | 03101-L | 13cm, 65cm, 104cm, 142cm |
| | Saltation Sensor | Sensit | H11-LIN | 6.4cm-7.6cm |
| | Sonic Anemometer | Campbell-Scientific | CSAT3 | 300cm |
| | PM2.5 Aerosol Sensor | Met-One | E-Sampler | 290cm |
| | Prandtl Tube Sensor | Michigan Prandtl System | n/a | 350cm |
| | Barometric Pressure | Campbell-Scientific | CS106 | 200cm |
| | Air Temperature | Campbell-Scientific | CS215 | 200cm |
| | Relative Humidity | Campbell-Scientific | CS215 | 200cm |
| Tower 2 | Solar & Terrestrial Radiation | Campbell-Scientific | CNR4 | 150cm |
| | Air Temperature | Campbell-Scientific | CS107 | 150cm |
| Surface | Soil Moisture | Campbell-Scientific | CS616 | -5cm |
| | Soil Temperature | Campbell-Scientific | CS105-E | -5cm |
| | Saltation Sampler | Big Springs Number Eight (BSNE) | n/a | * |

Tower 1 supports most of the meteorological instruments in addition to the instruments used for measurements of saltation. Four 3-cup anemometers are mounted vertically, aligned with each other. These anemometers are mounted on arms extending westward from the west edge of the tower in order to record wind speeds without interference from the tower. A Campbell

43

Scientific 3D Sonic Anemometer (3DSA) is vertically aligned with the 3-cup anemometers and mounted near the top of the tower. A MetOne E-Sampler co-located with the 3DSA is used for measuring $PM_{2.5}$ concentrations. A Michigan Prandtl System (MPS) Prandtl tube mast as described in Chapter 2 is mounted on tower 1 to measure the static and stagnation pressures. The MPS was designed to make accurate pressure measurements in convective vortices.

Tower 2 supports instruments for radiometric measurements. A horizontal arm is mounted to tower 2 and a CNR4 net radiometer is mounted on the end of this arm. Also mounted on tower 2 is a temperature sensor to provide an accurate baseline temperature for the radiometric measurements.

Detailed measurements of soil properties are made with instrumentation on or just below the surface. Soil moisture and temperature measurements are made with sensors placed 5 m southeast of tower 1. Horizontally aligned soil moisture and soil temperature sensors are buried 5 cm below the soil surface and placed 15 cm from each other. A series of Big Springs Number Eight (BSNE) sand collectors are mounted 10 m west of tower 1 on two separate posts, separated by ~1 m (enough room to allow the collectors to rotate freely). The posts are aligned so that a wind from the prevailing direction (~330°) will allow the collectors on each post to function without interference from the neighboring post.

Data is recorded by a Campbell Scientific CS3000 datalogger, processed with a custom-designed computer, and transmitted to the University of Michigan in real time via cellphone modem. These three components are all located within an electronics box placed about 10 m from both towers. The ACI instrument suite is powered by solar energy with the power system placed 25 m east of the electronics box. The solar system is capable of providing 45 W of power continuously under average sky conditions.

### 3.3.2   Saltation mass flux

Data collected by the ACI project is used to model the strength of saltation, gauged by the mass flux of saltating particles that in turn is a function of the $u_*$ acting on the soil bed. The ACI project determines $u_*$ from wind speed measurements taken at various heights above the surface. The values of $u_*$, along with the local soil's particle size distribution, are the input for the modeling of saltation with COMSALT. The particle size distribution from simulations of

saltation mass flux with COMSALT is compared with direct measurements from the ACI project's BSNE collectors, and differences are investigated to determine what physical characteristics of saltation at Owens Lake are not well represented by the model.

The ACI project determines $u_*$ as a function of the change of wind speeds with height. Variations of wind speed with height are modeled by the "law of the wall," a relationship between the wind profile, friction velocity, and roughness length

$$u(z) = \frac{u_*}{\kappa} \ln\left(\frac{z}{z_0}\right)$$

(3.6)

where $u(z)$ is the horizontal wind speed at height $z$, $z_0$ is the roughness length, and $\kappa$ is the von Kármán constant, approximately equal to 0.4. Eq. (3.6) assumes a neutrally-stable atmospheric surface layer, an assumption we feel is reasonable for the high-wind conditions within which we calculate friction velocity. Using a least-squares linear regression technique, the friction velocity is calculated by

$$u_* = m\kappa$$

(3.7)

where $m$ is the slope resulting from the linear regression between $u(z)$ and $\ln(z)$. This technique has already been used successfully to study sand transport at Owens Lake [*Lancaster and Baas, 1998; Ono, 2006*].

As explained below, assumptions required when applying the least-squares linear regression must be made carefully to minimize uncertainties in the results. In calculating $u_*$ from the wind profile using the least-squares linear regression method we assume that the shear stress within the boundary layer and surface layer is constant with height, an assumption generally valid in places like the Owens Lake with a flat and homogeneous surface [e.g., *Kok et al.,* 2012]. The value of the linear regression coefficient $r^2$ used in the calculation of $u_*$ quantifies the validity of this assumption. Indeed, the value of this coefficient of correlation, between the ($u_*$, $\ln(z)$) data pairs and the calculated linear regression, ranges between 0 (indicating total lack of correlation) and 1 (indicating a "perfect" fit of experimental data to the

45

calculated regression values).  To control the quality of the data, only friction velocities obtained with $r^2 \geq 0.98$ are used in this study; lower $r^2$ values would provide values with uncertainties greater than 10% in all cases [*Sherman and Farrell*, 2008].  Unacceptably low $r^2$ values are often the result of near-surface measurements taken within the saltation layer where the wind speed is altered by the exchange of momentum between the air and the saltating particles.  When this is the case, we do not use the value of the wind speed measured within the saltation layer in the linear regression.  In this case, $u_*$ is calculated using only the values of the wind speed from measurements above the saltation layer.

The ACI project measures total horizontal saltation mass flux with nine BSNE sand collectors [*Fryrear*, 1986; *Appendix A*] designed to collect saltating particles.  The BSNE sand trap openings are opened and closed manually in order to control the beginning and end of each sand collection period.  Sand collection periods are chosen to provide maximum mass flux measurements for a variety of collection periods by opening the BSNE traps only once vigorous saltation has initiated and closing them immediately, should saltation cease.  Saltation conditions during the manned portion of ACI observations provided two short-term (< 30 minutes) collection periods, two one-hour collection periods, and one long-term (> six hours) collection period.

Sand collected from the BSNE collectors is analyzed using mechanical sieves with various mesh sizes and separated into bins with mean diameters of 78.5, 114.5, 138.5, 201.5, 336.5, 461.5, 549.5, 654.5, and 781.5 μm, with a final sieve collecting particles >853 μm.  These bins are referred to in this chapter as bins 1 through 10, respectively.  Each BSNE collection represents saltation mass flux at the height of the BSNE collector and is sifted into separate particle size bins and weighed.  From these measurements of bulk sediment mass, we compile both particle size density distributions and total horizontal mass flux as a function of height.  The latter is calculated by

$$F_{salt}(z_n) = \frac{m(z_n)}{\Delta t \cdot A_n} \tag{3.8}$$

where $F_{salt}(z_n)$ is the mass flux of saltated particles at height $z$ corresponding to BSNE trap $n$, $m(z_n)$ is the total mass collected in BSNE trap $n$, $\Delta t$ is the period of time of mass collection, and $A_n$ is the cross-sectional area of the BSNE aperture.

The particle size distribution calculated with the measured masses of saltated particles is then compared to COMSALT's predictions. COMSALT is a steady-state model and accepts a single friction velocity value as input. As $u_*$ is not constant for significant periods of time, we use a discrete, 20-value probability distribution function of input $u_*$ values to force COMSALT. When COMSALT is forced with each of these 20 $u_*$ inputs, the resulting COMSALT outputs are each weighed according to the frequency of each $u_*$ value. This method produces COMSALT-modeled particle size distributions and horizontal mass fluxes as a function of height that accurately reflects the variations in $u_*$ observed during the sampling period.

### 3.3.3   Vertical dust flux in the absence of convective plumes and vortices

We use the eddy covariance technique to calculate vertical dust flux in wind regimes characterized by moderate to strong turbulence with small mean vertical velocity. This technique was successfully used in prior studies of vertical dust fluxes [*Koch and Rennó*, 2005; *Fratini et al.*, 2007]. In general, the eddy covariance technique requires accurate, high-frequency measurements of both vertical wind velocity and the concentration of the atmospheric constituent of interest. Although appropriate use of the eddy covariance technique requires that the multiple conditions described below be satisfied, it is one of the most reliable methods for calculating fluxes when those conditions are met.

First, the terrain surrounding the measurement system must be generally flat and homogeneous. *Wieringa* [1993] describes minimum fetch lengths upwind of the collection site necessary to eliminate boundary effects caused by terrain features. For the measurement height of 3 m used in this study, the upwind fetch length must be at least 500 m. The ACI location at Owens Lake has a fetch in its predominant wind direction (~330°) of 1,500 m where the terrain is flat and the surface is generally uniform.

Second, most of the vertical flux must be a result of turbulent eddies and not from topographic forcing or strong, discrete convective events like convective plumes. To avoid topographic effects, we consider dust events that occur only when the primary wind direction is

parallel to the direction of the valley where the fetch terrain is flat. The ACI project verifies a horizontal wind by calculating the 15-minute average vertical wind speed ($\overline{w}_{15}$). When $\overline{w}_{15} \approx 0$, vertical flux is assumed to be due to turbulent eddies alone.

Finally, the vertical dust flux from gravitational setting must be negligible when compared to other processes such as turbulent transport. The ACI study measures particles with a cut cyclone of 2.5 μm, significantly below the threshold of 7 μm above which gravitational settling becomes important [*Fratini et al.*, 2007].

In the ACI project, the dust flux is calculated with the eddy covariance method only when the three conditions listed above are met. When the eddy covariance method is applied to suspended dust concentrations, the vertical dust flux $F_d$ is

$$F_d = \overline{\left( \rho_d' w' \right)} \tag{3.9}$$

where $\rho_d'$ and $w'$ are the perturbations of dust concentration and vertical velocity about their mean values, respectively.

Eq. (3.9) shows that the product of the dust concentration perturbation with the vertical velocity perturbation is then averaged over a time period long enough to cover the significant turbulent eddy length scales. The ACI project uses a 15 minute running average of the 1 Hz measurement because a period this long is optimum for calculating the fluxes resulting from the turbulent eddies over flat terrains and wind strong enough to initiate saltation [*Aubinet et al.*, 2012].

The ACI project measures the aerosol concentration used in the eddy covariance calculation with a MetOne E-Sampler equipped with a $PM_{2.5}$ cut cyclone. This system measures the concentration of suspended aerosols of 2.5 μm of diameter and smaller. Larger particles would not stay airborne long enough to affect climate significantly. This limitation to particles of diameters smaller than 2.5 μm must be considered, though, when dusty phenomena capable of ejecting larger dust particles deep into the boundary layer are studied.

### 3.3.4 Vertical dust flux enhanced by convective plumes and vortices

Vertical dust flux in the presence of wind with large vertical velocity components as expected in dust devils, dusty plumes, and haboobs is calculated as the product of dust concentration within the phenomena and the magnitude of the vertical velocity on them,

$$F_{d,p} = \rho_d w \qquad (3.10)$$

where $F_{d,p}$ is the dust flux and $w$ is the vertical velocity in the convective plumes. The dust flux in convective phenomena is measured with the MetOne E-Sampler and the sonic anemometer described in Section 3.3. This bulk-flux technique has been used successfully in measurements under similar environmental conditions [*Rennó et al.,* 2004; *Koch and Rennó,* 2005].

The ACI project measures the wind speed and aerosol concentration in convective phenomena only when they pass over the ACI towers. Dust devils and dusty plumes are not expected to pass over the instruments frequently, but even occasional convective dust activity is studied carefully as the ACI project measures dust concentration and wind speed continuously.

### 3.3.5 Determination of Aerosol Optical Depth

The data collected by the ACI project supports studies of the link between perturbations in aerosol concentration and changes to the AOD in order to achieve the more general goal of studying changes to the surface flux of solar radiation caused by changes in concentrations of suspended dust. As discussed in section 3.2, the AOD connects mineral aerosols to their impact on climate. In order to evaluate aerosols' impact on the optical depth during the ACI project, only short-term variations in optical depth are considered.

Variations in AOD are calculated using Eq. (3.5) with short-term (< 1 day) variations in optical depth. AOD calculations assume optical thickness changes above the tropopause are negligible, including variations in the AOD caused by changes in concentrations of atmospheric chemicals like $O_3$ and $NO_2$. This procedure was motivated by a previous study of the variations of AOD at Owens Lake indicating that changes in optical depth above the stratosphere are negligible when compared to that below it [*Niemeyer et al.,* 1999].

In the absence of cloud cover, optical depth variations below the tropopause are assumed to be entirely due to changes in dust concentration. The existence of clouds is identified by changes in the values of solar shortwave radiation that could only be the result of direct blocking of the sun. Only data from days identified as being cloudless are used in the optical depth analysis. We also check visually the data for cloud cover using the three wide-field-of-view cameras mounted on tower 1. This visual check serves to determine the presence of high-level cirrus clouds, which would not cause large changes in the solar shortwave radiation. In the absence of cloud cover, short-term changes in the AOD provide an accurate measure of the effect of suspended dust particles on the radiation budget. Surface irradiance measured with a CNR4 Net Radiometer is used to calculate the AOD using Eq. (3.5). Surface irradiance measurements are compared to TOA irradiance, which is calculated using a solar constant of 1361 W/m$^2$. Measurements of aerosol concentration with the E-sampler are used to identify the initiation of dust-lifting events and to quantify the change in the suspended PM$_{2.5}$ dust concentration before and after each event.

## 3.4 INITIAL RESULTS

### 3.4.1 Measurement periods

Data from the five measurement periods listed in Table 3.2 are analyzed in this chapter and represent the initial results of the ACI project. Each measurement period is characterized by intervals of vigorous saltation lasting more than 30 minutes, determined by particle impacts against the Sensit sensor. This minimum 30 minute time scale is necessary to provide an adequate averaging interval with meaningful shear velocity and vertical dust flux values, critical components of our data analysis. On average, friction velocities from most measurement periods are similar to each other and are consistent with those observed in previous studies at the Owens Lake [*Lancaster and Baas,* 1998]. Period 1 occurred when an observer was present at the ACI project site, while periods 2, 3, 4, and 5 contain only autonomously recorded data. The latter four measurement periods occurred during wind events driven by synoptic scale activity characterized by northerly winds over the Owens Valley, while measurements during period 1 were made with a nearby large dusty plume and represent saltation and dust ejection forced by

that plume's surface inflow.  The initial data set analyzed in this chapter does not include data from direct measurements in dust devils, dusty plumes, and haboobs.

Table 3.2: Dusty events analyzed in this study.

| Period | Date | Time (PDT) | Duration | $\bar{u}_*$ [m/s] | Peak $u_*$ [m/s] | Total $F_d$ [mg/m$^2$] |
|--------|------|-----------|----------|-------------------|------------------|------------------------|
| 1 | 18 Dec 2012 | 14:04-18:04 | 4h 0 min | 0.24 | 0.31±0.01 | n/a |
| 2 | 29 Jan 2013 | 11:53-17:27 | 5h 34 min | 0.25 | 0.40±0.01 | 172±63 |
| 3 | 20 Feb 2013 | 07:20-16:21 | 9h 01 min | 0.26 | 0.34±0.01 | 309±25 |
| 4 | 09 Mar 2013 | 09:34-14:08 | 4h 34 min | 0.23 | 0.34±0.01 | 46.2±18 |
| 5 | 08 Apr 2013 | 10:45-17:28 | 6h 43 min | 0.38 | 0.47±0.01 | 201±68 |

*Period 1:* Measurement period 1 began with light (< 4 m/s) winds of variable direction, but northerly winds prevailed by 07:00.  Around 10:00 a cold front boundary passed over Owens Lake, bringing strong northerly winds with peak wind speed of about 18 m/s in mid-afternoon as recorded by the 3DSA.  During period 1, conditions were favorable for formation of convective plumes over Owens Lake, with two dust devils developing near its south end and a non-rotating dusty plume forming near its center.  None of the dust devils passed over the ACI project instruments, but the large dusty plume passed close enough to produce vertical wind speeds large enough to invalidate the use of the eddy covariance technique in the determination of the dust flux.

*Period 2:* Measurement period 2 was characterized by light wind at the ACI instrument site until shortly after 10:00, when the wind speed increased quickly as the large-scale wind direction shifted to northerly and in-line with Owens Valley.  Peak wind speeds, dust concentrations, and saltation impact counts were measured shortly before noon.  Relative humidity measurements during period 2 indicate a mean value of 24±0.04% with respect to the air and 23±0.5% with respect to the soil temperature. This is the highest soil relative humidity value of all measurement periods.

*Period 3*: Measurements from period 3 are shown in Figure 3.3 and display wind, saltation, and dust flux trends typical of dusty days with vigorous saltation at Owens Lake. Weak westerly winds shifted to northerly later in the previous day, and intensified throughout the early morning hours.  The peak wind gust during this period was 21.1 m/s in at 09:44.  Ambient PM2.5 measurements after the saltation event shows an increase in baseline dust concentration of more than 100%, demonstrating the persistent local impact these events have on local radiative

forcing. The relative humidity was elevated during period 3 compared to the two subsequent measurement periods. The average relative humidity value of the air was 26±0.04%, and the average value with respect to the soil temperature was 22±0.3%. This elevated humidity was possibly because period 3 was earlier in the morning than the other measurement periods.
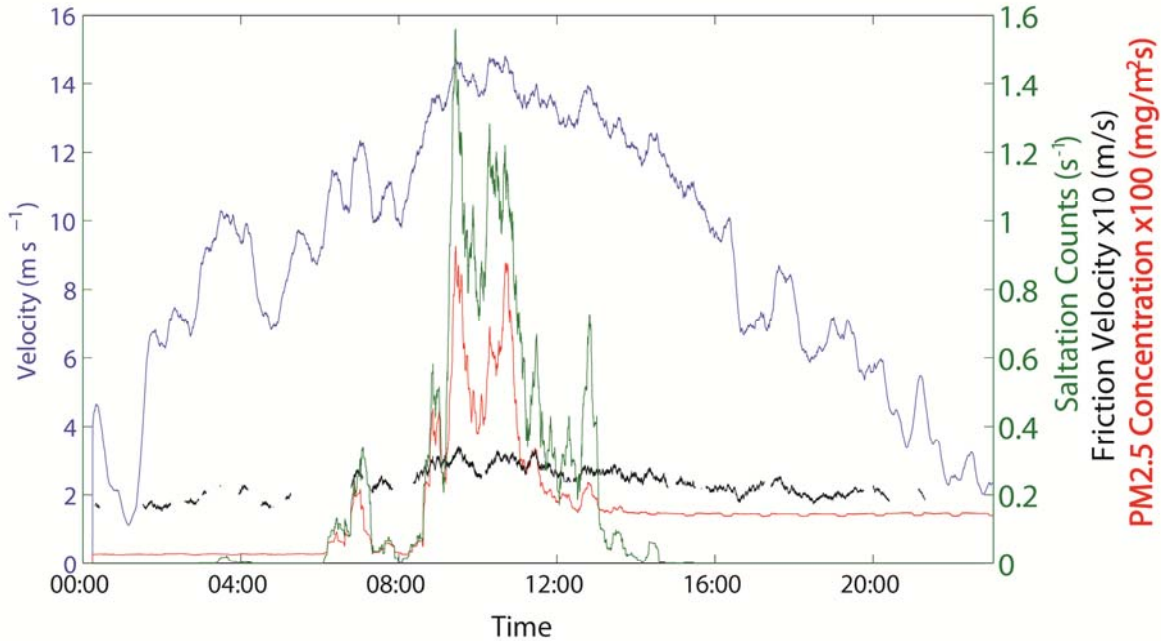


Figure 3.3: Strong saltation during period 3. The peak in wind speed averaged over 15 minutes (blue) seen shortly after 09:00 PST is accompanied by a coincident peak in 15-minute averaged $PM_{2.5}$ concentration (red), saltation strength (green) as measured by the Sensit sensor, and friction velocity (black).

*Period 4:* Saltation initiated intermittently during measurement period 4 from 08:34 until around 10:00, then intensified and quickly reached peak intensity at 10:23. Saltation activity then abated slowly and eventually subsided completely by 13:08. Measurements show that during period 4, saltation was driven by a slowly increasing horizontal wind speed throughout the early morning that averaged around 8 m/s at 04:00 then increased to greater than 10 m/s around 06:30.

*Period 5:* Data collected during measurement period 5 includes the most vigorous case of saltation studied, as indicated by the frequency of particle counts by the Sensit sensor. The mean $u_*$ during period 5 was larger than during any other measurement period with $\overline{u_*} = 0.38$ m/s. Peak 15-minute-averaged $u_*$ during this period is also the largest from any measurement period reaching $u_{*max} = 0.47$ m/s. Despite these elevated $u_*$ values, the mean $PM_{2.5}$ concentration

during this period was only 1.2 mg/m$^3$, not the highest value of all measurement periods. This indicates that there may have been an impediment to dust ejection during period 5. The mean relative humidity relative with respect to the soil temperature was 11±0.2% during this period, the lowest value of all measurement periods.

All five measurement periods include vigorous saltation and thus provide valuable data for analysis of the saltation and dust ejection. Only measurement periods 1 and 2 were cloud-free and thus provided reliable radiation flux data for comparison with measurements of aerosol concentrations. As described below, measurement period 1 is the only one that includes manually-collected samples of saltating particles for comparison with results of simulations with COMSALT.

### 3.4.2 Saltation measurements

3.4.2.1 Particle size distributions

During measurement period 1, the BSNE sand collectors provided saltation mass flux data that is compared to COMSALT's prediction of the size distributions of saltating particles. Five saltation mass flux samples (labeled A through E) were collected using the BSNE array during period 1, and the time periods of sample collection are detailed in Table 3.3. Samples A and B were taken early in period 1 before continuous saltation started, and the BSNE collectors were opened for two short time intervals to collect these samples (14 minutes for sample A and 17 minutes for sample B, as each sample was "closed" when saltation abated). Samples C and D were collected during the peak of the period 1 saltation event as evidenced by the Sensit particle counts, $\bar{u}_*$ values, and mean PM$_{2.5}$. Samples C and D each represent a 60-minute period of saltation mass flux collection, the target collection length for the study. Sample E was collected overnight, but although the BSNE collectors were open for more than 16 hours, the Sensit measurements indicate saltation was active for only the first one hour of this collection period. Thus, for the purposes of comparison with saltation particle size distribution resulting from simulations with COMSALT, sample E is assumed to have been collected only when saltation was vigorous.

Table 3.3: Saltation Collection periods analyzed in this study.

| Sample | Date | Time (PDT) | Duration [min] | $\bar{u}_*$ [m/s] | $\sigma_{u_*}$ [m/s] | $F_{salt}(z=5cm)$ [g/m²s] | $\bar{\rho}_d$ [mg/m³] |
|---|---|---|---|---|---|---|---|
| A | 18 Dec 2012 | 13:18-13:32 | 14 | 0.43±0.001 | 0.13 | 3.28±.003 | 0.195±0.0005 |
| B | 18 Dec 2012 | 13:53-14:10 | 17 | 0.39±0.001 | 0.12 | 2.89±.002 | 0.221±0.0005 |
| C | 18 Dec 2012 | 14:29-15:29 | 60 | 0.52±0.001 | 0.09 | 27.13±0.01 | 0.283±0.0004 |
| D | 18 Dec 2012 | 15:48-16:48 | 60 | 0.54±0.001 | 0.10 | 36.41±0.02 | 0.272±0.0004 |
| E | 18-19 Dec 2012 | 17:10-09:20 | 970 | 0.33±0.001 | 0.10 | 3.10±0.002 | 0.173±0.0001 |

Figure 3.4 compares the particle size distribution collected with the BSNE collectors to that predicted by COMSALT and that of the parent soil at the ACI location. The size distributions of the saltating particles predicted by COMSALT and those collected by the BSNE collectors are similar to the particle size distribution of the soil itself (up to an upper size limit) in all five sampling periods. Neither direct mass collection via BSNE collectors, nor prediction by COMSALT indicates significant saltation of particles with diameters larger than 600 μm. This occurs despite the existence of larger particles in the soil because the $u_*$ required to lift these large particles rarely occurs during the collection periods. Despite the overall similarity in the size distributions of modeled and measured saltation particles, important differences occur.
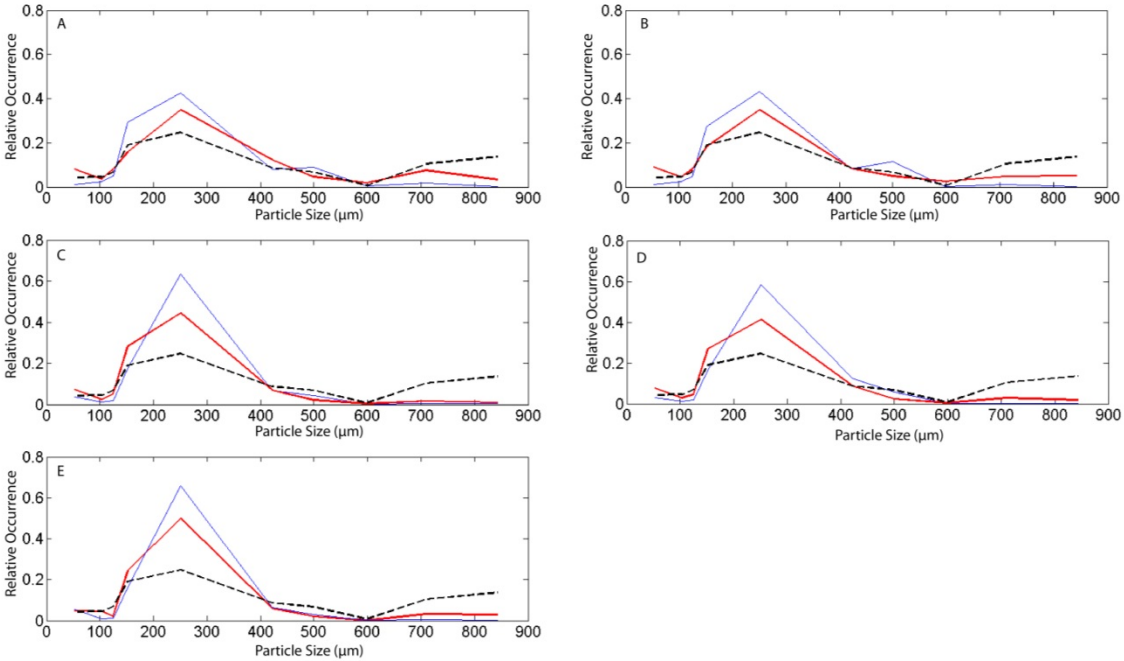
Figure 3.4: Particle size distributions from five collection periods, A through E, as measured by BSNE traps (red) and predicted by COMSALT (blue). The soil particle size distribution is shown for comparison (black). Periods A and B, during which saltation was intermittent, show an underestimation of smaller particles by COMSALT compared to field measurements, whereas periods C and D, when saltation was continuous and vigorous, show the opposite, possibly due to dust particle aggregates breaking apart when impacting the BSNE collectors, introducing a bias toward smaller particles.

For the measurement periods in which samples A and B were collected, COMSALT overestimates the proportion of particles smaller than 150-300 μm as indicated in Figure 3.4. For this same period, COMSALT also overestimates the proportion of particles with diameters of about 500 μm. We hypothesize that the overestimation of the smaller particles is due to the intermittent nature of saltation during these two shorter measurement periods. We postulate that in general the saltation mass flux is overestimated by simulations of steady state saltation with COMSALT when saltation is intermittent. During collection periods A and B, friction velocities present a broader distribution, with standard deviations of 0.13 and 0.12 m/s, respectively, indicating larger variability than during other observation periods.

The time intervals on which samples C and D were collected display a different behavior to that of the previous two periods. During these intervals, COMSALT underestimates the proportion of particles with diameter of about 125 μm. Because of the normalized nature of the analysis, COMSALT's prediction of the particle size distribution has a larger peak for particles

of diameters of about 250 μm than observed in the BSNE collectors, as indicated in Figure 3.4. This deviation between modeled and measured particle size distribution at particles with diameter of about 125 μm may be the result of a physical mechanism not accounted for by COMSALT.

The most significant discrepancy between the size distributions of saltating particles predicted by COMSALT and those measured by the ACI project's BSNE collectors is that a larger amount of particles with diameter of about 125 μm are observed in the BSNE collectors than predicted. It is interesting that this discrepancy is not observed during the periods characterized by intermittent saltation. The discrepancy between COMSALT's predictions and the measurements can be explained by the presence of significant amounts of dust aggregates at the field site. If a large enough fraction of the saltating particles are aggregates, the bias toward the smaller particles with diameter of 125 μm in the BSNE collectors could be the result of the breaking of aggregates when impacting into the collectors. Particle aggregates with diameters larger than 125 μm would be less likely to saltate during periods of smaller $u_*$ [*Kok et al.,* 2012], as observed when samples A and B were collected. This results is consistent with the hypothesis that particle aggregation may be a common process in this Owens Lake salty playa.


3.4.2.2   Saltation in different wind regimes

Preliminary results show excellent agreement between the values of $u_*$ and the intensity of saltation quantified by counts of particle impacts against the Sensit saltation sensor. The most intense saltation periods coincide with the largest friction velocities, and this is most clearly seen in the data collected during period 5 (Figure 3.5). This is consistent with established theory that saltation mass flux increases with increases in $u_*$ [e.g. *Bagnold,* 1941; *Owen,* 1964; *Kok et al.,* 2012]. The values of $u_*$ corresponding to the onset and termination of saltation periods also provide valuable information on saltation and the conditions of the soil.
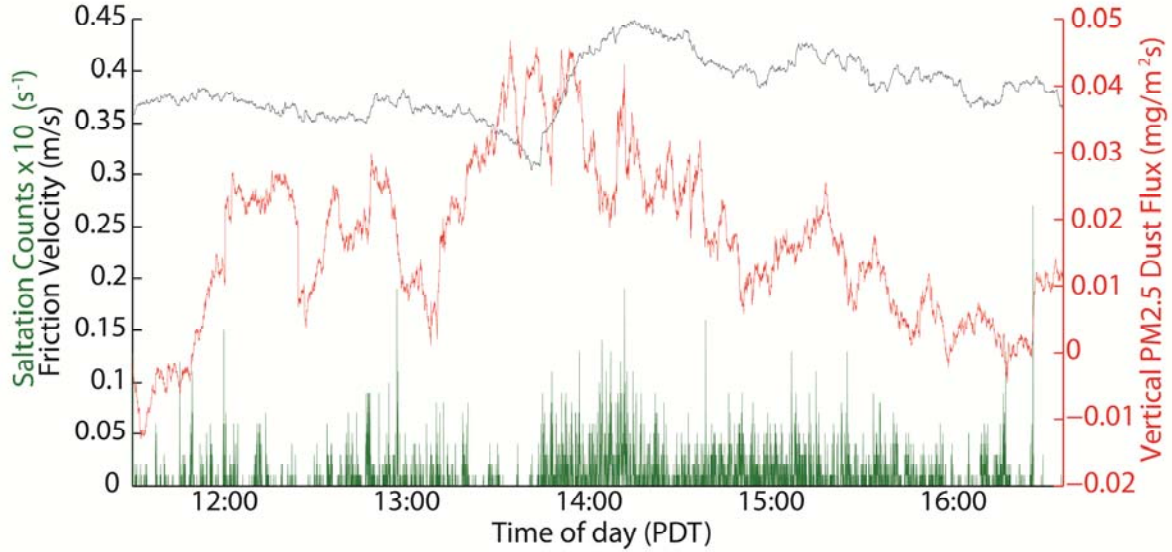
Figure 3.5: Friction velocity and saltation measurements during period 5. Saltation strength (green), as measured by particle counts impacting upon the Sensit sensor, is proportional to the 15-minute-averaged values of $u_*$ (black) and vertical flux of $PM_{2.5}$ dust (red). $u_*$ during period 5 is determined by a least-squares linear regression from wind speed measurements above the saltation layer, while vertical dust flux is calculated with the eddy covariance technique, as discussed in section 3.3. Gaps in the $u_*$ values occur when the regression fit is poor ($r^2 < 0.98$).

Observations of the onset and termination of the various saltation periods show that the approximate threshold friction velocity value changes throughout the day. For instance, saltation during period 5 is sustained continuously after 13:50 local time when $u_* > 0.31$ m/s, implying that $u_{*_t} \approx 0.31$ m/s. The absence of saltation in the late afternoon (after 16:30) during period 5, despite the fact that $u_* \approx 0.38$ m/s around 16:50, suggests that $u_{*_t}$ increased during period 5. This increase in the threshold friction velocity follows a slight increase in relative humidity with respect to the soil temperature throughout the day, supporting the relationship proposed by *Fécan et al.* [1999] between soil moisture and $u_{*_t}$. Recent studies of the effect of surface conditions on dust emission [*King et al.,* 2012] may provide additional hints of the effect of soil moisture on saltation. The changes in the $u_{*_t}$ value could be explained by exhaustion of the supply of sand particles or dust aggregates, or some other change in the properties of the soil throughout the day.

.

### 3.4.3 Vertical dust flux during saltation

3.4.3.1 Dust flux observations

Our observations at Owens Lake indicate that the vertical dust flux increases with friction velocity, a result that is consistent with previous investigations of this effect shown in Figure 3.6 [*Gillette,* 1977; *Nickling and Gillies,* 1993]. Data from locations that are supply-limited or characterized by high roughness-lengths presented by *Nickling and Gillies* [1993] show total dust fluxes similar to the values measured by the ACI project, which measures flux for particles of diameters smaller than 2.5 μm. Although measurements during each ACI sampling period indicate similar responses of the dust fluxes to increases in $u_*$, there are clear differences between periods. For example, measurements during period 2 indicate the highest values of vertical flux of $PM_{2.5}$ particles, while measurements during period 5 indicate the lowest $PM_{2.5}$ particle flux values, despite the values of $u_*$ being some of the highest. These changes in dust flux with $u_*$ are consistent with modeled dust flux estimates described by Eq. (3.4). Indeed, the data collected during all four measurement periods fit the predictions of Eq. (3.4) well.
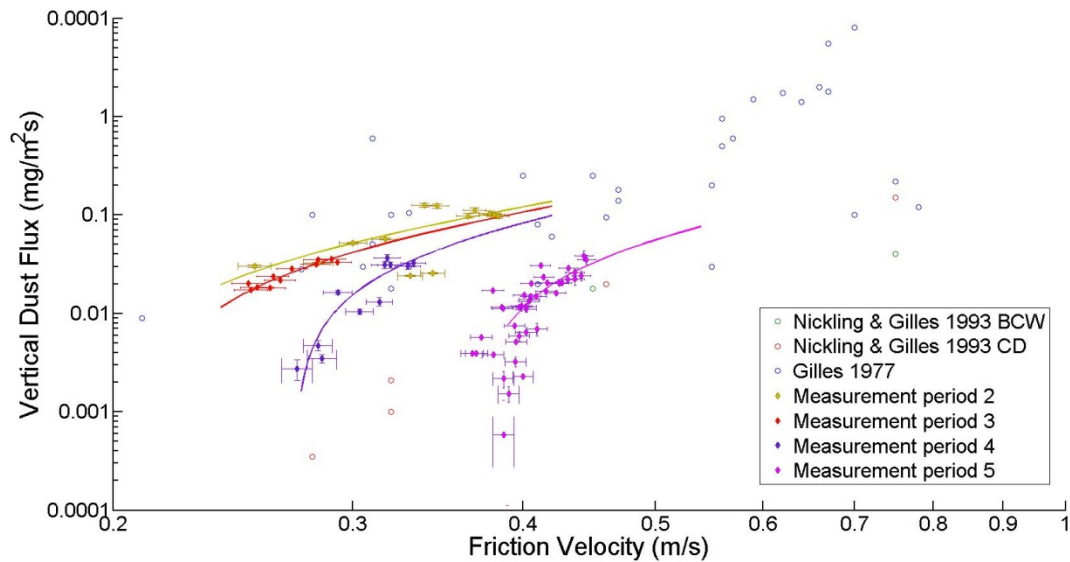
Figure 3.6: Vertical dust flux during saltation events with 95% confidence interval shown. Vertical dust flux measured during periods 2, 3, 4, and 5 is determined using the eddy-covariance technique and is compared with results from previous studies. Regression lines are the least-squares regression fit of Eq. (3.4) to collected data and represents changes to $u_{*_t}$ and $C_F$ determined through the regression. Steeper regression curves are modeled with higher $u_{*_t}$ and lower $C_F$ values, indicating that larger friction velocities are required to initiate saltation, but that dust is ejected more efficiently when saltation does occur.

### 3.4.3.2   Dust flux dependence on soil humidity

Four regression lines fitting the estimation of the dust flux by Eq. (3.4) to the data collected at the field are shown in Figure 3.6. Least-squares regression of each measurement period was used to determine $u_{*_t}$ and the dimensional constant $C_F$ used in Eq. (3.4), which are listed in Table 3.4. Unexpectedly, measurement periods characterized by higher mean soil relative humidity display smaller values of $u_{*_t}$.

Table 3.4: Physical parameters driving dust ejection
determined from data regression to Eq. (3.4).

| Period | $u_{*_t}$ [m/s] | $C_F$ [kg/J] | Mean Soil RH [%] |
|---|---|---|---|
| 2 | 0.20±0.03 | 4.0±0.6 | 23±0.5 |
| 3 | 0.18±0.04 | 3.5±0.8 | 22±0.3 |
| 4 | 0.26±0.03 | 2.9±0.4 | 16±0.3 |
| 5 | 0.26±0.02 | 1.6±0.1 | 11±0.2 |

Another surprising result is that the measurement periods with highest soil relative humidity are those with largest dust fluxes. A similar effect was discussed by *Reynolds et al.* [2007] who hypothesized that the effect is caused by the inhibition of saltation by surface crusting in dry playas (crusting was hypothesized to limit the supply of particles capable of saltating). In contrast to the observations of *Reynolds et al.* [2007], there were no visual signs of changes in the supply of saltating particles at the ACI project site. Moreover, we would not expect the particle supply to increase with increases in soil relative humidity.

We find through the regression analysis of the data collected at the field site, together with Eq. (3.4), that $C_F$ is larger during periods in which the amount of moisture available to the soil (represented by the soil relative humidity) is elevated. $C_F$ is the dimensional constant of Eq. (3.4) representing the efficiency with which saltating particles bombarding the surface eject smaller dust particles into the air. This increase in efficiency implies either weaker interparticle forces resisting dust or an enhanced ability of a bombarding saltation particle to eject dust because other soil properties such as composition and particle size distribution do not change.

The largest $C_F$ values inferred from our measurements represent the environmental conditions that best support efficient dust ejection from bombarding saltation particles. When conditions upwind of the ACI site become most favorable to efficient dust ejection, $C_F$ would be the largest. Since the area upwind (North) of the ACI site is protected from anthropogenic activity and the Owens River does not penetrate deep into the playa, artificial changes to the soil or changes in the river's flow rate are unlikely to have affected the ACI site. Indeed, measurements of soil volumetric moisture content 5 cm below the surface remain constant through all five measurement periods, indicating negligible changes to the water table depth. Thus, it is unlikely that anthropogenic effects or changes in the Owens River flow would have caused the increase in saltation with soil humidity measured at the ACI field site.

Changes in $C_F$ could be the result of surface soil crust formation and breakup. The soil at the Owens Lake site is subject to strong diurnal heating and nighttime cooling with diurnal temperature variations averaging ~20° C. Temperature variations this large may cause the breakup of surface crusts that could increase the amount of loosely held soil particles and thus increase $C_F$. Such a process would depend on atmospheric moisture because water absorption and evaporation are the primary drivers of surface crusting [*Chen et al.,* 1980; *Feng et al.,* 2013]. *Reynolds et al.* [2007] note that differences in soil crusts between wet and dry playas affect their capability for dust ejection significantly, but they did not observe changes to this capability within a single playa. Other studies have discussed the capability of surface crusts to inhibit dust ejection [e.g. *Belnap and Gillette,* 1998]. Water evaporation from wet soils forces the break-up of soil crusts [*Morris et al.,* 1992], though the high salt content of the Owens Lake soil may dampen this effect because salt inhibits evaporation [*Gran et al.,* 2011]. The measurement periods on which the $C_F$ values were the largest occurred in winter, when the soil relative humidity is greatest [*Costa-Cabral et al.,* 2013], supporting this idea. In addition, broken soil crusts are expected to be more erodible, providing lower values of $u_{*_t}$ like those observed when the $C_F$ values are highest. General seasonal variations in $u_{*_t}$ were not observed in a previous study at Owens Lake [*Ono,* 2006], but this could be because $u_{*_t}$ was highly variable in the previous study. These findings support our hypothesis that increases in soil moisture enhance surface crusting and breakup, producing a more erodible surface that increases $C_F$ and enhances dust ejection.

Since soil moisture increases interparticle forces significantly, an increase in the moisture could create dust aggregates with a sufficient concentration to increase $C_F$ significantly. Dust aggregates would act as larger diameter particles for the purpose of aerodynamic lifting in saltation, and therefore in addition to ejecting soil-bound dust particles upon bombardment, dust aggregates could eject dust particles when they disintegrate [*Kok et al.,* 2012]. Therefore, an increase in aggregates would be expected to increase $C_F$. This hypothesis is consistent with the observations that $C_F$ increases with increases in soil relative humidity. The accompanying decrease in $u_{*_t}$ could be explained by the fact that aggregates have more voids and therefore should be less dense than typical particles and would saltate at lower values of $u_{*_t}$.

### 3.4.4   Changes to aerosol optical depth with dust concentrations

Measurement periods 1 and 2 contained long enough cloud-free periods for variations of optical depth with aerosol concentrations to be determined.  In the absence of variations in atmospheric chemical composition that could affect the flux of radiation at the surface, we posited that variations of optical depths are caused by variations in the aerosol content.

Figure 3.7 shows that 15-minute averaged optical depth during both periods increases by ~0.2 coincident with an increase in the 15-minute average concentration of $PM_{2.5}$ particles of about 0.7 mg/m$^3$.  This is consistent with the finding by *Niemeyer et al.* [1999] that the passage of dusty plumes at the Owens Lake increases the optical depth by ~0.25.  The slightly higher aerosol optical depth values observed by *Niemeyer et al.* [1999] is not surprising because a dust plume would likely have ejected larger dust particles aloft than saltation alone.
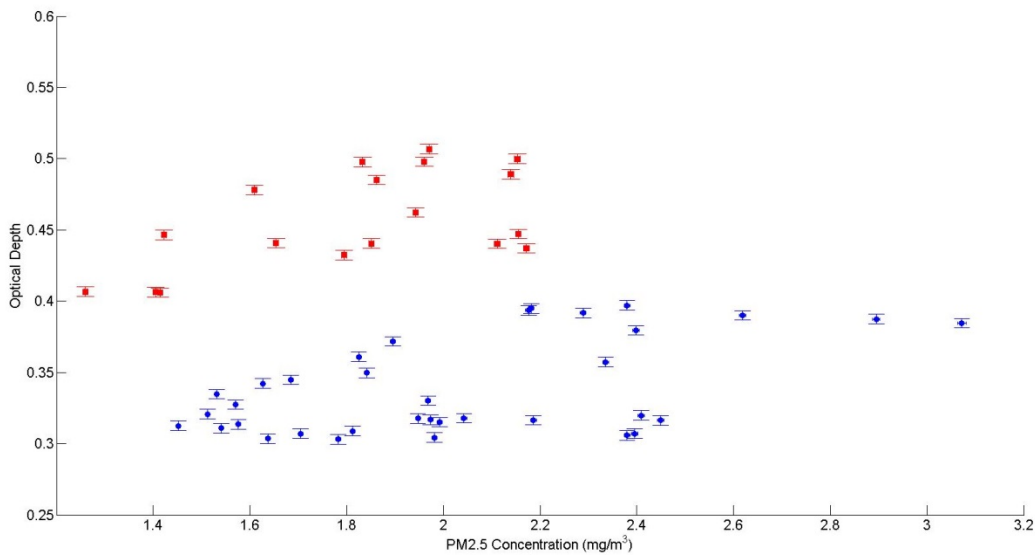


Figure 3.7: Optical depth perturbations from suspended dust with 95% confidence interval shown.  Increases in 15-minute average $PM_{2.5}$ concentrations are coincident with increases to 15-minute averages of the local optical depth during period 1 ( ● ) and period 2 (■).  Only two of the four measurement periods contain data with negligible cloud cover allowing optical depth changes to be approximated as being solely due to changes in the aerosol optical depth.

## 3.5 CONCLUSION

This chapter introduces the University of Michigan Aerosols-Climate Interaction project, designed to study the physical processes that eject dust into the atmosphere and the effects of changes in the atmospheric dust content on flux of radiation at the surface. Data collected during the initial phase of the ACI project indicates that saltation increases with increases in friction velocity as predicted by well-established theories, and that aerosol optical depth increases with increases in the concentrations of $PM_{2.5}$ particles. Initial measurements also indicate a surprising decrease in the threshold friction velocity and increase in the efficiency of dust ejection with increases in soil moisture. The ACI's initial results support the hypothesis that increases in soil moisture lead to the formation of dust aggregates that enhance saltation and dust lifting at the Owens Lake salty playa.

Climatological variations of humidity and diurnal variation of temperature support a second hypothesis that the dust lifting increases with soil moisture because of the expansion and breakup of soil crusts. Additional measurements must be conducted to test these two hypotheses. In particular, direct measurements of dust aggregate frequency, soil moisture content, and diurnal soil crust strengths must be made simultaneously. Our findings may indicate that dust remediation efforts like those being conducted at Owens Lake must consider the effects of the composition of the local soil because the formation of aggregates can increase the emission of dust in wetter soils.

# CHAPTER 4

# A DUST LIFTING MODEL FOR SALTY PLAYAS

## 4.1 INTRODUCTION

Under typical conditions, mineral dust is ejected when saltating particles bombard the surface and transfer kinetic energy to particles on the soil surface [*Grini et al.,* 2002]. The ejection of dust during saltation is a function of both the resistance of the soil to release dust particles, represented by the soil's threshold friction velocity ($u_{*t}$) [*Gillette and Passi,* 1988; *Anderson and Haff,* 1988; *Shao et al.,* 1993; *Shao and Lu,* 2000; *Kok et al.,* 2012], and the efficiency by which the bombardment by saltating particles transfer energy to soil particles [*Kok et al.,* 2012]. The role that $u_{*t}$ plays in the overall mechanics of dust ejection has been studied extensively, but less attention has been given to changes in the bombardment efficiency. This chapter addresses this issue.

## 4.2 DUST EJECTION MODEL

### 4.2.1 Dust flux over saltation

Since saltating particles eject dust proportionally to their kinetic energy and the efficiency by which they eject dust upon impacting the surface [*Kok et al.,* 2012], the vertical dust flux above saltation can be described as

$$F_d = n_s \overline{E}_s \varepsilon \tag{4.1}$$

where $F_d$ is the dust flux in units of kg/m$^2$s just above the saltation layer, $n_s$ is the number of saltators impacting the surface per second, $\varepsilon$ is the mean mass of ejected dust per unit energy of

the impactors (a measure of efficiency of dust ejection by saltation), and $\overline{E}_s$ is the mean kinetic energy of the saltators impacting the surface.

Eq. (4.1) can be expanded by using the fact that the mean impact energy increases with the square of the mean velocity of the saltators when they impact the surface [*Kok et al,* 2012] and an expression for $n_s$ derived by *Shao et al.* [1993] assuming horizontal momentum balance. Substituting the relationships for $n_s$ and $\overline{E}_s$ in Eq. (4.1), we find that the total dust flux is

$$F_d = 2\rho_a \overline{v}_{imp} \varepsilon \left( u_*^2 - u_{*t}^2 \right) \tag{4.2}$$

where $\rho_a$ is the air density, $u_*$ is the friction velocity, $u_{*t}$ is threshold friction velocity, and $\overline{v}_{imp}$ is the mean impact velocity of the saltators.

The impact velocity $\overline{v}_{imp}$ is generally assumed to depend on $u_*$ [*Shao et al.,* 1993], but recent studies in areas where the supply of particles is not limited suggest that $\overline{v}_{imp}$ is instead proportional to the threshold friction velocity $u_{*t}$ [*Kok et al.,* 2012], thus

$$\overline{v}_{imp} = \alpha u_{*t} \tag{4.3}$$

where $\alpha$ is a proportionality constant. Substituting Eq. (4.3) into Eq. (4.2), we get

$$F_d = \left( C_F \rho_a u_*^2 \right) u_{*t} - \left( C_F \rho_a \right) u_{*t}^3 \tag{4.4}$$

where $C_F = 2\alpha\varepsilon$ is a constant of proportionality representing the bombarding particles' efficiency at ejecting dust.

*Kok et al.* [2012] were the first to use Eq. (4.4) for calculating the dust flux above the saltation layer and to realize that it indicates that the dust flux is not proportional to $u_*^3$ as suggested by classical theories [*e.g. Bagnold,* 1941; *Owen,* 1964]. This represents a shift from the idea that the dust flux depends mostly on meteorological conditions like wind stress, to the idea that factors impacting $u_{*t}$ like soil composition and moisture content have a large impact on the dust flux.

### 4.2.2 Moisture dependence of dust flux

In order to understand the observations that dust flux varies with soil moisture content, we analyze the impact of changes in soil moisture to Eq. (4.4). Taking $\rho_a$ and $u_*$ to be constant, the partial derivative of dust flux with soil moisture content ($w$) is

$$\frac{\partial F_d}{\partial w} = \left(\rho_a u_*^2\right)\left(u_{*t}\frac{\partial C_F}{\partial w} + C_F\frac{\partial u_{*t}}{\partial w}\right) - \rho_a\left(u_{*t}^3\frac{\partial C_F}{\partial w} + C_F\frac{\partial u_{*t}^3}{\partial w}\right). \tag{4.5}$$

The volumetric soil moisture content $w$ represents the moisture content of the soil through

$$w = \frac{V_w}{V_t} \tag{4.6}$$

where $V_w$ is the volume of water within a soil sample and $V_t$ is the total volume a soil sample.

Since the dust flux vanishes when $u_* < u_{*t}$, it follows from Eq. (4.5) that

$$\frac{1}{\rho_a}\frac{\partial F_d}{\partial w} = u_{*t}\left(u_*^2 - u_{*t}^2\right)\frac{\partial C_F}{\partial w} + C_F\left(u_*^2 - 3u_{*t}^2\right)\frac{\partial u_{*t}}{\partial w} \qquad \text{for } u_* \geq u_{*t}. \tag{4.7}$$

The second term on the right of Eq. (4.7) indicates that $\dfrac{\partial F_d}{\partial w}$ is directly proportional to

$\dfrac{\partial u_{*t}}{\partial w}$ when $u_* > \sqrt{3}\,u_{*t}$. Although this term appears to indicate that the dust flux always increases with soil moisture, this is not correct. As soil moisture increases, $u_{*t}$ also increases limiting the extent to which increases in soil moisture can produce increases in the dust flux.

### 4.3 DISCUSSION

### 4.3.1 Analysis of the dust ejection-moisture relationship

Eq. (4.7) suggests an interesting relationship between $F_d$, $u_{*t}$, and $w$ during saltation (that is, when $u_* \geq u_{*t}$). The first term on the right-hand side of Eq. (4.7) indicates that the dust flux increases with increases in dust ejection efficiency. The second term represents the dual ability

of soil moisture to increase the efficiency by which particle bombardment ejects dust particles from the surface, while simultaneously decreasing the intensity of saltation by increasing the threshold friction velocity. We postulate that the overall extent by which the dust flux varies with soil moisture depends on the soil particle size distribution and composition (i.e., salt content) because they affect the intensity of the interparticle forces that bind the dust and soil particles together.

The relationship between dust ejection efficiency and soil moisture, $\dfrac{\partial C_F}{\partial w}$, is critically important in the analysis of Eq. (4.7), but unfortunately not well understood yet. Chapter 3 describes a regression technique used to estimate the values of $C_F$ as a function of soil relative humidity (Table 4.1). The result indicates that at Owens Lake playa, $C_F$ increases with environmental moisture, implying $\dfrac{\partial C_F}{\partial w} > 0$. Indeed, observations during the ACI project as described in Chapter 3 indicate that in the Owens Dry Lake salty playa $\dfrac{\partial C_F}{\partial w}$ is large enough to make the first term on the right hand of Eq. (4.7) dominate, making $\dfrac{\partial F_d}{\partial w} > 0$ on nearly all, except the weakest, saltation regimes. Although the relationship between $\dfrac{\partial F_d}{\partial w}$ and $\dfrac{\partial C_F}{\partial w}$ is straightforward, the complexity by which $u_{*t}$ influences dust flux requires a careful analysis of Eq. (4.7).

Table 4.1: Threshold friction velocity ($u_{*_t}$) and dust ejection efficiency ($C_F$) estimated via least-squares regression of data collected during saltation events at the Owens Lake playa during the ACI project.

| Event Date (2013) | $u_{*t}$ [m/s] | $C_F$ [kg/J] | Mean Soil RH [%] |
|---|---|---|---|
| January 29 | 0.19 | 4.32 | 22.8 |
| February 20 | 0.21 | 3.71 | 22.1 |
| March 9 | 0.27 | 2.99 | 15.5 |
| April 8 | 0.37 | 1.13 | 11.3 |

The dependence of $F_d$ on $u_{*_t}$ represents the tendency for moisture to inhibit saltation by increasing interparticle forces [*Herminghaus,* 2005]. The relationship between $F_d$ and $u_{*t}$ is also driven by the tendency of soil moisture to increase the efficiency by which the bombardment by saltators ejects dust particles from the surface as described in Chapter 3, perhaps by forming dust aggregates that saltate and eject dust more easily.

*Fécan et al.* [1999] show that $u_{*t}$ increases with soil moisture content according to the relationship

$$u_{*t} = u_{*t,dry} \sqrt{1 + 1.21(w - w')^{0.68}} \qquad\qquad w \geq w' \qquad\qquad (4.8)$$

where $u_{*t,dry}$ is the threshold friction velocity of dry soil and $w'$ is a parameter that depends on the clay content of the soil.

Eq. (4.8) is consistent with the idea that $u_{*t}$ increases with soil moisture because of increases in the interparticle forces binding the soil material together. The contribution of water to interparticle forces is a result of the capacity of the soil particles to adsorb water and build capillary bridges between soil particles [*Cornelis,* 2006]. Different types of soils will adsorb water and build capillary bridges to different degrees, and thus $\dfrac{\partial u_{*t}}{\partial w}$ is a function of soil type. The estimate for $u_{*t}$ represented by Eq. (4.8) ignores the possible contribution of solutes such as salts, which are often prevalent in regions of strong dust emission such as dry lake beds. Thus, it might under predict the increases in $u_{*t}$ with increases in soil moisture content.

Differentiating Eq. (4.8) to determine $\dfrac{\partial u_{*t}}{\partial w}$ yields,

$$\frac{\partial u_{*t}}{\partial w} = u_{*t,dry} \frac{0.8228(w - w')^{-0.32}}{2\sqrt{1 + 1.21(w - w')^{0.68}}} \qquad\qquad (4.9)$$

which indicates that $\dfrac{\partial u_{*_t}}{\partial w}$ is always positive for sandy soils ($w' \approx 0$), and that its magnitude increases with soil moisture content ($w$).

Although for sandy soils $\dfrac{\partial u_{*_t}}{\partial w}$ is always positive, it is useful to determine its approximate value in order to assess the effect of changes in the threshold friction velocity on $\dfrac{\partial F_d}{\partial w}$. Figure 4.1 shows friction velocity and saltation strength (particle counts) in a typical vigorous saltation event that occurred during the Aerosols-Climate Interaction project. Saltation started when $u_*$ exceeded ~0.28 m/s, providing a reasonable approximation of $u_{*t}$ during this event. Applying Eq. (4.7) to dry sandy soil ($w' \approx 0$), we estimate the dry threshold friction velocity $u_{*_t} \approx 1.08 u_{*_t, dry}$. Measurements of $w$ at the Owens Lake playa are typically ~10%, larger than typical values for arid soils because the Owens Lake salty playa has a relatively shallow water table (~1.5 m below the surface) [*Groeneveld et al.,* 1985]. Using these typical values for the Owens Lake playa, we find that $\dfrac{\partial u_{*_t}}{\partial w} \approx 0.2 \, m/s$.
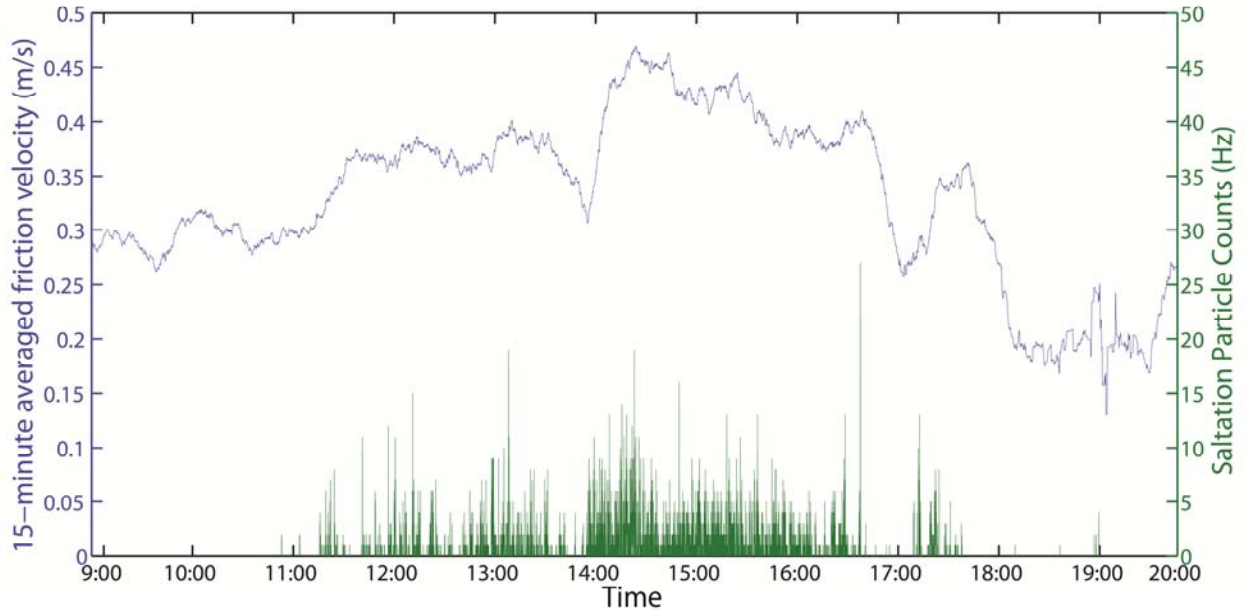
Figure 4.1: Friction velocity (blue) and saltation counts (green) during a typical saltation event at the Owens Lake playa on April 8, 2013. Quasi-steady saltation starts when the friction velocity is larger than ~0.28 m/s, indicating this is approximately the value of the threshold friction velocity. The average value of the friction velocity during this event ~0.39 m/s indicates environmental conditions that support the increases of dust flux by increases in the efficiency of dust ejection by particle bombardment.

Because $\frac{\partial u_{*_t}}{\partial w} > 0$ and $\frac{\partial C_F}{\partial w} > 0$, Eq. (4.7) indicates that $\frac{\partial F_d}{\partial w} > 0$ only when $u_* > u_{*_t}\sqrt{3}$, a condition that implies in vigorous saltation at the Owens Lake playa. During weaker saltation events on which $u_{*_t}\sqrt{3} > u_* > u_{*_t}$, the sign of $\frac{\partial F_d}{\partial w}$ depends on the soil moisture's effect on $\frac{\partial u_{*_t}}{\partial w}$ and $u_{*_t}$. Figure 4.2 shows values of $F_d$ for various soil moisture and $u_*$ values, calculated taking $\frac{\partial C_F}{\partial w} = 10$ to represent typical conditions at the Owens Lake playa. The larger values of $u_*$ necessary to produce a positive $\frac{\partial F_d}{\partial w}$ under moister conditions represent the dust ejection limit at which soil moisture is high enough to inhibit saltation.

70
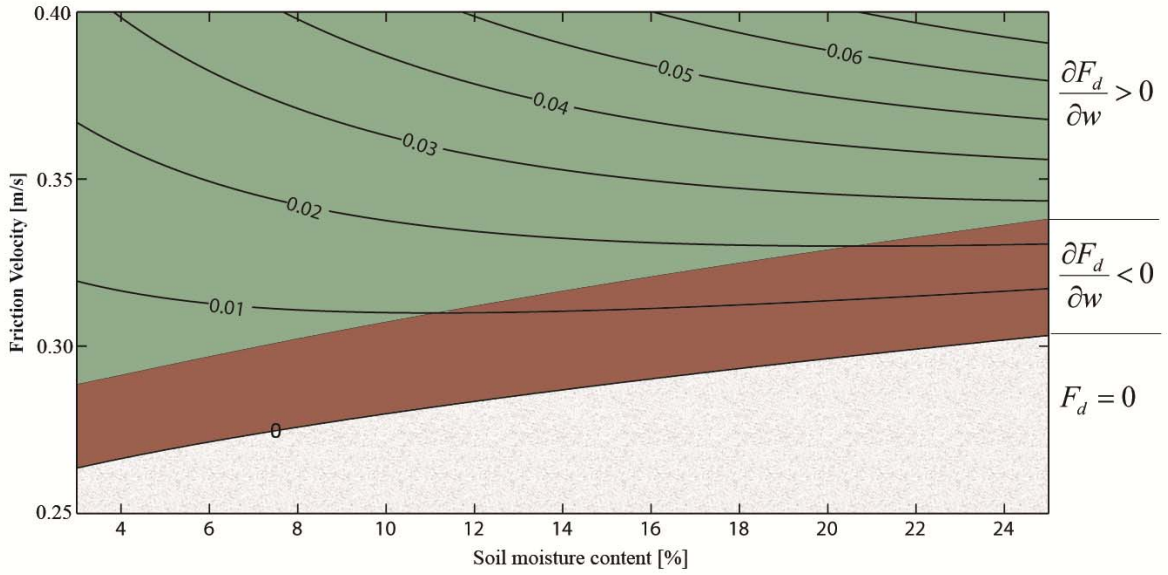
Figure 4.2: Contour plot of dust flux values ($F_d$) predicted using Eq. (4.7) and a wide range of $w$ and $u_*$ values typical of the Owens Lake playa. The green shaded area indicates the region where the dust flux increases with soil moisture content ($\frac{\partial F_d}{\partial w} > 0$), the red area represents the region of negative values, and the gray area indicates the region where $u_* < u_{*_t}$ and thus $F_d = 0$. $F_d$ increases with increases in $w$ in vigorous saltation (that is, when $u_*$ is large) and in dry conditions (that is, when $w$ is small).

The linear relationship between $\frac{\partial F_d}{\partial w}$ and $\frac{\partial C_F}{\partial w}$ described by Eq. (4.7) under vigorous saltation implies that increases in the efficiency of dust ejection (with soil moisture) increase the overall dust flux despite increases in $u_{*_t}$. As $u_*$ approaches $u_{*_t}$, this dependence vanishes because the first term on the right hand side of Eq. (4.7) tends to zero and the second term is negative.

### 4.3.2    Application of the dust ejection-moisture relationship

The theory developed in section 4.2 highlights an interesting consequence of the effects of changes in soil moisture to dust lifting at the Owens Lake playa. The increases in dust flux ($F_d$) with increases in soil moisture content ($w$) observed at the Owens Dry Lake indicates that increases in dust ejection efficiency dominate the effect of decreases in the number of saltators for the typical conditions observed during saltation at the Owens Lake salty playa. Physically, this means that as long as saltation occurs, increases in the mass of dust ejected per saltator more

71

than compensate for the decrease in the number of saltators in motion. This is significant because classical saltation theories consider only the effects of soil moisture content on $u_{*t}$ and therefore assume that soil moisture produces decreases in the dust flux [*Shao et al.,* 1993]. Recent studies of dust ejection in Asia suggest that soil moisture contributes to models' underestimation of the dust flux [*Tanaka et al.,* 2011], supporting the idea that Owens Lake might not be unique in this regard. *Kok et al.* [2012] briefly discuss field experiments that show increases in $C_F$ with increases in $u_*$, but they do not discuss the effects of soil moisture on it.

As explained below, the relationship represented by Eq. (4.7) provides an interpretation for the observations of increases in the dust flux with soil moisture content observed by the ACI project. Figure 4.3 shows that the dust flux values measured during four separate periods monotonically decrease when the soil moisture content decreases. Table 4.1 lists the values of $C_F$, representing the efficiency of dust ejection introduced in Eq. (4.3). It shows that the dust flux increases with increases in the relative humidity of the air with respect to the soil temperature. Similarly, it shows that $C_F$ increases with relative humidity. These observations demonstrate the direct relationship between $\dfrac{\partial F_d}{\partial w}$ and $\dfrac{\partial C_F}{\partial w}$ suggested by Eq. (4.7).
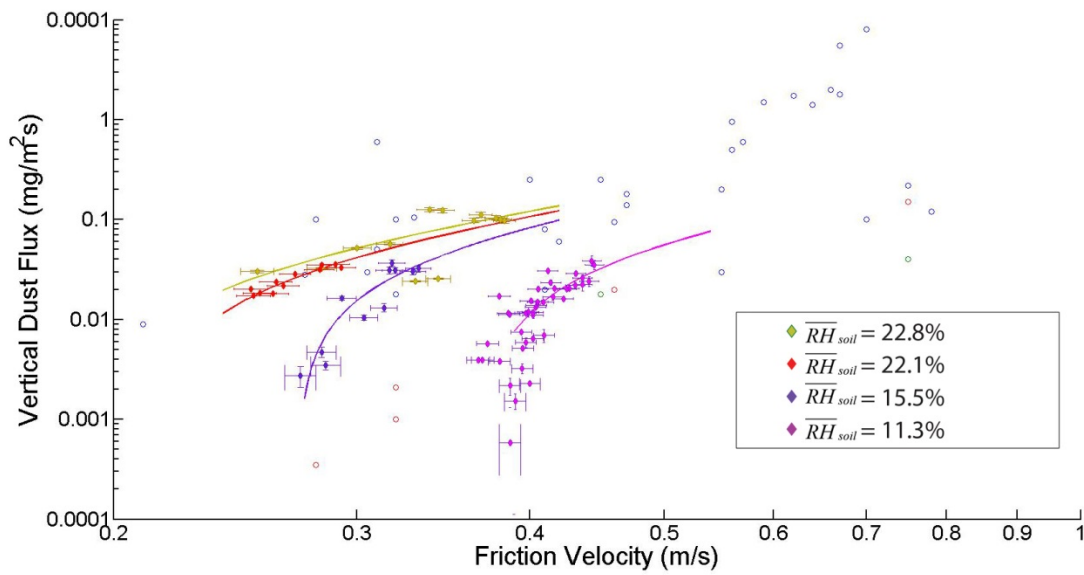
Figure 4.3: Vertical dust flux measured at the Owens Lake during periods of quasi-steady saltation events in 2013 with 95% confidence interval shown. The vertical dust flux as a function of friction velocity calculated using Eq. (4.2) (solid lines) decreases with increases in soil humidity. This counterintuitive relationship is caused by increases in the efficiency of dust ejection by particle bombardment, hypothesized to be via the formation of particle aggregates or the breakup of soil crusts.

Soil properties are implicitly included in Eq. (4.7). For example, the soil at the University of Michigan field site at the Owens Lake contains high salt content which readily absorbs atmospheric water vapor and enhances cohesive forces between particles [*Gill et al.,* 2002; *Quick and Chadwick,* 2011]. A high salt content results in a large $u_{*t}$ in erodible soils [*Nickling,* 1984]. Although *Fécan et al.* [1999] do not include the effects of salts in their equation for predicting $u_{*t}$ (Eq. (4.7) of this article), the relationship represented by Eq. (4.7) indirectly includes the effects of salts because these hygroscopic materials will tend to enhance the effect of $w$ on $C_F$. However, caution should be taken when applying Eq. (4.7)'s estimation of $u_{*t}$ to Eq. (4.7) because under similar atmospheric conditions the absorption of atmospheric moisture is expected to increase with soil hygroscopy [*Yakirevich et al.*, 1997]. Change in a soil's capacity to build capillary bridges is implicitly included into Eq. (4.7) through $C_F$, whether or not the change is a result of water absorption.

The results of the field observations detailed in chapter 3 lead to a hypothesis that changes in a bombarding particle's efficiency in ejecting dust can be caused either by the

breakup of soil crusts or the creation of dust aggregates. The higher $u_{*t}$ values that are observed during drier conditions implies that crusting plays a role in this process, and indeed it is possible that surface crusts are more likely to eject aggregates when bombarded by saltating particles than a surface of loose soil. Aggregates' role in enhancing dust ejection is limited to small aggregates that could saltate, as increases in the proportion of large aggregates tend to inhibit dust ejection [*Hagen*, 1991]. Both surface crust strength and the estimation of the proportion of saltating particles that are aggregates will be the focus of a future study of the effects of moisture on dust ejection.

## 4.4 CONCLUSION

We present in this chapter a theory for the interpretation of how soil water content changes the vertical dust flux above the saltation layer. This theory explains why the vertical dust flux increases with environmental moisture content at the Owens Lake playa as observed during the ACI project. As soil water content changes, saltation-forced dust flux changes proportionally to the change in the ability of bombarding sand particles to eject dust. At Owens Lake salty playa, the moisture-induced enhancement of the dust ejection efficiency of saltating particles exceeds the decreases in dust flux caused by increases in the threshold friction velocity. The increase in a bombarding particle's efficiency in ejecting dust must be either due to increases in the soil's ability to release dust or due to increases in the bombarding particle's ability to drive dust ejection. The change in efficiency is hypothesized to be the result of changes in soil surface crust or of changes in the proportion of dust aggregates among the saltating particles.

Future studies of the influence of soil water on dust ejection from saltation should employ techniques to measure directly the soil water content of the particles in the top-most layer of the soil. Additionally, direct observations of the proportion of soil aggregates among the saltating particles can shed light on effects of changes in soil moisture on the formation of such aggregates. Indeed, visual identification of soil aggregates via time-lapse photography may also be a viable avenue for study. Measurements of changes in soil crust strength with soil moisture using the methods described in *Reynolds et al.* [2007] may provide insights into the crust's role

in the formation of particle aggregates. These direct measurements can test the theory here presented and more generally shed light on dust ejection mechanisms.

# CHAPTER 5
# CONCLUSIONS AND FUTURE WORK

The goal of this dissertation was to improve our understanding of the physical process that initiate saltation and thus lift dust into suspension. Chapter 1 discusses the means by which this goal is accomplished, outlining the investigations into dust devil dynamics, dust lifting via saltation, and predicting the effect of changing environmental conditions- including soil moisture- on dust lifting.

## 5.1 ACCURATE MEASUREMENTS WITHIN A DUST DEVIL

The characterization and testing of a new instrument to accurately measure static and total pressures within a wind flow with a rapidly-changing direction was described in Chapter 2. When the Michigan Prandtl System's rotating vane is aligned with the wind flow direction, the measurements of the difference between static and total pressure have a mean error of less than 7.7% for wind speeds up to 35 m s$^{-1}$. I further show that for nearly all of the wind shifts expected in a typical dust devil, the MPS maintains its vane's alignment with the wind direction to within 30°, and most measurements within a typical dust devil will see alignment between the vane and wind direction within 12°. Such alignment between the vane and wind direction allows for measurement errors by the MPS to be smaller than +4% in most cases, and always positive, as misalignments always result in an increase to the static pressure measurement.

Accurate measurements detailing the dynamics of dust devils can provide a basis for estimating surface wind vector strengths and thus estimates of wind shear against the surface that can initiate saltation and lift dust. When the dust lifting capacity of dust devils can be parameterized as a function of their overall strength via maximum pressure perturbation and soil and environmental conditions, statistical analyses of dust devil frequencies and strengths can provide an estimate for the mean contribution of dust devils as mineral aerosol sources.

## 5.2 A FIELD EXPERIMENT TO STUDY DUST LIFTING FROM SALTATION-INDUCING PHENOMENA

Chapter 3 outlines the goals, implementation, and initial results from the Aerosols-Climate Interactions project designed to study dust lifting by saltation in Owens Lake salty playa. The project's overall goal of studying dust lifting is divided between studies of the more fundamental processes of saltation and the subsequent dust ejection processes.

The ACI project has been making measurements of the mass flux of saltating material, frequency of the counts of the impacts by saltating particles on a piezoelectric sensor, and meteorological measurements of the friction velocity. Initial results from the ACI project indicate the local threshold friction velocity for which saltation initiates at Owens Lake is ~0.30 m/s and may change during a single saltation event. Furthermore, the threshold friction velocity is observed to be higher in saltation events characterized by drier conditions at Owens Lake, a surprising result that might be caused by surface crusting enhanced by the soil's high salt content.

Another surprising initial result from the ACI project is that vertical dust flux, determined using the eddy covariance technique, increases when the environment is moister. A regression analysis of the vertical dust flux and corresponding friction velocities against a model proposed by *Kok et al.* [2012] reveals that the efficiency by which bombardment by saltating particles eject dust increases as the soil humidity increases. I hypothesize in Chapter 3 that the increase in dust flux may be a result of either enhanced dust aggregate formation- aggregates that are then pulverized after they lift into saltation- or a consequence of soil crust breakup when the soil at Owens Lake is subjected to the rapid diurnal heating and cooling that is characteristic of the local climate.

## 5.3 A THEORY FOR DUST LIFTING'S SOIL MOISTURE DEPENDENCE

A new theory that is detailed in Chapter 4 explains the surprising initial results discussed in Chapter 3. In light of the unexpected increases to both threshold friction velocity and vertical dust flux in moister environmental conditions observed at Owens Lake, I analyze the soil

moisture dependence of the *Kok et al.* [2012] model for dust flux from saltation. The result is a theory describing the relationship between changes in dust flux and a saltating particle's dust ejection efficiency with changes in the soil's volumetric moisture content. The theory explains a direct, proportional relationship between $\dfrac{\partial F_d}{\partial w}$ and $\dfrac{\partial C_F}{\partial w}$ under most environmental conditions where saltation is vigorous. In weak or intermittent saltation, or when soil moisture is low, the relationship between $\dfrac{\partial F_d}{\partial w}$ and $\dfrac{\partial C_F}{\partial w}$ becomes inverted, possibly due to limiting quantities of soil particles entering into saltation.

## 5.4 FUTURE WORK

The research presented in this dissertation implies multiple natural avenues for more detailed studies. A few particular studies that could complement this dissertation's findings are discussed below.

1) Parameterizing dust devil dust ejection as a function of peak vortex pressure perturbation and the surrounding environmental conditions. The MPS described in Chapter 2 allows for detailed measurements of pressures and wind speeds within dust devils. Correlating dust ejection quantities with such pressure perturbations can provide a parameterization of dust ejection from individual dust devil events.

2) Collecting dust aggregates during saltation and determining the proportion of saltating particles that are aggregates during different soil moisture regimes. Initial results from the BSNE collectors and COMSALT modeling detailed in Chapter 3 implies dust aggregation in saltating particles is common at Owens Lake. Using a saltation trap specifically designed to collect aggregates- a "sticky" trap or other device that prevents aggregate break-up upon collection- a new study can determine the proportion of saltating particle that are aggregates. This measured aggregate proportion should then be compared to differences between collected and modeled particle size distributions and soil moisture measurements to test the hypothesis in Chapter 3 of frequent dust aggregation in saltators.

3) Evaluating the crust strength at Owens Lake during different soil moisture regimes. A study to measure the strength of the soil crust at Owens Lake during different seasons and environmental conditions should be conducted to test the hypothesis discussed in Chapters 3 and 4 of crust break-up causing enhanced dust emission efficiency in saltation. Using a technique similar to *Reynolds et al.* [2007] where a pen penetrometer was used to gauge crust strength and measurements of volumetric soil moisture, a correlation between crust strength and soil moisture at Owens Lake could provide valuable insight into changes in the source of saltatable material when soil moisture changes.

**APPENDICES**

# APPENDIX A

## SUPPLEMENTAL MATERIAL FOR CHAPTER 3

### A.1.　Instrument details

*Campbell-Scientific 03101-L 3-cup anemometer*
|  |  |
|---|---|
| Height: | 65 cm, 104 cm, 142 cm |
| Measurement resolution: | ± 1 m/s |
| Measurement frequency: | 1 Hz |

*Davis 3-cup anemometer*
|  |  |
|---|---|
| Height: | 13 cm |
| Measurement resolution: | ± 1 m/s |
| Measurement frequency: | 1 Hz |

*Sensit H11-LIN Saltation Sensor*
|  |  |
|---|---|
| Height: | 6.4-7.6 cm |
| Measurement resolution: | 1 particle impact |
| Measurement frequency: | 1 Hz |

*Campbell-Scientific CSAT3 Sonic Anemometer*
|  |  |
|---|---|
| Height: | 300 cm |
| Measurement uncertainty: | Horizontal: ± 0.08 m/s |
|  | Vertical: ± 0.04 m/s |
| Measurement frequency: | 10 Hz |

*Met-One E-Sampler Aerosol Sensor with PM2.5 cut-cyclone*
|  |  |
|---|---|
| Height: | 290 cm |
| Measurement uncertainty: | 8% |
| Measurement frequency: | 1 Hz |
| Measurement range: | 0.001 to 65 mg/m^3 |

*Michigan Prandtl System Prandtl Tube Sensor*
|  |  |
|---|---|
| Height: | 350 cm |
| Measurement uncertainty: | ~7.7% for most wind flows, up to ~35% for extremely rapidly changing wind directions. |
| Measurement frequency: | 1 Hz |

*Campbell-Scientific CS106 Barometric Pressure Sensor*
|  |  |
|---|---|
| Height: | 200 cm |

Measurement uncertainty: ± 0.3 hPa
Measurement frequency: 1 Hz


*Campbell-Scientific CS215 Temperature and Relative Humidity Sensor*
Height: 200 cm
Measurement uncertainty: Temperature: ± 0.3 °C
Humidity: ± 2%
Measurement frequency: 1 Hz


*Campbell-Scientific CNR4 Net Radiometer*
Height: 150 cm
Measurement uncertainty: < 5%
Measurement frequency: 1 Hz
Measurement range: 305 to 2800 nm


*Campbell-Scientific CS107 Air Temperature Sensor*
Height 150 cm
Measurement uncertainty: ± 0.2 °C
Measurement frequency: 1 Hz


*Campbell-Scientific CS616 Soil Moisture Sensor*
Depth 5 cm
Measurement uncertainty: ± 2.5% VWC
Measurement frequency: 10 Hz


*Campbell-Scientific CS105E Soil Temperature Sensor*
Depth 5 cm
Measurement uncertainty: < 0.3°C
Measurement frequency: 10 Hz


*Big Springs Number Eight (BSNE) Sand Collectors*
Aperature size $2.5 \text{ cm}^2$ (small)
$10 \text{ cm}^2$ (large)
Placement Heights
Small-aperature: 5 cm, 7.5 cm, 9 cm, 11.5 cm
Large-aperature: 16.5 cm, 19 cm, 35 cm, 52 cm, 81.25 cm

## APPENDIX B

## LIST OF PUBLICATIONS GENERATED BY THIS DISSERTATION

*Peer Review*

Halleaux, D. G., and N. O. Rennó (2013), A Dust Lifting Model for Changes in Soil Moisture, *In Review*.

Halleaux, D. G., and N. O. Rennó (2013), Aerosols-Climate Interactions at the Owens "Dry" Lake, California, *In Review*.

Halleaux, D. G., J. M. Sussman, and N. O. Rennó (2013), The Michigan Prandtl System: An Instrument for Accurate Pressure Measurements in Convective Vortices, *J. Atm. Ocean. Tech., 30,* 2426-2433, doi: 10.1175/JTECH-D-12-00246.1.

Rennó, N. O., D. Halleaux, H. Elliott, and J. F. Kok (2013), The Lifting of Dust Aerosols and their Effects on Atmospheric Dynamics. A Chapter on the book "Comparitive Climatology of Terrestrial Planets." University of Arizona Press, in press.

*Conference*

Halleaux, D. G., S. F. Braswell, and N. O. Rennó (2012), Dust Forecasting for Human Exploration of Mars. *Concepts and Approaches for Mars Exploration.*

Halleaux, D., and N. Rennó (2012), Measurements Confirm a Thermodynamical Theory for Convective Vortices, *European Geophysical Union General Assembly 2012, 14,* EGU2012-11268.

Rennó, N. O., D. G. Gossiaux, F. Saca, S. Rogacki, R. Gillespie, and S. Musko (2009), A Generalization of Bernoulli's Equation to Convective Vortices, *41$^{st}$ Lunar and Planetary Science Conference.*

Saca, F. A., N. O. Rennó, D. G. Halleaux, S. Rogacki, R. Gillespie, and S. Musko (2009), A portable Instrument for Atmospheric Measurements, *41$^{st}$ Lunar and Planetary Science Conference.*

Spiga, A., A. Pathare, M. Balme, N. Rennó, F. Saca, D. Halleaux, and S. Metzger (2009), In Situ Studies of Terrestrial Dust Devils and Ambient Meteorology: Field Measurements of Vorticity. *41st Lunar and Planetary Science Conference.*

**APPENDIX C**

**THE UNIVERSITY OF MICHIGAN – STATE OF CALIFORNIA LAND LEASE**
**AGREEMENT FOR OWENS LAKE, CALIFORNIA**

_SPACE ABOVE THIS LINE FOR RECORDER'S USE_

County: Inyo

W 26639

## LEASE No. PRC 9031.9

This Lease consists of this summary and the following attached and incorporated parts:

| | |
|---|---|
| Section 1 | Basic Provisions |
| Section 2 | Special Provisions Amending or Supplementing Section 1 or 3 |
| Section 3 | General Provisions |
| Exhibit A | Description of Lease Premises |

---

## SECTION 1

### BASIC PROVISIONS

**THE STATE OF CALIFORNIA**, hereinafter referred to as Lessor acting by and through the **CALIFORNIA STATE LANDS COMMISSION** (100 Howe Avenue, Suite 100-South, Sacramento, California 95825-8202), pursuant to Division 6 of the Public Resources Code and Title 2, Division 3 of the California Code of Regulations, and for consideration specified in this Lease, does hereby lease, demise, and let to the **Regents of the University of Michigan**, hereinafter referred to as Lessee, those certain lands described in Exhibit A subject to the reservations, terms, covenants, and conditions of this Lease.

MAILING ADDRESS:    The Regents of the University of Michigan
2455 Hayward Street
Ann Arbor, MI 48109

LEASE TYPE:    General Lease – Public Agency Use

LAND TYPE:    Sovereign

LOCATION:    Owens Lake, Inyo County

LAND USE OR PURPOSE:    Installation, use and maintenance of two monitoring towers, a data collection and transmission box, and a solar panel power collection station.

TERM: 2 years 6 months; beginning December 5, 2012; ending June 4, 2015, unless sooner terminated as provided under this Lease.

CONSIDERATION: No monetary consideration as the information collected will result in a public benefit; the State reserves the right at any time to set a monetary rent if the State Lands Commission finds such action to be in the State's best interest. Subject to modification by Lessor as specified in Paragraph 2(b) of Section 3 - General Provisions.

AUTHORIZED IMPROVEMENTS:

N/A  EXISTING: N/A

N/A  TO BE CONSTRUCTED; CONSTRUCTION MUST BEGIN BY: December 5, 2012

AND BE COMPLETED BY: January 1, 2013

LIABILITY INSURANCE:    N/A

SURETY BOND OR OTHER SECURITY:    N/A

---

## SECTION 2
## SPECIAL PROVISIONS

BEFORE THE EXECUTION OF THIS LEASE, ITS PROVISIONS ARE AMENDED, REVISED, OR SUPPLEMENTED AS FOLLOWS:

1. Lessee shall provide photos of the study site before installation, after installation, and after removal of the structures.

2. Lessee shall install Nixalite or other form of bird barrier spikes on all structures greater than 72 inches in height.

3. All personal property, tools, or equipment taken onto or placed upon the Lease Premises shall remain the personal property of the Lessee or its contractor. Such personal property shall be promptly removed by the Lessee, at its sole risk and expense upon the completion of the study. Lessor does not accept any responsibility for any damage, including damages to any personal property, including any equipment, tools, or machinery on the Lease Premises.

4. Any equipment to be used on the Lease Premises is limited to that which is directly required to perform the authorized use and shall not include any equipment that may cause damage to the Lease Premises or on other lands subject to Lessor's jurisdiction.

5. No refueling, repairs, or maintenance of vehicles or equipment will take place on the Lease Premises or on lands subject to Lessor's jurisdiction.

6. Lessee shall not add or permit any additional improvements to be placed on the Lease Premises without Lessor's consent.

7. Lessee shall obtain all authorizations and approvals of any adjacent property owners prior to accessing the Lease Premises.

8. Lessee is prohibited from operating motor vehicles on the Lease Premises or other lands subject to Lessor's jurisdiction. All project equipment shall be hand carried to the Lease Premises.

9. Lessee shall avoid any cultural resources within the Lease Premises.

10. Lessee shall contact the Lone Pine Paiute-Shoshone Reservation 48 hours in advance to allow a voluntary cultural monitor to be present during project installation and removal.

11. Lessee's staff shall receive Snowy Plover Avoidance training prior to the start of the project. In addition, if installation or removal occurs within Snowy Plover season, a pre-construction survey of the Lease Premises will be conducted by a qualified biologist.

12. All covenants pertaining to bond, insurance, indemnification, restoration obligations, default, and remedies shall survive the expiration or earlier termination of this Lease until Lessee has restored the Lease Premises as required by this lease.

In the event of any conflict between the provisions of Section 2 and Section 3 of this Lease, the provisions of Section 2 shall prevail.

## GENERAL PROVISIONS

### 1. GENERAL

These provisions are applicable to all leases, permits, rights-of-way, easements, or licenses or other interests in real property conveyed by the State Lands Commission.

### 2. CONSIDERATION

**(a) Categories**

**(1) Rental**

Lessee shall pay the annual rental as stated in this Lease to Lessor without deduction, delay, or offset, on or before the beginning date of this Lease and on or before each anniversary of its beginning date during each year of the Lease term.

**(2) Non-Monetary Consideration**

If the consideration to Lessor for this Lease is the public use, benefit, health, or safety, Lessor shall have the right to review such consideration at any time and set a monetary rental if the State Lands Commission, at its sole discretion, determines that such action is in the best interest of the State.

**(b) Modification**

Lessor may modify the method, amount, or rate of consideration effective on each fifth anniversary of the beginning date of this Lease. Should Lessor fail to exercise such right effective on any fifth anniversary it may do so effective on any one (1) of the next four (4) anniversaries following such fifth anniversary, without prejudice to its right to effect such modification on the next or any succeeding fifth anniversary. No such modification shall become effective unless Lessee is given at least thirty (30) days notice prior to the effective date.

**(c) Penalty and Interest**

Any installments of rental accruing under this Lease not paid when due shall be subject to a penalty and shall bear interest as specified in Public Resources Code Section 6224 and the Lessor's then existing administrative regulations governing penalty and interest.

### 3. BOUNDARIES

This Lease is not intended to establish the State's boundaries and is made without prejudice to either party regarding any boundary claims which may be asserted presently or in the future.

### 4. LAND USE

**(a) General**

Lessee shall use the Lease Premises only for the purpose or purposes stated in this Lease and only for the operation and maintenance of the improvements expressly authorized in this Lease. Lessee shall commence use of the Lease Premises within ninety (90) days of the beginning date of this Lease or within ninety (90) days of the date set for construction to commence as set forth in this Lease, whichever is later. Lessee shall notify Lessor within ten (10) days after commencing the construction of authorized improvements

and within sixty (60) days after completing them. Lessee's discontinuance of such use for a period of ninety (90) days shall be conclusively presumed to be an abandonment.

**(b) Continuous Use**

Lessee's use of the Lease Premises shall be continuous from commencement of the Lease until its expiration.

**(c) Repairs and Maintenance**

Lessee shall, at its own expense, keep and maintain the Lease Premises and all improvements in good order and repair and in safe condition. Lessor shall have no obligation for such repair and maintenance.

**(d) Additions, Alterations, and Removal**

(1) Additions - No improvements other than those expressly authorized in this Lease shall be constructed by the Lessee on the Lease Premises without the prior written consent of Lessor.

(2) Alteration or Removal - Except as provided under this Lease, no alteration or removal of improvements on or natural features of the Lease Premises shall be undertaken without the prior written consent of Lessor.

**(e) Conservation**

Lessee shall practice conservation of water, energy, and other natural resources and shall prevent pollution and harm to the environment. Lessee shall not violate any law or regulation whose purpose is to conserve resources or to protect the environment. Violation of this section shall constitute grounds for termination of the Lease. Lessor, by its executive officer, shall notify Lessee, when in his or her opinion, Lessee has violated the provisions of this section and Lessee shall respond and discontinue the conduct or remedy the condition within 30 days.

**(f) Toxics**

Lessee shall not manufacture or generate hazardous wastes on the Lease Premises unless specifically authorized under other terms of this Lease. Lessee shall be fully responsible for any hazardous wastes, substances, or materials as defined under federal, State, or local law, regulation, or ordinance that are manufactured, generated, used, placed, disposed, stored, or transported on the Lease Premises during the Lease term and shall comply with and be bound by all applicable provisions of such federal, State, or local law, regulation or ordinance dealing with such wastes, substances, or materials. Lessee shall notify Lessor and the appropriate governmental emergency response agency(ies) immediately in the event of any release or threatened release of any such wastes, substances, or materials.

**(g) Enjoyment**

Subject to the provisions of paragraph 5 (a) (2) below, nothing in this Lease shall preclude Lessee from excluding persons from the Lease Premises when their presence or activity constitutes a material interference with Lessee's use

and enjoyment of the Lease Premises as provided under this Lease.

### (h) Discrimination

Lessee in its use of the Lease Premises shall not discriminate against any person or class of persons on the basis of race, color, creed, religion, national origin, sex, age, or handicap.

### (i) Residential Use

No portion of the Lease Premises shall be used as a location for a residence or for the purpose of mooring a structure which is used as a residence. For purposes of this Lease, a residence or floating residence includes but is not limited to boats, barges, houseboats, trailers, cabins, or combinations of such facilities or other such structures which provide overnight accommodations to the Lessee or others.

## 5. RESERVATIONS, ENCUMBRANCES, AND RIGHTS-OF-WAY

### (a) Reservations

(1) Lessor expressly reserves all natural resources in or on the Lease Premises, including but not limited to timber and minerals as defined under Public Resources Code Sections 6401 and 6407, as well as the right to grant leases in and over the Lease Premises for the extraction of such natural resources; however, such leasing shall be neither inconsistent nor incompatible with the rights or privileges of Lessee under this Lease.

(2) Lessor expressly reserves a right to go on the Lease Premises and all improvements for any purposes associated with this Lease or for carrying out any function required by law, or the rules, regulations, or management policies of the State Lands Commission. Lessor shall have a right of reasonable access to the Lease Premises across Lessee owned or occupied lands adjacent to the Lease Premises for any purpose associated with this Lease.

(3) Lessor expressly reserves to the public an easement for convenient access across the Lease Premises to other State-owned lands located near or adjacent to the Lease Premises and a right of reasonable passage across and along any right-of-way granted by this Lease; however, such easement or right-of-way shall be neither inconsistent nor incompatible with the rights or privileges of Lessee under this Lease.

(4) Lessor expressly reserves the right to lease, convey, or encumber the Lease Premises, in whole or in part, during the Lease term for any purpose not inconsistent or incompatible with the rights or privileges of Lessee under this Lease.

### (b) Encumbrances

This Lease may be subject to pre-existing contracts, leases, licenses, easements, encumbrances, and claims and is made without warranty by Lessor of title, condition, or fitness of the land for the stated or intended purpose.

## 6. RULES, REGULATIONS, AND TAXES

(a) Lessee shall comply with and be bound by all presently existing or subsequently enacted rules, regulations, statutes or ordinances of the State Lands Commission or any other governmental agency or entity having lawful authority and jurisdiction.

(b) Lessee understands and agrees that a necessary condition for the granting and continued existence of this Lease is that Lessee obtains and maintains all permits or other entitlements.

(c) Lessee accepts responsibility for and agrees to pay any and all possessory interest taxes, assessments, user fees or service charges imposed on or associated with the leasehold interest, improvements or the Lease Premises, and such payment shall not reduce rental due Lessor under this Lease and Lessor shall have no liability for such payment.

## 7. INDEMNITY

(a) Lessor shall not be liable and Lessee shall indemnify, hold harmless, and, at the option of Lessor, defend Lessor, its officers, agents, and employees against and for any and all liability, claims, damages or injuries of any kind and from any cause, arising out of or connected in any way with the issuance, enjoyment or breach of this Lease or Lessee's use of the Lease Premises except for any such liability, claims, damage or injury solely caused by the negligence of Lessor, its officers, agents and employees.

(b) Lessee shall notify Lessor immediately in case of any accident, injury, or casualty on the Lease Premises.

## 8. INSURANCE

(a) Lessee shall obtain and maintain in full force and effect during the term of this Lease comprehensive general liability insurance and property damage insurance, with such coverage and limits as may be reasonably requested by Lessor from time to time, but in no event for less than the sum(s) specified, insuring Lessee and Lessor against any and all claims or liability arising out of the ownership, use, occupancy, condition, or maintenance of the Lease Premises and all improvements.

(b) The insurance policy or policies shall name the State of California, its officers, employees and volunteers as insureds as to the Lease Premises and shall identify the Lease by its assigned number. Lessee shall provide Lessor with a certificate of such insurance and shall keep such certificate current. The policy (or endorsement) must provide that the insurer will not cancel the insured's coverage without thirty (30) days prior written notice to Lessor. Lessor will not be responsible for any premiums or other assessments on the

Form 51.15 (Rev. 6/06)

90

policy. The coverage provided by the insured (Lessee) shall be primary and non-contributing.

(c) The insurance coverage specified in this Lease shall be in effect at all times during the Lease term and subsequently until all of the Lease Premises have been either accepted as improved, by Lessor, or restored by Lessee as provided elsewhere in this Lease.

## 9. SURETY BOND

(a) Lessee shall provide a surety bond or other security device acceptable to Lessor, for the specified amount, and naming the State of California as the assured, to guarantee to Lessor the faithful observance and performance by Lessee of all of the terms, covenants, and conditions of this Lease.

(b) Lessor may require an increase in the amount of the surety bond or other security device to cover any additionally authorized improvements, alterations or purposes and any modification of consideration.

(c) The surety bond or other security device shall be maintained in full force and effect at all times during the Lease term and subsequently until all of the Lease Premises have been either accepted as improved, by Lessor, or restored by Lessee as provided elsewhere in this Lease.

## 10. ASSIGNMENT, ENCUMBRANCING OR SUBLETTING

(a) Lessee shall not either voluntarily or by operation of law, assign, transfer, mortgage, pledge, hypothecate or encumber this Lease and shall not sublet the Lease Premises, in whole or in part, or allow any person other than the Lessee's employees, agents, servants and invitees to occupy or use all or any portion of the Lease Premises without the prior written consent of Lessor, which consent shall not be unreasonably withheld.

(b) The following shall be deemed to be an assignment or transfer within the meaning of this Lease:

(1) If Lessee is a corporation, any dissolution, merger, consolidation or other reorganization of Lessee or sale or other transfer of a percentage of capital stock of Lessee which results in a change of controlling persons, or the sale or other transfer of substantially all the assets of Lessee;

(2) If Lessee is a partnership, a transfer of any interest of a general partner, a withdrawal of any general partner from the partnership, or the dissolution of the partnership.

(c) If this Lease is for sovereign lands, it shall be appurtenant to adjoining littoral or riparian land and Lessee shall not transfer or assign its ownership interest or use rights in such adjoining lands separately from the leasehold rights granted herein without the prior written consent of Lessor.

(d) If Lessee desires to assign, sublet, encumber or otherwise transfer all or any portion of the Lease Premises, Lessee shall do all of the following:

(1) Give prior written notice to Lessor;

(2) Provide the name and complete business organization and operational structure of the proposed assignee, sublessee, secured third party, or other transferee; and the nature of the use of and interest in the Lease Premises proposed by the assignee, sublessee, secured third party or other transferee. If the proposed assignee, sublessee, or secured third party is a general or limited partnership, or a joint venture, provide a copy of the partnership agreement or joint venture agreement, as applicable;

(3) Provide the terms and conditions of the proposed assignment, sublease, or encumbrance or other transfer;

(4) Provide audited financial statements for the two most recently completed fiscal years of the proposed assignee, sublessee, secured party or other transferee; and provide pro forma financial statements showing the projected income, expense and financial condition resulting from use of the Lease Premises; and

(5) Provide such additional or supplemental information as Lessor may reasonably request concerning the proposed assignee, sublessee, secured party or other transferee.

Lessor will evaluate proposed assignees, sublessees, secured third parties and other transferees and grant approval or disapproval according to standards of commercial reasonableness considering the following factors within the context of the proposed use: the proposed party's financial strength and reliability, their business experience and expertise, their personal and business reputation, their managerial and operational skills, their proposed use and projected rental, as well as other relevant factors.

(e) Lessor shall have a reasonable period of time from the receipt of all documents and other information required under this provision to grant or deny its approval of the proposed party.

(f) Lessee's mortgage or hypothecation of this Lease, if approved by Lessor, shall be subject to terms and conditions found in a separately drafted standard form (Agreement and Consent to Encumbrancing of Lease) available from Lessor upon request.

(g) Upon the express written assumption of all obligations and duties under this Lease by an assignee approved by Lessor, the Lessee may be released from all liability under this Lease arising after the effective date of assignment and not associated with Lessee's use, possession or occupation of

Form 51.15 (Rev. 6/06)

91

or activities on the Lease Premises; except as to any hazardous wastes, substances or materials as defined under federal, state or local law, regulation, or ordinance manufactured, generated, used, placed, disposed, stored or transported on the Lease Premises.

(h) If the Lessee files a petition or an order for relief is entered against Lessee, under Chapters 7,9,11 or 13 of the Bankruptcy Code (11 USC Sect. 101, et seq.) then the trustee or debtor-in-possession must elect to assume or reject this Lease within sixty (60) days after filing of the petition or appointment of the trustee, or the Lease shall be deemed to have been rejected, and Lessor shall be entitled to immediate possession of the Lease Premises. No assumption or assignment of this Lease shall be effective unless it is in writing and unless the trustee or debtor-in-possession has cured all defaults under this Lease (monetary and non-monetary) or has provided Lessor with adequate assurances (1) that within ten (10) days from the date of such assumption or assignment, all monetary defaults under this Lease will be cured; and (2) that within thirty (30) days from the date of such assumption, all non-monetary defaults under this Lease will be cured; and (3) that all provisions of this Lease will be satisfactorily performed in the future.

## 11. DEFAULT AND REMEDIES

(a) **Default**

The occurrence of any one or more of the following events shall immediately and without further notice constitute a default or breach of the Lease by Lessee:

(1) Lessee's failure to make any payment of rental, royalty, or other consideration as required under this Lease;

(2) Lessee's failure to obtain or maintain liability insurance or a surety bond or other security device as required under this Lease;

(3) Lessee's vacation or abandonment of the Lease Premises (including the covenant for continuous use as provided for in paragraph 4) during the Lease term;

(4) Lessee's failure to obtain and maintain all necessary governmental permits or other entitlements;

(5) Lessee's failure to comply with all applicable provisions of federal, state or local law, regulation or ordinance dealing with hazardous waste, substances or materials as defined under such law;

(6) Lessee's Failure to commence to construct and to complete construction of the improvements authorized by this Lease within the time limits specified in this Lease; and/or

(7) Lessee's failure to comply with applicable provisions of federal, State or local laws or ordinances relating to issues of Health and Safety, or whose purpose is to conserve resources or to protect the environment.

(b) Lessee's failure to observe or perform any other term, covenant, or condition of this Lease to be observed or performed by the Lessee when such failure shall continue for a period of thirty (30) days after Lessor's giving written notice; however, if the nature of Lessee's default or breach under this paragraph is such that more than thirty (30) days are reasonably required for its cure, then Lessee shall not be deemed to be in default or breach if Lessee commences such cure within such thirty (30) day period and diligently proceeds with such cure to completion.

(c) **Remedies**

In the event of a default or breach by Lessee and Lessee's failure to cure such default or breach, Lessor may at any time and with or without notice do any one or more of the following:

(1) Re-enter the Lease Premises, remove all persons and property, and repossess and enjoy such premises;

(2) Terminate this Lease and Lessee's right of possession of the Lease Premises. Such termination shall be effective upon Lessor's giving written notice and upon receipt of such notice, Lessee shall immediately surrender possession of the Lease Premises to Lessor;

(3) Maintain this Lease in full force and effect and recover any rental, royalty, or other consideration as it becomes due without terminating Lessee's right of possession regardless of whether Lessee shall have abandoned the Lease Premises; and/or

(4) Exercise any other right or remedy which Lessor may have at law or equity.

## 12. RESTORATION OF LEASE PREMISES

(a) Upon expiration or sooner termination of this Lease, Lessor upon written notice may take title to any or all improvements, including fills, or Lessor may require Lessee to remove all or any such improvements at its sole expense and risk; or Lessor may itself remove or have removed all or any portion of such improvements at Lessee's sole expense. Lessee shall deliver to Lessor such documentation as may be necessary to convey title to such improvements to Lessor free and clear of any liens, mortgages, loans or any other encumbrances.

(b) In removing any such improvements Lessee shall restore the Lease Premises as nearly as possible to the conditions existing prior to their installation or construction.

Form 51.15 (Rev. 6/06)

(c) All plans for and subsequent removal and restoration shall be to the satisfaction of Lessor and shall be completed within ninety (90) days after the expiration or sooner termination of this Lease or after compliance with paragraph 12(d), whichever is the lesser.

(d) In removing any or all the improvements Lessee shall be required to obtain any permits or other governmental approvals as may then be required by lawful authority.

(e) Lessor may at any time during the Lease term require Lessee to conduct at its own expense and by a contractor approved by Lessor an independent environmental site assessment or inspection for the presence or suspected presence of hazardous wastes, substances or materials as defined under federal, State or local law, regulation or ordinance manufactured, generated, used, placed, disposed, stored, or transported on the Lease Premises during the term of the Lease. Lessee shall provide the results of the assessment or inspection to Lessor and the appropriate governmental response agency(ies) and shall further be responsible for removing or taking other appropriate remedial action regarding such wastes, substances or materials in accordance with applicable federal, state or local law regulation or ordinance.

### 13. QUITCLAIM

Lessee shall, within ninety (90) days of the expiration or sooner termination of this Lease, execute and deliver to Lessor in a form provided by Lessor a good and sufficient release of all rights under this Lease. Should Lessee fail or refuse to deliver such a release, a written notice by Lessor reciting such failure or refusal shall, from the date of its recordation, be conclusive evidence against Lessee of the termination of this Lease and all other claimants.

### 14. HOLDING-OVER

Any holding-over by Lessee after the expiration of the Lease term, with or without the express or implied consent of Lessor, shall constitute a tenancy from month to month and not an extension of the Lease term and shall be on the terms, covenants, and conditions of this Lease, except that the annual rental then in effect shall be increased by twenty-five percent (25%).

### 15. ADDITIONAL PROVISIONS

(a) Waiver

(1) No term, covenant, or condition of this Lease and no default or breach of any such term, covenant or condition shall be deemed to have been waived, by Lessor's acceptance of a late or nonconforming performance or otherwise, unless such a waiver is expressly acknowledged by Lessor in writing.

(2) Any such waiver shall not be deemed to be a waiver of any other term, covenant or condition of any other default or breach of any term, covenant or condition of this Lease.

(b) Time
Time is of the essence of this Lease and each and all of its terms, covenants or conditions in which performance is a factor.

(c) Notice
All notices required to be given under this Lease shall be given in writing, sent by U.S. Mail with postage prepaid, to Lessor at the offices of the State Lands Commission and the Lessee at the address specified in this Lease. Lessee shall give Lessor notice of any change in its name or address.

(d) Consent
Where Lessor's consent is required under this Lease its consent for one transaction or event shall not be deemed to be a consent to any subsequent occurrence of the same or any other transaction or event.

(e) Changes
This Lease may be terminated and its term, covenants, and conditions amended, revised, or supplemented only by mutual written agreement of the parties.

(f) Successors
The terms, covenants, and conditions of this Lease shall extend to and be binding upon and inure to the benefit of the heirs, successors, and assigns of the respective parties.

(g) Joint and Several Obligation
If more than one Lessee is a party to this Lease, the obligations of the Lessees shall be joint and several.

(h) Captions
The captions of this Lease are not controlling and shall have no effect upon its construction or interpretation.

(i) Severability
If any term, covenant or condition of this Lease is determined by a court of competent jurisdiction to be invalid, it shall be considered deleted and shall not invalidate any of the remaining terms, covenants and conditions.

Form 51.15 (Rev. 6/06)

STATE OF CALIFORNIA - STATE LANDS COMMISSION

LEASE NO. PRC 9031.9
W26639

    This Lease shall become effective only when approved by and executed on behalf of the State Lands Commission of the State of California and a duly executed copy has been delivered to Lessee. The submission of this Lease by Lessor, its agent or representative for examination by Lessee does not constitute an option or offer to lease the Lease Premises upon the terms and conditions contained herein, or a reservation of the Lease Premises in favor of Lessee. Lessee's submission of an executed copy of this Lease to Lessor shall constitute an offer to Lessor to lease the Lease Premises on the terms and conditions set forth herein.
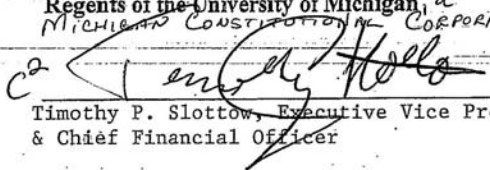
    **IN WITNESS WHEREOF**, the parties hereto have executed this Lease as of the date hereafter affixed.

| LESSEE: | LESSOR: |
|---|---|
| Regents of the University of Michigan, a MICHIGAN CONSTITUTIONAL CORPORATION | STATE OF CALIFORNIA STATE LANDS COMMISSION |
| Timothy P. Slottow, Executive Vice President & Chief Financial Officer | By: Colin Connor |
| | Title: Assistant Chief Land Management Division |
| | Date: DEC 06 2012 |

This Lease was authorized by the
California State Lands Commission on
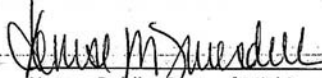
**ACKNOWLEDGEMENT**

December 5, 2012
(Month   Day   Year)

Form 51.15 (Rev. 6/06)

State of California-State Lands Commission (Lease)

STATE OF MICHIGAN    )
                             )SS

COUNTY OF WASHTENAW  )

The foregoing instrument was acknowledged before me this 3rd of December 2012 by Timothy P. Slottow, Executive Vice President and Chief Financial Officer, of The Regents of the University of Michigan, a Michigan constitutional corporation on behalf of the said corporation, in Washtenaw County, Michigan.

Notary Public, State of Michigan,

County of Washtenaw

My commission expires: 12/1/15

Acting in the County of Washtenaw

DENISE M. TRUESDELL
NOTARY PUBLIC - STATE OF MICHIGAN
COUNTY OF WASHTENAW
My Commission Expires December 1, 2015
Acting in the County of Washtenaw

95

# EXHIBIT A

## LAND DESCRIPTION

A parcel of state-owned sovereign land in the bed of Owens Lake in the County of Inyo, State of California, and more particularly described as follows:

BEGINNING at a point having NAD83 UTM Zone 11 North coordinates of Northing (Y) 4043715.1 meters, Easting (X) 416349.3 meters; thence in a clockwise direction through the following three (3) points;

1. Northing (Y) 4043744.1 meters, Easting (X) 416391.0 meters;
2. Northing (Y) 4043662.0 meters, Easting (X) 416448.1 meters;
3. Northing (Y) 4043633.4 meters, Easting (X) 416407.1 meters; thence to the POINT OF BEGINNING.

## END OF DESCRIPTION

Prepared November 29, 2012 by the Boundary Unit of the California State Lands Commission.

*(Surveyor's stamp: PROFESSIONAL LAND SURVEYOR, JAMES A. KOEB___, Exp. 12/31/12, No. 8487, STATE OF CALIFORNIA)*

## Appendix D

## Error Calculations

**D.1.** $\delta u_*$ Calculation

Calculation of the friction velocity, $u_*$, results from a linear regression of a 15-minute averaged vertical series of 1 Hz wind speed measurements at heights $z_1, z_2, z_3, z_4,$ and $z_5$ $(z_h)$, $u(z_h)$. The error in the final calculated $u_*$ is determined through a 1000-iteration monte-carlo simulation of linear regressions of potential wind speed inputs. The error in each individual wind speed measurement is

$$\delta u(z_h) = 0.5\frac{m}{s}$$

and the error of the average wind speed at each height is then

$$\delta \bar{u}(z_h) = \frac{0.5\frac{m}{s}}{\sqrt{900}} = 0.0167\frac{m}{s}$$

As an example of the full error calculation, the wind speed values from Measurement Period 3 are used. The mean wind speed measurements at each height for this measurement period are

| Height (z), [m] | Mean wind speed ($\bar{u}$), [m/s] | Mean wind speed error ($\delta\bar{u}$), [m/s] |
|---|---|---|
| 0.648 | 6.959 | 0.0167 |
| 1.04 | 10.716 | 0.0167 |
| 1.42 | 11.365 | 0.0167 |
| 3.0 | 12.057 | 0.0167 |

A Gaussian distribution of the mean wind speeds and their standard errors is used as inputs to the friction velocity linear regression in a Monte Carlo simulation. The distribution of the resulting friction velocities are shown in Figure D1. The simulation produces a mean friction velocity of $\bar{u}_* = 0.388$ with standard deviation $\sigma_{\bar{u}_*} = 0.007$. A 1000-iteration Monte Carlo simulation is used to ensure convergence of the standard deviation to within $\pm.001$ of its long-term value. Figure D2 shows the standard deviation output for different Monte Carlo simulation lengths, indicating adequate convergence is met after 500 iterations.
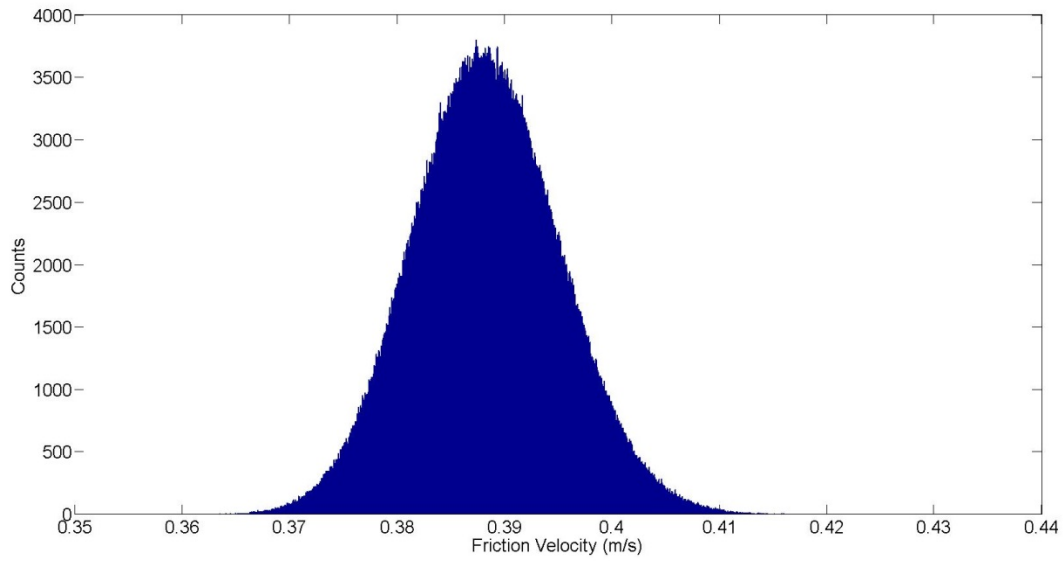
Figure D.1: Example of a 1000-iteration Monte Carlo simulation of the estimation for friction velocity from linear regression of the "law of the wall" equation.
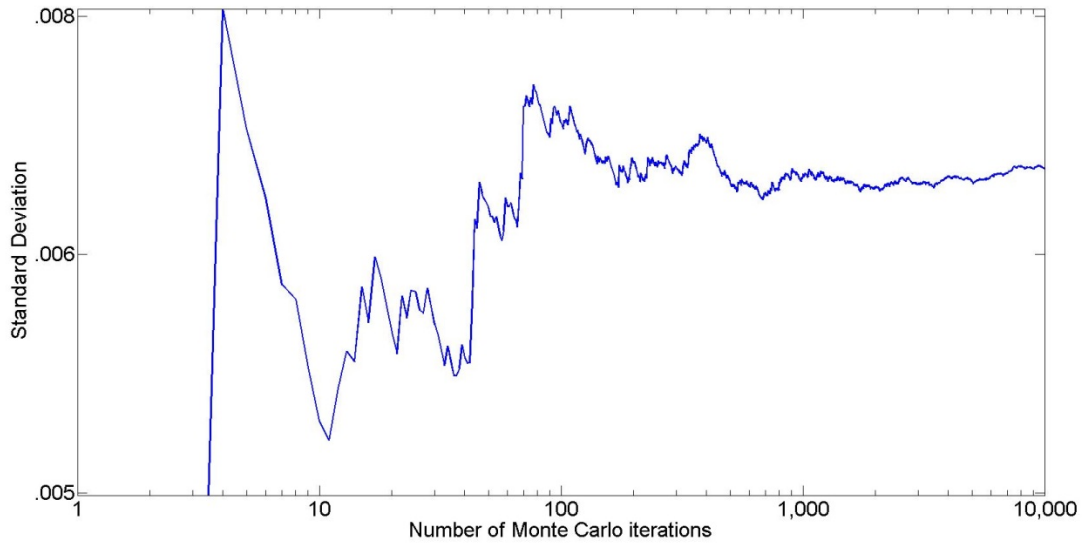


Figure D.2: The standard deviation of the Monte Carlo simulations as a function of the number of iterations performed. After 500 iterations, the standard deviation converges to within ±.001 m/s, providing a reasonable minimum number of iterations for this study.

### D.2. $\delta F_d$ Calculation

Uncertainty in the calculation of vertical dust flux is performed through error propagation through the eddy covariance calculations. Using the eddy covariance method, vertical dust flux is calculated by:

$$F_d = \overline{(\rho'w')}$$

The pressure perturbation around a local mean is then

$$\rho' = \rho - \bar{\rho}$$

where $\bar{\rho}$ is a 15-minute average of 1 Hz measurements about the value $\rho$. The error of $\bar{\rho}$ is then calculated by

$$\delta\bar{\rho} = \frac{\sigma_\rho}{\sqrt{n}} = \frac{0.08\bar{\rho}}{\sqrt{900}}$$

and the error in $\rho'$ is then

$$\delta\rho' = \sqrt{(\delta\bar{\rho})^2 + (\delta\rho)^2}$$

Similarly, the vertical wind speed perturbation is the difference between the current wind speed and the local mean. The local mean wind speed is a 15-minute moving average of 1 Hz measurements, and its error is calculated by

$$\delta\bar{w} = \frac{\sigma_w}{\sqrt{n}} = \frac{0.04m/s}{\sqrt{900}} = 0.0013\frac{m}{s}$$

and the error in $w'$ is then

$$\delta w' = \sqrt{(\delta\bar{w})^2 + (\delta w)^2}$$

The error in a single calculation of the product of density and vertical velocity perturbations is

$$\delta(\rho'w') = (\rho'w')\sqrt{\left(\left(\frac{\delta\rho'}{\rho'}\right)^2 + \left(\frac{\delta w'}{w'}\right)^2\right)}$$

and the 15-minute mean of the perturbation products then gives the vertical dust flux, whose error is then

$$\delta F_d = \frac{\sigma_{\rho'w'}}{\sqrt{n}} = \frac{(\rho'w')\sqrt{\left(\left(\frac{\delta\rho'}{\rho'}\right)^2 + \left(\frac{\delta w'}{w'}\right)^2\right)}}{\sqrt{900}}$$

**BIBLIOGRAPHY**

Albrecht, B. (1989), Aerosols, Cloud Microphysics, and Fractional Cloudiness, *Science, 245,* 1227-1230.

Alexander, J. M., O. Laskina, B. Meland, M. A. Young, V. H. Grassian, and P. D. Kleiber (2013), A combined laboratory and modeling study of the infrared extinction and visible light scattering properties of mineral dust aerosol, *J. Geophys. Res. Atmos., 118,* 435-452, doi:10.1029/2012JD018751.

Alfaro, S. C., J. L. Rajot, and W. Nickling (2004), Estimation of PM20 emissions by wind erosion: main sources of uncertainties, *Geomorphology, 59*, 63-74.

Anderson, R. S., and P. K. Haff (1988), Simulation of Eolian Saltation, *Science, 241*, 820-823.

Aubinet, M., T. Vesala, and D. Papale (2012), *Eddy Covariance,* Springer Verlag, Berlin.

Bagnold, R. A. (1941), The physics of blown sand and desert dunes, Methuen, New York.

Balme, M., and R. Greeley (2006), Dust devils on Earth and Mars, *Rev. Geophys., 44,* RG3003, doi: 10.1029/2005RG000188.

Balme, M., S. Metzger, M. Towner, T. Ringrose, R. Greeley, and J. Iversen (2003), Friction wind speeds in dust devils: A field study, *Geophys. Res. Lett., 30,* 1860, doi:10.1029/2003GL017493.

Beladjine, D., M. Ammi, L. Oger, and A. Valance (2007), Collision process between an incident bead and a three-dimensional granular packing, *Phys. Rev. E, 75,* 061305.

Belnap, J. and D. A. Gillette (1998), Vulnerability of desert biological soil crusts to wind erosion: the influences of crust development, soil texture, and disturbance, *J. Arid Env., 39,* 133-142.

Bou Karam, D., C. Flamant, J. Cuesta, J. Pelon, and E. Williams (2010), Dust emission and transport associated with a Saharan depression: February 2007 case, *J. Geophys. Res., 115,* D00H27.

Campbell Scientific Inc. (2012), CSAT3 three-dimensional sonic anemometer, Instrument manual.

Cantrell, W., C. McCrory, and G. E. Ewing (2002), Nucleated deliquescence of salt, *J. Chem. Phys., 116,* 2116-2120.

Castellanos, A (2005), The relationship between attractive interparticle forces and bulk behavior in dry and uncharged fine powders, *Adv. Phys., 54*, 263-376.

Chen, W. and D. W. Fryrear (2002), Sedimentary characteristics of a haboob dust storm, *Atmos. Res., 61,* 75-85.

Chen, Y., J. Tarchitzky, J. Brouwer, J. Morin, and A. Banin (1980), Scanning electron microscope observations on soil crusts and their formation, *Soil Sci., 130,* 49-55.

Cole-Dai, J. (2010), Volcanoes and climate, *Wiley Interdiscip. Rev.: Clim. Change, 1,* 824-839, doi:10.1002/wcc.76.

Cornelis, W. M. (2006), Hydroclimatology of wind erosion in arid and semiarid environments, In *Dryland Ecohydrology*, Springer, Dordrecht, 141-159.

Costa-Cabral, M., S. B. Roy, E. P. Maurer, W. B. Mills, and L. Chen (2013), Snowpack and runoff response to climate change in Owens Valley and Mono Lake watersheds, *Climatic Change, 116,* 97-109.

Dahlgren, R. A., J. H. Richards, and Z. Yu (1997), Soil and groundwater chemistry and vegetation distribution in a desert playa, Owens Lake, California, *Arid Soil Res. And Rehabilitation,* 11, 221-244.

Fécan, F., B. Marticorena, and G. Bergametti (1999), Parameterization of the increase of the Aeolian erosion threshold wind friction velocity due to soil moisture for arid and semi-arid areas, *Ann. Geophysiae, 17,* 149-157.

Feng, G., B. Sharratt, and V. Vaddella (2013), Windblown soil crust formation under light rainfall in a semiarid region*, Soil Till. Res., 128,* 91-96.

Fratini, G., P. Ciccioli, A. Febo, A. Forgione, and R. Valentini (2007), Size-segregated fluxes of mineral dust from a desert area of northern China by eddy covariance, *Atmos. Chem. Phys., 7,* 2839-2854.

Fryrear, D. W. (1986), A field dust sampler, *J. Soil and Water Conservation, 41,* 117.

Giles, J., (2005), The dustiest place on Earth, *Nature, 434,* 816-819.

Gill, T. E., D. A. Gillette, T. Niemeyer, and R. T. Winn (2002), Elemental geochemistry of wind-erodible playa sediments, Owens Lake, California, *Nucl. Instrum. Meth. B, 189,* 209-213.

Gillette, D. A. (1977), Fine particulate emissions due to wind erosion. *Trans. Am Soc. Agricultural Engrs., 20,* 890-897.

Gillette, D. A. (1981), Production of dust that may be carried great distances, *Geol. Soc. Am. Spec. Pap., 186,* 11-26.

Gillette, D. A. and P. C. Sinclair (1990), Estimation of suspension of alkaline material by dust devils in the United States, *Atmos. Environment, 24A,* 1135-1142.

Gillette, D. A., and R. Passi (1988), Modeling Dust Emission Caused by Wind Erosion, *J. Geophys. Res., 93,* 14233-14242.

Ginoux, P., M. Chin, I. Tegen, J. Prospero, B. Holben, O. Dubovik, and S. Lin (2001), Sources and distributions of dust aerosols simulated with the GOCART model, *J. Geophys. Res., 106,* 20255-20273.

Gran, M., J. Carrera, J. Massana, M. W. Saaltink, S. Olivella, C. Ayora, and A. Lloret (2011), Dynamics of water vapor flux and water separation processes during evaporation from a salty dry soil, *J. Hydrol., 396,* 215-220.

Greeley, R., and J. D. Iversen (1985), Wind as a Geological Process on Earth, Mars, Venus, and Titan, Cambridge University Press, New York.

Grini, A., C. S. Zender, and P. R. Colarco (2002), Saltation sandblasting behavior during mineral dust aerosol production, *Geophys. Res. Lett., 29,* 1868, doi:10.1029/2002GL015248.

Groeneveld, D. P., D. L. Grate, P. J. Hubbard, D. S. Munk, P. J. Novak, B. Tillemans, D. C. Warren, and I. Yamashita (1985), A field assessment of above- and below-ground factors affecting phreatophyte transpiration in the Owens Valley, California, *North American Riparian Conf.,* Tucson, Ariz., April 16-18, 1985.

Groeneveld, D. P., R. P. Watson, D. D. Barz, J. B. Silverman, and W. M. Baugh (2010), Assessment of two methods to monitor wetness to control dust emissions, Owens Dry Lake, California, *Int. J. Rem. Sens., 31,* 3019-3035.

Gu, Y., K. N. Liou, Y. Xue, C. R. Mechoso, W. Li, and Y. Luo (2006), Climatic effects of different aerosol types in China simulated by the UCLA general circulation model, *J. Geophys. Res., 111.*

Hagen, L. J., S. van Pelt, B. Sharratt (2010), Estimating the saltation and suspension components from field wind erosion, *Aeolian Res., 1,* 147-153.

Hagen, L. J. (1991), Wind erosion mechanics: Abrasion of aggregated soil, *Transactions of the ASAE, 34,* 831-837.

Hamaker, H. C. (1937), The London-Van der Waals attraction between spherical particles, *Physica, 4,* 1058-1072.

Hansen, J. E., M. Sato, A. Lacis, R. Reudy, I. Tegen, and E. Matthews (1998), Climate forcings in the Industrial era, *Proc. Natl. Acad. Sci., 95,* 12753-12758.

Haywood, J., and O. Boucher (2000), Estimates of the direct and indirect radiative forcing due to tropospheric aerosols: a review, *Rev. Geophys., 38,* 513-543.

Herminghaus, S. (2005), Dynamics of wet granular matter, *Adv. in Phys., 54,* 221-261.

Hillel, D (1980), Fundamentals of Soil Physics, Academic, San Diego.

Holben, B. N., D. Tanré, A. Smirnov, T. F. Eck, I. Slutsker, N. Abuhassan, W. W. Newcomb, J. S. Schafer, B. Chatenet, F. Lavenu, Y. J. Kaufman, J. Vande Castle, A. Setzer, B.

Markham, D. Clark, R. Frouin, R. Halthore, A. Karneli, N. T. O'Neill, C. Pietras, R. T. Pinker, K. Voss, and G. Zibordi (2001), An emerging ground-based aerosol climatology: Aerosol optical depth from AERONET, *J. Geophys. Res., 106,* 12067-12097.

Huneeus, N., M. Schulz, Y. Balkanski, J. Griesfeller, and J. Prospero (2011), Global dust model intercomparison in AeroCom phase I, *Atmos. Chem. Phys., 11,* 7781-7816.

IPCC (2007), IPCC (The Intergovernmental Panel on Climate Change) Fourth Assessment Report on scientific aspects of climate change for researchers, students and policymakers, Cambridge University Press, Cambridge, U.K.

Ito, J., H. Niino, and M. Nakanishi (2010), Large eddy simulation on dust suspension in a convective mixed layer, *SOLA, 6*, 133-136.

Jacobson, M. C., H. C. Hansson, K. J. Noone, and R. J. Charlson (2000), Organic atmospheric aerosols: review and state of the science, *Rev. of Geophys., 38,* 267-294.

Jiang, Q., M. Liu, and J. D. Doyle (2011), Influence of Mesoscale dynamics and turbulence on fine dust transport in Owens Valley, *J. App. Meteorol. Climatol., 50.1,* 28-38.

Johnson, K. L., K. Kendall, and A. D. Roberts (1971), Surface energy and the contact of elastic solids, *Proc. R. Soc. Lond. A, 324,* 301-313.

Kaplan, M. L., R. K. Vellore, J. M. Lewis, and M. Young (2011), The role of unbalanced Mesoscale circulations in dust storms, *J. Geophys. Res., 116,* D23101, doi:10.1029/2011JD016218.

King, J., G. F. S. Wiggs, F. D. Eckardt, D. S. G. Thomas, R. G. Bryant, and R. Washington (2012), DO4 Models: A new generation of model dust emission schemes based on source area process data, *EGU General Assembly 2012, 14,* Vienna, Austria, Abstract 9779.

Koch, J. and N. O. Rennó (2005), The role of convective plumes and vortices on the global aerosol budget, *Geophys. Res. Lett., 32*, L18806.

Kok, J. F. and N. O. Rennó (2009), A comprehensive numerical model of steady state saltation (COMSALT), *J. Geophys. Res., 114*, D17204.

Kok, J. F., E. J. R. Parteli, T. I. Michaels, and D. B. Karam (2012), The physics of wind-blown sand and dust, *Rep. Prog. Phys., 75,* 106901.

Kravchenko, A. G., and P. Moin (2000), Numerical studies of flow over a circular cylinder at $Re_D$=3900. *Phys. Fluids,* **12**, 403-417.

Lancaster, N., and A. Baas (1998), Influence of vegetation cover on sand transport by wind: Field studies at Owens Lake, California, *Earth Surf. Proc. And Landforms, 23,* 69-82.

Laurent, B., B. Marticorena, G. Bergametti, I. Tegen, K. Schepanski, and B. Heinhold (2009), Modelling mineral dust emissions, *IOP Conf. Ser.: Earth Env. Sci., 7,* 012006, doi:10.1088/1755-1307/7/1/012006.

Li, Z., F. Niu, J. Fan, Y. Liu, D. Rosenfeld, and Y. Ding (2011), Long-term impacts of aerosols on the vertical development of clouds and precipitation, *Nature Geosci., 4,* 888-894, doi:10.1038/NGEO1313.

Lohmann, U., and J. Feichter (2005), Global indirect aerosol effects: a review, *Atmos. Chem. Phys., 5,* 715-737.

Loosmore, G. A., and J. R. Hunt (2000), Dust resuspension without saltation, *J. Geophys. Res., 105,* 20663-20671.

Maisel, D. (2005), The Owens Lake Project, *Nieman Reports, 59,* 17-19.

Marks, L. S. (1934), The determination of the direction and velocity of flow of fluids. *J. Franklin Inst.*, **217**, 201-212.

Marsham, J. H., P. Knippertz, N. S. Dixon, D. J. Parker, and G. M. S. Lister (2011), The importance of the representation of deep convection for modeled dust-generating winds over West Africa during summer, *Geophys. Res. Lett., 38,* L16803, doi:10.1029/2011GL048368.

Marticorena, M. and G. Bergametti (1995), Modeling the atmospheric dust cycle: 1. Design of a soil-derived dust emission scheme, *J. Geophys. Res., 100*, 16415-16430.

McLaughlin, J. B. (1991), Inertial migration of a small sphere in linear shear flows, *J. Fluid Mech., 224,* 261-274.

Metzger, S. M. (1999), Dust devils as aeolian transport mechanisms in southern Nevada and the Mars Pathfinder landing site, Ph.D. dissertation, Univ. of Nev., Reno.

Moller, A. R. (1978), The improved NWS storm spotters' training program at Ft. Worth, Tex. *Bull. Amer. Meteor. Soc., 59*, 1574-1582.

Morris, P. H., J. Graham, and D. J. Williams (1992), Cracking in drying soils, *Can. Geotech. J., 29,* 263-277.

Neakrase, L. D. V., and R. Greeley (2010), Dust devil sediment flux on Earth and Mars: Laboratory simulations, *Icarus, 206,* 306-318.

Neakrase, L. D. V., R. Greeley, J. D. Iversen, M. R. Balme, and E. E. Eddlemon (2006), Dust flux within dust devils: Preliminary laboratory simulations, *Geophys. Res. Lett., 33,* L19S09, doi:10.1029/2006GL026810.

Nickling, W. G. (1984), The stabilizing role of bonding agents on the entrainment of sediment by wind, *Sedimentology, 31,* 111-117.

Nickling, W. G., and C. McKenna Neuman (2009), Aeolian sediment transport, *Geomorphology of Desert Environments*, ed A. Parsons and A. D. Abrahams, Springer, New York.

Nickling, W. G., and J. A. Gillies (1993), Dust emission and transport in Mali, West Africa, *Sedimentology, 40,* 859-868.

Niemeyer, T. C., D. A. Gillette, J. J. Deluisi, Y. J. Kim, W. F. Niemeyer, T. Ley, T. E. Gill, and D. Ono (1999), Optical depth, size distribution and flux of dust from Owens Lake, California, *Earth Surf. Process. Landforms, 24,* 463-479.

Ono, D. (2006), Application of the Gillette model for windblown dust at Owens Lake, CA, *Atmos. Env., 40,* 3011-3021.

Owen, P. R. (1964), Saltation of uniform grains in air, *J. Fluid Mech., 20*, 225-242, doi: 10.1017/S0022112064001173.

Park, S. H., S. L. Gong, T. L. Zhao, R. J. Vet, V. S. Bouchet, W. Gong, P. A. Makar, M. D. Moran, C. Stroud, and J. Zhang (2007), Simulation of entrainment and transport of dust particles within North America in April, 2001 ("Red Dust Episode"), *J. Geophys. Res., 112,* D20209, doi:10.1029/2007JD008443.

Pilewskie, P. (2007), Aerosols heat up, *Nature, 448,* 541-542.

Prandtl, L. (1952), Essentials of Fluid Dynamics: With applications to hydraulics aeronautics, meteorology, and other subjects. Hafner Pub. Co., 452 pp.

Prospero, J. M., P. Ginoux, O. Torres, S. E. Nicholson, and T. E. Gill (2002), Environmental characterization of global sources of atmospheric soil dust identified with the NIMBUS 7 total ozone mapping spectrometer (TOMS) absorbing aerosol product, *Rev. Geophys., 40,* 1002, doi:10.1029/2000RG000095.

Quick, D. J., and O. A. Chadwick (2011), Accumulation of salt-rich dust from Owens Lake playa in nearby alluvial soils, *Aeolian Res., 3,* 23-29.

Rajot, J. L., S. C. Alfaro, L. Gomes, and A. Gaudichet (2003), Soil crusting on sandy soil sand its influence on wind erosion*, Catena, 53*, 1-16.

Rennó, N. O. (2008), A thermodynamically general theory for convective vortices, *Tellus, Ser. A, 60*, 688-699.

Rennó, N. O., D. G. Halleaux, F. Saca, S. Rogacki, R. Gillespie, S. Musko (2010), A generalization of Bernoulli's equation to convective vortices. Abstract, *41$^{st}$ Lunar and Planetary Science Conference*, *The Woodlands,* TX, Lunar Planet. Inst., 1745.

Rennó, N. O., V. J. Abreu, J. Koch, P. H. Smith, O. K. Hartogensis, H. A. R. De Bruin, D. Burose, G. T. Delory, W. M. Farrell, C. J. Watts, J. Garatuza, M. Parker, and A. Carswell

(2004), MATADOR 2002: A pilot field experiment on convective plumes and dust devils, *J. Geophys. Res., 109,* E07001, doi:10.1029/2003JE002219.

Rennó, N. O., M. L. Burkett, M. P. Larkin (1998),  A simple thermodynamical theory for dust devils. *J. Atmos. Sci.,* **55**, 3244-3252.

Reynolds, R. L., J. C. Yount, M. Reheis, H. Goldstein, P. Chavez, R. Fulton, J. Whitney, C. Fuller, and R. M. Forester (2007), Dust emission from wet and dry playas in the Mojave Desert, USA, *Earth Surf. Proc. And Landforms, 32,* 1811-1827.

Ringrose, T. J. (2005), Inside dust devils, *Astronomy Geophys., 46,* 5.16-5.19.

Roberts, A., and P. Knippertz (2012),  Haboobs: convectively generated dust storms in West Africa, *Weather, 67,* 311-316.

Saca, F. A., N. O. Rennó, D. G.  Halleaux, S. Rogacki, R. Gillespie, S. Musko (2010), A portable instrument for atmospheric measurements. Abstract, *41$^{st}$ Lunar and Planetary Science Conference, The Woodlands,* TX, Lunar Planet. Inst., 1767.

Saffman, P. G. (1965), Lift on a small sphere in a slow shear flow, *J. Fluid Mech., 22,* 385.

Shannon, S., and D. J. Lunt (2011), A new dust cycle model with dynamic vegetation: LPJ-dust version 1.0, *Geosci. Model Dev., 4,* 85-105.

Shao, Y. (2005), A similarity theory for saltation and application to aeolian mass flux, *Boundary Layer Meteorology, 115*, 319-338.

Shao, Y. (2008), Physics and Modelling of Wind Erosion 2$^{nd}$ Edn., Springer, Heidelberg.

Shao, Y. and H. Lu (2000), A simple expression for wind erosion threshold friction velocity, *J. Geophys. Res., 105*, 22437-22443.

Shao, Y., and A. Li (1999), Numerical modeling of saltation in the atmospheric surface layer, *Boundary Layer Meteorol., 91*, 199-225.

Shao, Y., M. R. Raupach, and P. A. Findlater (1993), Effect of saltation bombardment on the entrainment of dust by wind, *J. Geophys. Res., 98,* 12719-12726.

Sherman, D. J. and E. J. Farrell (2008), Aerodynamic roughness lengths over movable beds: Comparison of wind tunnel and field data, *J. Geophys. Res., 113*, F02S08.

Sherman, D. J., D. W. T. Jackson, S. L. Namikas, and J. Wang (1998), Wind-blown sand on beaches: an evolution of models, *Geomorphology, 22*, 113-133.

Sinclair, P. C. (1964), Some preliminary dust devil measurements, *Mon. Wea. Rev., 92,* 363-367.

Sinclair, P. C. (1973), The Lower Structure of Dust Devils, *J. Atmos. Sci., 30,* 1599-1619.

Smirnov, A., B. N. Holben, T. F. Eck, I. Slutsker, B. Chatenet, and R. T. Pinker (2002), Diurnal variability of aerosol optical depth observed at AERONET (Aerosol Robotic Network) sites, *Geophys. Res. Lett., 29,* 2115, doi: 10.1029/2002GL016305.

Sokolik, I. N., D. M. Winker, G. Bergametti, D. A. Gillette, G. Carmichael, Y. J. Kaufmann, L. Gomes, L. Schuetz, and J. E. Penner (2001), Introduction to special section: Outstanding problems in quantifying the radiative impacts of mineral dust, *J. Geophys. Res., 106,* D16, 18015-18027.

Sow, M., S. C. Alfaro, J. L. Rajot, and B. Marticorena (2009), Size resolved dust emission fluxes measured in Niger during 3 dust storms of the AMMA experiment, *Atmos. Chem. Phys., 9*, 3881-3891.

Tanaka, T. Y., T. T. Sekiyama, T. Maki, and M. Mikami (2011), The effects of snow cover and soil moisture on Asian dust: I. A numerical sensitivity study, *SOLA, 7A,* 036-039, doi: 10.2151/sola.71-010.

Tegen, I., A. A. Lacis, and I. Fung (1996), The influence of climate forcing on mineral aerosols from disturbed soils. *Nature, 380,* 419-422.

Tegen, I., and I. Fung (1995), Contribution to the atmospheric aerosol load from land surface modification, *J. Geophys. Res., 100*, 18707-18726.

Tegen, I., and K. Schepanski (2009), The global distribution of mineral dust, *IOP Conf. Ser.: Earth and Env. Sci., 7,* 012001, doi:10.1088/1755-1307/7/1/012001.

Tegen, I., M. Werner, S. P. Harrison, and K. E. Kohfeld (2004), Relative importance of climate and land use in determining present and future global soil dust emission, *Geophys. Res. Lett., 31*, L05105, doi: 10.1029/2003GL019216.

Tegen, I., S. P. Harrison, K. Koheld, and I. C. Prentice (2002), Impact of vegetation and preferential source areas on global dust aerosol: Results from a model study, *J. Geophys. Res., 107*, doi:10.1029/2001JD000963.

Titus, J., R. S. Nowak, and S. D. Smith (2002), Soil resource heterogeneity in the Mojave Desert, *J. Arid Environ., 52,* 269-292.

Twomey, S. (1977), The influence of pollution on the shortwave albedo of clouds, *J. Atmos. Sci., 34,* 1149-1152.

Washington, R., M. C. Todd, S. Engelstaedter, S. Mbainayel, and F. Mitchell (2006), Dust and the low-level circulation over the Bodélé Depression, Chad: Observations from BoDEx 2005, *J. Geophys. Res., 111,* D03201, doi:10.1029/2005JD006502.

Wieringa, J. (1993), Representative roughness parameters for homogeneous terrain, *Boundary Layer Meteorology, 63*, 323-363.

Wieringa, J. (1967), Evaluation and Design of Wind Vanes. *J. Appl. Meteor., 6*, 1114-1122.

Williams, E. R. (2008), Comment on "Atmospheric controls on the annual cycle of North African dust" by S. Engelstaedter and R. Washington, *J. Geophys. Res., 113*, D23109.

Yakirevich, A., P. Berliner, and S. Sorek (1997), A model for numerical simulating of evaporation from bare saline soil, *Water Resources Research, 33,* 1021-1033.

Yang, P., Q. Feng, G. Hong, G. W. Kattawar, W. J. Wiscombe, M. I. Mishchenko, O. Dubovik, I. Laszlo, and I. N. Sokolik (2007), Modeling of the scattering and radiative properties of nonspherical dust-like aerosols, *Aerosol Sci., 38,* 995-1014.

Yin, D., S. Nickovic, B. Barbaris, B. Chandy, and W. A. Sprigg (2005), Modeling wind-blown desert dust in the southwestern United States for public health warning: A case study, *Atmos. Env., 39,* 6243-6254.

Zender, C.S., R. L. Miller, and I. Tegen (2004), Quantifying mineral dust mass budgets: Terminology, constraints, and current estimates, *Eos Trans. AGU, 85,* 509-512, doi: 10.1029/2004EO480002.

Zucrow, M. J., and J. D. Hoffman (1976), *Gas Dynamics.* Wiley, 772 pp.